ABSTRACT

Title of Dissertation: COSMOLOGY AND PARTICLE PHYSICS BEYOND THE STANDARD MODEL

Kaustubh Deshpande
Doctor of Philosophy, 2021

Dissertation Directed by: Professor Raman Sundrum
Department of Physics

The Standard Models (SM) of particle physics and cosmology have been great successes so far, but various observational and theoretical hints point towards new physics beyond them. In this thesis, we first briefly discuss these shortcomings, including puzzles for the initial state of the early universe and how they can be solved via Cosmic Inflation. We then focus on constructing microscopic models for inflation which are theoretically natural, Effective Field Theory (EFT) controlled, and observationally consistent, while also looking for possible new signals. We develop a supersymmetric (SUSY) bi-axion model of high-scale inflation, in which the axionic structure originates from gauge symmetry in an extra dimension. While local SUSY is necessarily Higgsed at high scales during inflation we show that it can naturally survive down to the $\sim$ TeV scale in the current era in order to resolve the electroweak hierarchy problem. In the face of improving constraints on the tensor-to-scalar ratio, we also investigate inflation at lower energy scales via the very well-motivated mechanism of Hybrid Inflation. We construct a technically natural and EFT-controlled model for this, "Twinflation", incorporating a discrete

"twin" symmetry.

If a SUSY extension of the SM does survive down to $\sim$ TeV scales, although not yet observed at the collider searches so far, it may have structures giving rise to novel Long-Lived Particle (LLP) signatures. LLPs also feature in a variety of other new physics scenarios. We show that future electron-proton colliders, forming an interesting hybrid of leptonic and hadronic colliders, can probe LLPs with soft decay products and very short lifetimes, thus offering a complimentary reach into the new physics parameter space.

COSMOLOGY AND PARTICLE PHYSICS BEYOND THE STANDARD MODEL

by

Kaustubh Deshpande

Dissertation submitted to the Faculty of the Graduate School of the
University of Maryland, College Park in partial fulfillment
of the requirements for the degree of
Doctor of Philosophy
2021

Advisory Committee:
Professor Raman Sundrum, Chair/Advisor
Professor Paulo Bedaque
Professor Anson Hook
Professor Rabindra Mohapatra
Professor Richard Wentworth

Preface

Some chapters of this thesis are based on my work in collaboration with other people. Chapter 2 is mostly JHEP 1908 (2019) 029 [1] co-authored with Raman Sundrum. Chapter 3 is mostly arXiv:2101.06275 (submitted to JHEP) [2] co-authored with Soubhik Kumar and Raman Sundrum. Chapter 4 is mostly JHEP 1807 (2018) 024 [3] which is work in collaboration with David Curtin, Oliver Fischer, and Jose Zurita.

Dedication

To the spirit of inquiry among all humans...

Acknowledgments

I owe my gratitude to all those countless people without whom this PhD journey would never have been possible for me. This is a great opportunity for me to acknowledge at least some of them.

I would like to start by thanking my advisor Prof. Raman Sundrum. His deep thinking and insightful perspective towards physics has always inspired me. I would also like to thank other faculty in the Particle Theory Group at the Maryland Center for Fundamental Physics (MCFP) - Prof. Kaustubh Agashe, Prof. Zackaria Chacko, Prof. Anson Hook, and Prof. Rabindra Mohapatra - for the tremendous learning I had from them through all these years, directly or indirectly, through graduate courses, discussions, seminars, teaching assistantship, and general advising. I would especially like to thank Prof. David Curtin for the incredible opportunities and guidance during our collaborative work. Let me also thank Oliver Fischer and Jose Zurita for their wonderful help during this collaboration which was a great learning experience for me. I am thankful to Prof. Richard Wentworth as well as Profs. Sundrum, Hook, Mohapatra, and Prof. Paulo Bedaque for agreeing to serve on my thesis committee.

Enormous thanks to the past and present post-docs and graduate students at MCFP, with whom I had a chance to interact, collaborate with and learn from. They include Stefano Antonini, Batoul Banihashemi, Arushi Bodas, Dawid Brzeminski, Dan Carney,

Jack Collins, David Curtin, Saurav Das, Abhish Dev, Sanket Doshi, Peizhi Du, Reza Ebadi, Majid Ekhterachian, Anton de la Fuente, Michael Geller, Sungwoo Hong, Saurabh Kadam, Soubhik Kumar, Zhen Liu, Rashmish Mishra, Arif Mohd, Simon Riquelme, Prashant Saraswat, Matthew Severson, Antony Speranza, Gustavo Marques Tavares, Yuhsin Tsai, Christopher Verhaaren, and Yixu Wang. I would like to thank Majid Ekhterachian again for his help and support, especially while navigating the initial years of the graduate school together.

I would like to acknowledge the financial support from MCFP and National Science Foundation for my research. Many thanks to Heather Markle and Melanie Knouse for help in various administrative processes at MCFP. I would also like to thank Jessica Crosby and Josiland Chambers for their immense help as graduate program coordinators in the Physics Department at UMD.

I would like to express my gratitude towards the friends whom I lived with, had close interactions with, and who contributed to make my life in the College Park area more enjoyable and meaningful. They include Omkar Joshi, Saurabh Kadam, Amar Kurane, Harshad Oak, and Arpith Shanbhag.

I am deeply grateful to my Indian classical music (vocal) teacher, Dr. Pradeep Sathe, as well as other fellow learners in the class. This soul-enriching art form has been a very important part of my life since the last few years, and I would like to thank Dr. Sathe for all his efforts to inculcate it in me.

I am extremely grateful to the Vedanta Center of Greater Washington DC and all of the people associated with it. I consider it my great fortune to be able to come in contact with this place and the thought it represents. No words will be sufficient to express my

gratitude towards the spiritual support I have received from here.

Finally, let me thank my close relatives and family. I would like to thank my two sisters and their families for constant support, love, and care. About my father, my mother, and lastly, my wife Kalyani... no amount of gratitude I might express here would be worth the love I have received from them!

Table of Contents

List of Tables

List of Figures

List of Abbreviations

1PI	One-particle irreducible
4(5)D	Four (five) dimensional
AdS	Anti-de Sitter
BSM	Beyond the Standard Model
CC	Cosmological Constant
CDM	Cold dark matter
CFT	Conformal Field Theory
CMB	Cosmic Microwave Background
DIS	Deep inelastic scattering
DM	Dark matter
DV	Displaced vertex
DW	Domain walls
EFT	Effective Field Theory
EW	Electroweak
EWinos	Electroweakinos
FCC	Future Circular Collider
GW	Gravitational waves
HERA	Hadron-Electron Ring Accelerator
HL-LHC	High-luminosity Large Hadron Collider
IR	Infra-red
ISR	Initial state radiation
KK	Kaluza-Klein
KLR	Kallosh-Linde-Rube
LEP	Large Electron-Positron Collider
LHC	Large Hadron Collider
LHeC	Large Hadron Electron Collider
LLP	Long-Lived Particle
MET	Missing transverse energy
MSSM	Minimal Supersymmetric Standard Model
NG	Non-Gaussianities
NGB	Nambu Goldstone boson
PDF	Parton Distribution Function
pNGB	Pseudo-Nambu Goldstone boson
PQ	Peccei-Quinn

PV	Primary vertex
QCD	Quantum Chromodynamics
RH	Right-handed
SM	Standard Model
SUGRA	Supergravity
SUSY	Supersymmetry
UV	Ultra-violet
VBF	Vector boson fusion
VEV	Vacuum expectation value
WGC	Weak Gravity Conjecture

Chapter 1: Introduction

1.1 Success of the Standard Model and the need for new physics

The Standard Model of particle physics (see [13] for a review) has been a great achievement of the human mind! It provides a microscopic theory of the constituent building blocks of almost all the physical world that we know so far, amazingly spanning ~ 40 orders of magnitude in length scales, valid from sub-nuclear (about a hundredth of a femtometer) to the cosmological scales (Gigaparsecs).

However, there are strong reasons to believe, from both observational and theoretical perspectives, that this is not the "end of particle physics", and that there should exist new physics beyond the Standard Model (BSM). A variety of astrophysical and cosmological observations, e.g. galaxy rotation curves, gravitational lensing, and cosmic microwave background (CMB), suggest that $\sim 85\%$ of all matter and $\sim 26\%$ of all the energy density in the universe is made up of the Dark Matter (DM) (see [14, 15] for a review), which does not interact like the SM particles except gravitationally. There is no good SM candidate for DM (except probably primordial black holes [16]) and hence DM is most likely consists of BSM particle(s). Also, the tiny neutrino masses, observed from neutrino oscillation experiments, are much smaller than all the other scales in the SM and do not have an explanation for their origin within it (see [17] for a review). Furthermore,

the observable universe around us has much more matter than antimatter. This asymmetry cannot be generated just by the SM and the standard cosmological evolution (see e.g. [18]). All of these experimental results call for new BSM physics.

Apart from these observational hints, SM has some striking theoretical and conceptual puzzles as well, pointing to its possible incompleteness. The SM Higgs boson, a fundamental scalar field which plays the crucial role of spontaneous breaking of electroweak symmetry and giving masses to all of the SM particles that couple to it, has been observed and its SM interactions verified so far (see [14] for a review). However, SM has no explanation for the fundamental origin of the Higgs mass, neither is it calculable within it. Furthermore, any extension of SM which is able to calculate it, predicts a mass much larger than the observed one (125 GeV) over the majority of the parameter space, due to quadratic sensitivity to the UV mass scales. In order to get a small mass as observed, one needs to fine-tune totally unrelated contributions to within an extraordinary precision, which is highly unnatural. This is the so-called Higgs Hierarchy Problem.

A similar problem exists in the case of the Cosmological Constant (CC) which receives quantum corrections quartically sensitive to the UV scales, generically giving a value much bigger than the observed one ($\sim \mathrm{meV}^4$). This requires fine-cancellations between unrelated contributions to a precision even higher than that in the Higgs case. This is the so-called Cosmological Constant Problem (see [19, 20] for a review). Finally, there is also the Strong CP Problem (see [21] for a review), which is the puzzle that why is the CP-violating θ-parameter of QCD constrained to be so small, even though it is expected to be $\mathcal{O}(1)$, especially considering that similar CP-violating phases in the electroweak sector are $\mathcal{O}(1)$.

The evolution of the universe on cosmological scales is governed very well by the ΛCDM "standard model" of cosmology (see e.g. [22]). This describes the cosmological expansion as driven by the CC and cold DM, with a small fraction of SM matter and radiation. This description is consistent with almost all of the observations so far, except for some anomalies still being examined, e.g. H_0 tension [23, 24], EDGES 21-cm observation [25], and DM core-cusp issue [26].

However, there exist various puzzles regarding the initial state of the early universe (see [4] for a review). The observable universe today on large scales is extremely homogeneous, e.g. the CMB temperature is uniform to ~ 1 in 10^5 across all of the sky. But this requires that the patches of the universe which would never have been in causal contact since Big Bang, according to the standard ΛCDM evolution, to still be approximately in thermal equilibrium today. This is the so-called Horizon Problem. Similarly, there exists the Flatness Problem. The universe today is spatially flat to a good accuracy, even though a little curvature at early times would grow considerably, thus requiring the initial state to be flat to an extraordinary accuracy. Furthermore, the CMB shows small fluctuations on top of the uniform background, even on the scales bigger than the horizon, which is puzzling. The origin of these super-horizon fluctuations cannot be explained by ΛCDM evolution since they cannot be produced by any causal processes, and need to be imprinted on the initial state. As we will see next, these initial state issues can be addressed robustly via Cosmic Inflation.

1.2 Cosmic inflation

The initial state puzzles faced by the standard ΛCDM cosmology, as reviewed above, can be addressed by introducing an early universe phase of accelerated expansion, called as Cosmic Inflation. Such an expansion can be powered by vacuum energy dominated dynamics, giving an approximately exponential expansion of the space-time, as we will see below. Such a rapid expansion dilutes any prior "irregularities" (e.g. spatial curvature), blows up a causally connected patch into the entire observable universe at late times, while also imprinting quantum fluctuations on the super-horizon scales. Here we give a brief overview of the classical and quantum inflationary evolution, including the main aspects used in this thesis. For a review and detailed discussion, see [4].

Inflation can be implemented minimally with a single real scalar field, inflaton, slowly rolling down its nearly flat potential (see Fig. 1.1). The general metric describing a 3+1 dimensional expanding, homogeneous and isotropic space-time is given by

$$ds^2 = -dt^2 + a(t)^2 d\vec{x}^2, \tag{1.1}$$

with the Hubble parameter

$$H(t) = \frac{\dot{a}}{a}(t) \tag{1.2}$$

characterizing the rate of expansion. Here, overdot denotes derivative with respect to t. The coupled classical dynamics of the inflaton field in this background is given by the

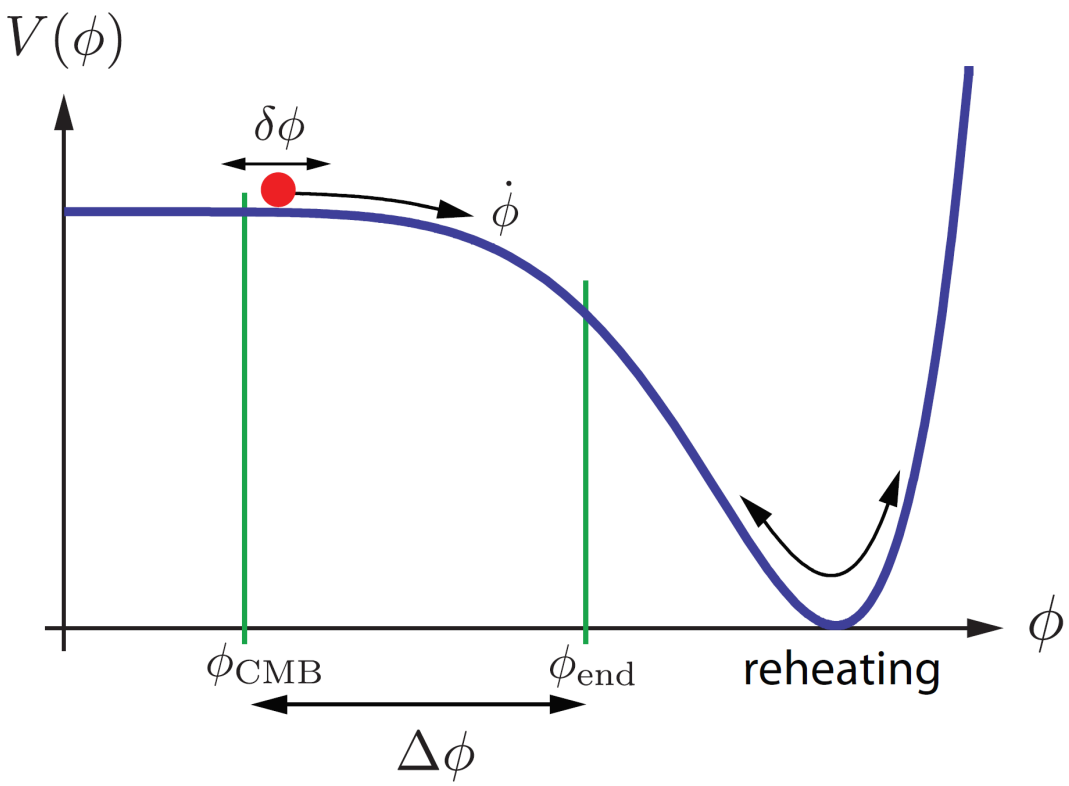

Figure 1.1: Example of a slow-roll potential for inflaton [4]: Inflation can happen on a nearly flat part of the potential as shown. $\phi_{\rm end}$ refers to the onset of slow-roll violation and end of inflation. $\phi_{\rm CMB}$ corresponds to the initial field value to get sufficient e-folds of expansion to address the horizon problem at the CMB. $\delta\phi$ are the spatially varying inflaton quantum fluctuations.

following equations of motion:

$$\begin{aligned} \ddot{\phi} + 3H\dot{\phi} + V'(\phi) &= 0, \\ \frac{\dot{\phi}^2}{2} + V(\phi) &= 3H^2 M_{\rm Pl}^2. \end{aligned} \tag{1.3}$$

During slow-roll inflation, potential energy dominates over the kinetic energy, i.e. $\dot{\phi}^2 \ll V(\phi)$, which then implies from above that H remains approximately constant (since $V(\phi)$ is also nearly flat in the slow-roll phase). Then, using Eq. (1.2), one can clearly see that $a(t) \sim e^{Ht}$, i.e. slow-roll inflation powers the exponential space-time expansion. The

slow-roll potential is characterized by the so-called slow-roll parameters defined as below:

$$\epsilon(\phi) \equiv \frac{1}{2}\left(\frac{V'}{V}\right)^2 M_{\rm Pl}^2 \ , \ \ \eta(\phi) \equiv \frac{V''}{V} M_{\rm Pl}^2. \tag{1.4}$$

The slow-roll is satisfied when $\epsilon, \eta \ll 1$. As ϕ rolls down such a potential, at some $\phi_{\rm end}$, ϵ or η grows and becomes ≈ 1. Beyond this point, the inflaton undergoes a fast-roll to the minimum of the potential, quickly releases the vacuum energy and thus ends the phase of inflation. Later, through its perturbative decay or through non-perturbative conversion processes, it can reheat the universe with SM (and DM) particles. In order to address e.g. the horizon problem, the scale factor needs to expand by at least 50-60 e-folds ($\mathcal{N}_e$) as given by

$$\mathcal{N}_e = \int d\ln a = \int H dt \approx \int_{\phi_{\rm ini}}^{\phi_{\rm end}} \frac{d\phi}{M_{\rm Pl}\sqrt{\epsilon(\phi)}}. \tag{1.5}$$

To achieve this, ϕ needs to roll over large $\Delta\phi$, which might also be super-Planckian (see Lyth bound [27]).

Classical evolution of inflaton addresses the initial state issues for the homogeneous background universe on the large scales. Furthermore, its quantum fluctuations give rise to small primordial inhomogeneities and anisotropies as observed, and also primordial gravitational waves. The inflaton field fluctuations can be written as $\phi(\vec{x}, t) = \phi_0(t) + \delta\phi(\vec{x}, t)$, where $\phi_0(t)$ and $\delta\phi(\vec{x}, t)$ are the inflaton classical background and quantum fluctuations, respectively. At sufficiently early times during inflation, a mode $\delta\phi_k$ with comoving momentum k, is sub-horizon, i.e. its physical momentum $\left(= \frac{k}{a}\right) \gg H$. Its quantum evolution then is approximately described by a simple harmonic oscillator in flat space-time, since curvature effects can be neglected at momenta much higher than H.

When one analyses $\delta\phi_k$ at late times, one finds that it effectively becomes classical. Its linearized equation of motion in the background inflationary space-time, neglecting the small slow-roll potential, is given by

$$\delta\ddot{\phi}_k + 3H\delta\dot{\phi}_k + \left(\frac{k}{a}\right)^2 \delta\phi_k = 0. \tag{1.6}$$

When the mode becomes super-horizon, i.e. for $\frac{k}{a} \ll H$, the second term in the above equation dominates over the third, and hence its evolution gets frozen at its value during horizon-crossing, i.e. for $\frac{k}{a} \sim H$. These inflationary fluctuations imprinted on super-horizon scales, after the end of inflation, enter back into the horizon during standard ΛCDM evolution, and provide seeds for late-time structure formation.

As we mentioned earlier, the trajectory of ϕ plays the role of a "clock" governing when inflation ends as a function of space. Spatially varying fluctuations $\delta\phi(\vec{x}, t)$ hence imply that different regions of the universe inflate by slightly different amount, leading to variations in the local energy densities in the post-inflationary universe, resulting e.g. in the temperature fluctuations in the CMB as observed. These can be calculated in a gauge-invariant way, i.e. taking into account scalar fluctuations of the metric, via the comoving curvature perturbation $(\mathcal{R})$. The two-point correlation function of $\mathcal{R}$ defines the (dimensionless) power spectrum for the primordial scalar fluctuations (P_s) as

$$\langle \mathcal{R}_{\vec{k}} \mathcal{R}_{\vec{k'}} \rangle = (2\pi)^3 \, \delta(\vec{k} + \vec{k'}) \, \frac{2\pi^2}{k^3} P_s(k), \tag{1.7}$$

which is given by

$$P_s(k) = A_s \left(\frac{k}{k_*}\right)^{n_s-1} \;\; ; \;\; A_s = \frac{1}{8\pi^2}\frac{1}{\epsilon_*}\frac{H_*^2}{M_{\rm Pl}^2} \;\; , \;\; n_s = 1 - 6\epsilon_* + 2\eta_*. \tag{1.8}$$

Here k_* is a reference momentum scale corresponding to the largest length scale observable today and all other quantities with a subscript $*$ are evaluated at the horizon-crossing of this mode during inflation (i.e. when $k_* = aH_*$). Similarly, inflation also generates primordial tensor fluctuations to the spatial metric whose power spectrum is given by

$$P_t(k) = A_t \left(\frac{k}{k_*}\right)^{n_t} \;\; ; \;\; A_t = \frac{2}{\pi^2}\frac{H_*^2}{M_{\rm Pl}^2} \;\; , \;\; n_t = -2\epsilon_*. \tag{1.9}$$

The relative strength of these tensor fluctuations (gravitational waves) as compared to the scalar ones is the so-called "tensor-to-scalar ratio", given by

$$r \equiv \frac{A_t}{A_s} = 16\epsilon_*. \tag{1.10}$$

The current constraints on A_s, n_s, r from the Planck CMB observations [5] are

$$A_s = (2.097 \pm 0.1014) \times 10^{-9} \;\; , \;\; n_s = 0.9649 \pm 0.0042 \;\; , \;\; r < 0.064. \tag{1.11}$$

The bound on r can also be translated to an upper bound on the inflationary Hubble scale as

$$H_{\rm inf} = \left(\frac{\pi^2}{2} A_s r\right)^{1/2} M_{\rm Pl} \lesssim 10^{13}{\rm GeV}. \tag{1.12}$$

There are various upcoming and near-future proposed experiments [28, 29, 30, 31, 32] aiming at improving these constraints, and especially measuring r. These will be able to measure $r \gtrsim 10^{-3}$, corresponding to $H_{\rm inf} \gtrsim 10^{12}$ GeV. The measurement of $H_{\rm inf}$ would be a very important discovery as it gives a new fundamental energy scale in physics, which may open up many new avenues in BSM physics explorations.

1.3 Supersymmetry

As inflation can happen at energy scales as high as $H_{\rm inf} \sim 10^{13}$ GeV, it can be sensitive to new physics structures in the UV, e.g. supersymmetry (SUSY), grand unified theory etc. In Chap. 2, we explore the compatibility of high-scale inflation with SUSY, which is a highly motivated BSM framework. Here we give a brief overview of some of the main aspects of SUSY used in this thesis. For a review, see [33, 34, 35].

SUSY is a symmetry between bosons and fermions. We know that light fermions are perfectly natural due to the chiral symmetry that becomes exact in the massless limit. By contrast, a light Higgs scalar is ordinarily not protected by any symmetry and is quadratically sensitive to UV scales. However, when the SM is extended to become supersymmetric, the Higgs scalar becomes naturally as light as its fermionic superpartner. Thus, SUSY forms perhaps the most important and popular paradigm for addressing the Higgs Hierarchy Problem.

SUSY can be formulated by extending the space-time to include Grassmannian coordinates $(\theta^\alpha, \theta^\dagger_{\dot\alpha})$, which is now called the "superspace". SUSY is then realized as the

symmetry under superspace translations given by

$$\theta \to \theta + \epsilon \ , \ \theta^\dagger \to \theta^\dagger + \epsilon^\dagger \ , \ x^\mu \to x^\mu + \Delta^\mu \quad ; \Delta^\mu = i\left(\epsilon\sigma^\mu\theta^\dagger + \epsilon^\dagger\bar{\sigma}^\mu\theta\right). \tag{1.13}$$

A superfield $S\left(x, \theta, \theta^\dagger\right)$ is then a multiplet of fields, bosonic and fermionic, which has well-defined transformations under SUSY as $S \to S + \delta S$ where

$$\delta S = \left(\Delta^\mu \partial_\mu + \epsilon^\alpha \partial_\alpha + \epsilon^\dagger_{\dot{\alpha}} \partial^{\dot{\alpha}}\right) S, \tag{1.14}$$

which features bosons transforming into fermions and vice versa, due to the Grassmannian nature of coordinates involved.

Some of the especially useful superfields are chiral and vector superfields. A chiral superfield (Φ) is obtained by applying the constraint $\bar{D}^{\dot{\alpha}}\Phi = 0$, where the SUSY covariant derivative $\bar{D}^{\dot{\alpha}} = \partial^{\dot{\alpha}} - i\left(\bar{\sigma}^\mu\theta\right)^{\dot{\alpha}} \partial_\mu$. This constraint projects out all component fields in Φ except a complex scalar (ϕ), a Dirac fermion (ψ), and an auxiliary complex scalar (F). These transform under SUSY as

$$\delta\phi \sim \epsilon\psi \ \ , \ \ \delta\psi \sim \left(\sigma^\mu\epsilon^\dagger\right)\partial_\mu\phi + \epsilon F \ \ , \ \ \delta F \sim \epsilon^\dagger\bar{\sigma}^\mu\partial_\mu\psi, \tag{1.15}$$

which shows bosons transforming into fermions and vice versa, as alluded to before. On the other hand, a vector superfield (V) is a real superfield, i.e. satisfying the constraint $V = V^*$. It includes a gauge field (A_μ), its super-partner Dirac gaugino (λ), and an auxiliary real scalar (D). The general SUSY-invariant action for chiral superfields Φ_i

charged under a $U(1)$ gauge symmetry with charges q_i, respectively, is given by

$$\int d^4x\, \mathcal{L}(\Phi_i, V) = \int d^4x \left[\int d^4\theta\, \Phi_i^* e^{gq_i V} \Phi_i + \int d^2\theta \left(W(\Phi_i) + \frac{1}{4} f(\Phi_i) \mathcal{W}_\alpha^2 \right) + \text{h.c.} \right]. \tag{1.16}$$

The $\int d^4\theta$ term is called the Kähler potential. It includes the gauge-invariant kinetic terms for the fields in Φ_i. It can also include higher dimension terms in $\Phi_i^* e^{gq_i V} \Phi_i$ which then give higher dimensional derivative interactions. The $\int d^2\theta$ term is called the superpotential. The second term in it has $\mathcal{W}_\alpha$ which is the SUSY analog of the gauge-invariant field strength $F_{\mu\nu}$, and gives rise to the gauge kinetic term. $W(\Phi_i)$ and $f(\Phi_i)$ are holomorphic functions of Φ_i and are responsible for non-derivative but gauge-invariant interactions for Φ_i fields.

As mentioned before, SUSY can make light scalars natural and hence may play a role in the real world to address the SM Higgs Hierarchy Problem. However, for naturalness, this generically requires SUSY to be restored above $\sim$ TeV energy scales. There have been innumerable collider searches for TeV-scale SUSY so far, but unfortunately with null results to date. The exploration, however, still continues both on the theoretical and experimental side.

1.4 Outline of the thesis

The slow-roll scalar inflaton needs to have a nearly flat potential, which gives rise to its hierarchy problem, known as the "η problem" (see e.g. [36]), analogous to that of the SM Higgs. The simplest of natural models addressing this via a pseudo-Nambu Goldstone

boson (pNGB) nature of inflaton [37], however, require the scale of spontaneous breaking of the corresponding global symmetry to be above $M_{\rm Pl}$. This is in conflict with the arguments that fundamental global symmetries are ill-defined in the context of Quantum Gravity [38, 39, 40]. Also, in these models, inflaton needs to traverse super-Planckian distances in the field space, which offers the potential danger of poorly controlled $\phi/M_{\rm Pl}$ expansion in the effective potential. These issues, however, can be addressed with a sub-Planckian multi-axion structure, giving rise to an effective super-Planckian light field trajectory [41]. These 4D axions can arise via accidental (and not fundamental) global symmetries in the IR, originating from extra-dimensional gauge theories in the UV [42, 43, 44], thus satisfying the Quantum Gravity constraints mentioned above. (We review this in more detail in Chap. 2.) Furthermore, if SUSY plays a role in addressing the Higgs Hierarchy Problem, the above-mentioned well-motivated construction of axionic inflation has to be compatible with an approximate SUSY vacuum. In Chap. 2, which is based upon [1], we develop such a SUSY bi-axion model coupled to supergravity (SUGRA), with the axionic structure protected by extra-dimensional gauge symmetries. We also study the possible observable signals from this model which come naturally in the form of primordial non-Gaussianties and periodic modulations in the CMB.

The high-scale models of inflation have been tightly constrained by CMB observations [5], primarily via the non-observation of primordial gravitational waves. This motivates one to study mechanisms generating inflation at lower scales, which might also be motivated from various particle physics scenarios (see e.g. [45, 46, 47, 48, 49, 50]). However, realizing low-scale inflation via simple single-field models is typically fine-tuned. The general structure of Hybrid Inflation [51] is a well-motivated mechanism for

this, where a "waterfall" field ends inflation via its tachyonic transition. However, this waterfall mechanism gives rise to the inflaton hierarchy problem. In Chap. 3, which is based upon [2], we construct a natural, EFT-controlled and viable model of low-scale hybrid inflation, based on a discrete twin symmetry. Such symmetries were first used in the Twin Higgs mechanism [52] to address the little hierarchy problem of the SM Higgs.

As mentioned earlier, the collider searches for TeV-scale SUSY, highly motivated due to its possible role in addressing the Higgs Hierarchy Problem, have all returned with null results so far (see e.g. [14]). However, the SUSY extensions of SM may possibly give rise to novel but so-far hidden signatures at colliders. A prime example of this is the class of Long-Lived Particle (LLP) signatures (e.g. [53, 54, 55, 56, 57, 58]). Furthermore, such LLPs are generic features of a variety of BSM scenarios (e.g. [52, 59, 60, 61, 62, 63, 64, 65, 66, 67, 68, 69, 70, 71, 72, 73, 74, 75, 76, 77, 78, 79, 80, 81, 82, 83]), and not just SUSY, thus making their search highly motivated. Indeed there has been a rich LLP search program at the current and upcoming colliders (see e.g. [78, 83, 84, 85]), both hadronic and leptonic. In Chap. 4, which is based upon [3], we explore the unique capability of the future proposed electron-proton (ep) colliders in this regard. The proposed ep colliders, like LHeC [6, 86, 87] and FCC-eh [88], form an interesting hybrid of hadronic and leptonic colliders. They have higher center-of-mass energies and luminosities than the leptonic colliders, while also having a much cleaner environment as compared to the hadronic ones, with low pile-up and hadronic background. We demonstrate that LLPs with soft decay products and very short lifetimes, which are inaccessible at hadronic and leptonic colliders, can be probed at ep colliders, thus offering a complementary reach into the corresponding BSM parameter space.

Chapter 2: Supersymmetric Inflation From The Fifth Dimension

2.1 Introduction

Cosmic Inflation provides an attractive framework for understanding the robustness of the early state of our universe (see [4] for a review). Its simplest implementation driven by a slowly rolling scalar field (inflaton) requires a very flat inflaton potential, suggesting that the inflaton is a pseudo-Goldstone boson of a spontaneously broken global symmetry. A small explicit breaking of the symmetry can then give rise to a weak potential naturally varying on the scale of the spontaneous breaking, f. A canonical example is given by the model of "Natural Inflation" [37], with periodic inflaton potential,

$$V(\phi) = V_0 \left(1 - \cos \frac{\phi}{f}\right). \tag{2.1}$$

However, even a crude fit to the Cosmic Microwave Background (CMB) data [89] requires $f \gtrsim M_{\rm Pl}$[1], which conflicts with our general expectation that there should be no dynamical scales above the Planck scale, and with the particular arguments that global symmetries themselves are ill-defined in the context of Quantum Gravity [38, 39, 40].

These concerns can be resolved by (a) relating but not identifying the scale over

[1] This is an example of the model-independent Lyth bound [27] in the case of Natural Inflation model.

which the inflaton potential varies with the scale of spontaneous symmetry breaking, and (b) realizing the spontaneously broken approximate symmetries as accidental symmetries in the IR rather than fundamental global symmetries in the UV. The simplest version of (a) is given by beginning with two pseudo-Goldstone bosons, ϕ_A and ϕ_B, for two global symmetries $U(1)_A \times U(1)_B$ spontaneously broken at approximately the same scale $f_A, f_B \approx f \ll M_{\rm Pl}$ [41]. For suitable explicit symmetry breaking sources one can then generate a potential of the form

$$V(\phi_A, \phi_B) = V_0^{(1)} \left(1 - \cos \frac{\phi_B}{f_B}\right) + V_0^{(2)} \left[1 - \cos \left(\frac{\phi_A}{f_A} + N \frac{\phi_B}{f_B}\right)\right], \tag{2.2}$$

where N represents a large charge under $U(1)_B$ for one of the "spurions" characterizing the explicit breaking. Naively, this makes the problem worse, since the potential varies in the ϕ_A direction on the scale $f \ll M_{\rm Pl}$, and in the ϕ_B direction on the scale $f/N \ll f$, while CMB data suggests a potential varying more slowly than the Planck scale. However, just such a potential can arise when we properly consider the mass eigenstates. Taking for simplicity $V_0^{(1),(2)} \approx V_0$, these are given by heavy and light directions in field space,

$$\phi_h \equiv \phi_B + \frac{1}{N}\phi_A, \ \phi_l \equiv \phi_A - \frac{1}{N}\phi_B. \tag{2.3}$$

After setting the heavy ϕ_h to its vacuum expectation value (VEV), we can obtain the effective potential for the light field ϕ_l as

$$V_{\rm eff}(\phi_l)\big|_{\langle\phi_h\rangle \approx 0} \approx V_0 \left(1 - \cos \frac{\phi_l}{Nf}\right). \tag{2.4}$$

This corresponds to an effective Natural Inflation model, with inflaton ϕ_l and an emergent scale of potential variation $f_{\rm eff} = Nf$, which can be $> M_{\rm Pl}$ even though $f < M_{\rm Pl}$, for sufficiently large spurious charge N. We will refer to this as the "Bi-axion inflation" model.

An attractive microscopic realization of Bi-axion inflation satisfying (b), based on the mechanism of "extranatural inflation" [42], is provided by using gauge symmetry in an extra dimension [43]. If the higher-dimensional spacetime is highly warped so as to have an $\mathrm{AdS}_5/\mathrm{CFT}_4$ type holographic purely-4D dual description, then the dual interpretation is that the axions are composite Goldstone bosons of some strong dynamics (see e.g. [90]), analogous to the pions of QCD, and the spontaneously broken symmetries are accidental or emergent symmetries below the Planck scale. Here, we just briefly summarize the unwarped (or mildly warped) higher-dimensional case. The 4D axions above are realized as gauge-invariant Wilson-loops (or lines, given suitable boundary conditions) around (or across) the compact extra dimension,

$$\phi_A \equiv \int_0^L A_5 \, dx_5 \ , \ \phi_B \equiv \int_0^L B_5 \, dx_5 . \tag{2.5}$$

Charged matter propagating in the 5D bulk, H_1 and H_2, with mass m, can generate the potential (2.2) for ϕ_A and ϕ_B, given that they are charged under the two gauge groups as $(0,1)$ and $(1,N)$, respectively. The scales f_A, f_B emerge as

$$f_A = \frac{1}{g_A L}, \ f_B = \frac{1}{g_B L}. \tag{2.6}$$

The potential in (2.2) can be generated minimally by the loop contributions of H_1, H_2 via the "Hosotani mechanism" [91] which gives

$$V_0^{\text{loop}} \sim \frac{e^{-mL}}{L^4}, \tag{2.7}$$

in (2.4), as well as "higher harmonics" accompanied by higher powers of e^{-mL}. As studied in [44], bi-axion extranatural inflation can also non-trivially satisfy the plausible constraints of the Weak Gravity Conjecture (WGC) [92]. These quantum gravity constraints are an even stronger form of the arguments forbidding fundamental global symmetries, to also forbid UV gauge symmetries with very weak gauge couplings (relative to gravitational strength). These higher dimensional realizations of bi-axion inflation can be generalized to multiple-axion models, which then allow for more modest values of charge, N [43, 44].

In this chapter, we study compatibility of the bi-axion inflation scenario arising from higher dimensional gauge theory with the scenario of ∼TeV-scale supersymmetry (SUSY) for resolving the electroweak hierarchy problem. In the presence of SUSY, the loop contributions from the charged matter fields to the effective potential of 4D axions cancel out. We are hence forced to have tree-level contributions for the same, which can be achieved if H_1, H_2 have non-zero VEVs (v, v') at both the boundaries, which generates

$$V_0^{\text{tree}} \sim e^{-mL} m v v'. \tag{2.8}$$

Obviously, the question of whether the above-mentioned very plausible and robust forms

of inflation are naturally realizable within the constraints of supergravity (SUGRA) dynamics in the UV, with SUSY being present at $\sim$ collider energies today, is of considerable importance to our picture of fundamental physics and the prospects for experiments and observations. See [93, 94, 95, 96, 97, 98, 99] for other discussions of bi-axion inflation combined with SUSY, where the axions have alternative UV realizations. See [100, 101, 102, 103, 104, 105, 106] for other attempts to reconcile low energy SUSY and inflation from a UV perspective. We will also explore the possible new signatures from extra fields in the axion supermultiplets, most notably in the form of primordial non-Gaussianities (NG) in the cosmological collider physics program [107, 108, 109, 110, 111, 112, 113, 114, 115, 116, 117] as well as periodic modulations in the CMB [44, 118, 119, 120, 121, 122, 123, 124, 125, 126].

Models of single-field inflation with relatively simple potentials, such as Natural Inflation and its variants, necessarily operate at high scales in order to satisfy cosmological data, with inflationary Hubble scale $H_{\rm inf} \sim 10^{13} - 10^{14}$ GeV. The recently released Planck 2018 data places tight constraints on such high-scale models, especially given the non-observation of CMB B-modes induced by super-horizon gravitational waves [5]. Natural Inflation itself is now disfavored at 95% confidence level, but not ruled out. However, the bi-axionic structure of inflation from extra-dimensional gauge symmetry can generically produce multiple periodic terms in the potential (2.1), which can alleviate the tension above with a suitable and plausibly not very fine-tuned choice of parameters. We leave such a detailed analysis and appraisal for a future study. Furthermore, there are various ways discussed in the existing literature to relax these constraints for axion-based inflation, e.g. by realizing the structure of hybrid inflation from a bi-axion potential [127].

This chapter is organized as follows. In Section 2.2, we review a SUGRA-based inflation model, the "Kallosh-Linde-Rube model" [128, 129], which has many common features with our SUSY bi-axion model as developed in Sections 2.3 and 2.4. In Section 2.3, starting from the 5D SUSY gauge structure, we first construct a 4D effective theory of an axion supermultiplet. After generalizing it to the case of two axions, we account for (effective) 4D SUGRA couplings below the compactification scale. In Section 2.4, we discuss the inflationary trajectory along the lightest direction in the field space with an effective super-Planckian field range and periodic potential, also stabilized along all the other heavier directions. We then describe the picture of SUSY breaking (~~SUSY~~) during inflation which we find to be caused mostly by the heavy sector and not the inflaton sector. Furthermore, we also account for the post-inflationary ~~SUSY~~ vacuum that we occupy today, which we find not affecting the inflationary dynamics significantly as long as the ~~SUSY~~ scale is much below the inflationary energy scale. This model presents an interesting interplay of fine-tunings in the electroweak (EW) sector, cosmological constant (CC), and superpotential which are connected together after incorporating the ~~SUSY~~ today. The superpotential fine-tuning favors ~~SUSY~~ at high-scale, however the net fine-tuning, dominated by the EW and CC fine-tunings, can be shown to favor ~~SUSY~~ at low-scale i.e. somewhat above the EW scale. In Section 2.5, we discuss observable signals in the form of primordial NG and periodic modulations in the CMB. The "sinflaton", the real scalar partner of inflaton, can have $\mathcal{O}(H_{\rm inf})$ mass during inflation and sufficiently strong coupling to the inflaton to mediate primordial NG of observable strength in future experiments. A boundary-localized gauge singlet, in the presence of a shift-symmetric Kähler coupling, can also mediate sizeable primordial NG. Charged mat-

ter much heavier than the compactification scale, even only modestly below the 5D gauge theory cut-off, can contribute to periodic modulations in the CMB, within the sensitivity of ongoing searches. We conclude in Section 2.6.

We use units with the reduced Planck mass $M_{\rm Pl} = 1$ everywhere in this chapter, except Sections 2.4.4 and 2.5, where we explicitly write factors of $M_{\rm Pl}$ in order to get a better sense of the numbers.

2.2 The Kallosh-Linde-Rube model

We seek a locally supersymmetric description of high-scale inflation in which SUSY is only broken somewhat above the weak scale today. Since the weak scale is $\ll H_{\rm inf}$, we can first consider the supersymmetric limit of the ground state today. On the other hand, during inflation we know that the approximate de Sitter geometry is incompatible with SUSY. So inflation must be a spontaneous breaking (super-Higgsing) of SUSY within an excitation on top of today's SUSY vacuum, which we can also approximate to have zero vacuum energy (cosmological constant).

In order to have a light inflaton (ϕ), we will have an inflaton supermultiplet (Φ) with approximate shift symmetry. This can be implemented with $K(\Phi, \bar{\Phi}) = K(\Phi + \bar{\Phi})$ and $\phi = \mathrm{Im}(\Phi)$. A small explicit breaking of the shift symmetry from the superpotential can generate slow-roll potential for ϕ. Thus, the lightness of inflaton can be explained by its pseudo-Goldstone boson nature. However, implementing inflation with only this single supermultiplet is challenging [130]. In this case, the Goldstino of spontaneous ~~SUSY~~ during inflation would have to be the inflatino (then "eaten" by the gravitino). Consider

$K = \frac{1}{2}\left(\Phi + \bar{\Phi}\right)^2$ and $W = f(\Phi)$. Then, restricting to polynomial $f(\Phi)$ for illustration, in SUGRA, $V(\phi) \approx f'^2(\phi/\sqrt{2}) - 3f^2(\phi/\sqrt{2})$, which has a clear instability.[2] This can be avoided by introducing a separate supermultiplet for the Goldstino during inflation.

We see that the Goldstino multiplet must be part of a sector that Higgses SUSY *during* inflation. One of the simplest models to describe spontaneous ~~SUSY~~ coupled to SUGRA, is the Polonyi model [134]:

$$K = \bar{S}S - \lambda\left(\bar{S}S\right)^2, \; W = \mu S, \tag{2.9}$$

with the addition of the non-minimal Kähler coupling λ. The SUSY order parameter in the vacuum is $D_S W\big|_{\langle S\rangle \approx 0} \approx \mu \neq 0$. Spontaneous ~~SUSY~~ in this model gives rise to a massless Goldstino which however is eaten by the gravitino which then becomes massive ("super-Higgs mechanism"). The quartic term in the Kähler potential also makes the scalar heavy, with $m_S^2 \approx 4\lambda\mu^2$. Thus, there is no light particle in this sector. During inflation, in the limit of the slow-roll approximation i.e. for a fixed value of inflaton, the physics can be approximately described by this model. But we need to have a coupling between this sector (S) and the inflaton (Φ) such that there is no ~~SUSY~~ at $\Phi = 0$ (i.e. at the vacuum today) but with ~~SUSY~~ at $\Phi = \Phi_0 \neq 0$ (i.e. during inflation). In other words, the μ parameter of (2.9) needs to be made Φ-dependent in a suitable manner. This can be achieved with the following model [128, 129]:

$$K = \frac{1}{2}\left(\Phi + \bar{\Phi}\right)^2 + \bar{S}S - \lambda\left(\bar{S}S\right)^2, \; W = Sf(\Phi), \tag{2.10}$$

[2] However, see [131, 132, 133] for attempts towards building "sGoldstino inflation" model.

which we will refer to as the "Kallosh-Linde-Rube (KLR) model" and consider as a toy model for our SUSY bi-axion model. All scalars except for $\phi = \text{Im}(\Phi)$ can be shown to be heavy and thus the inflationary potential (see Appendix A for SUGRA scalar potential) can be obtained as,

$$\begin{aligned} V(\phi)\big|_{\langle S\rangle,\langle\eta\rangle} &= f^2(\phi/\sqrt{2}), \\ V_{\text{inf}} = 3H_{\text{inf}}^2 &= f^2(\phi_0/\sqrt{2}). \end{aligned} \tag{2.11}$$

The SUSY order parameters for Φ and S during inflation can be evaluated as follows:

$$D_\Phi W\big|_{\text{inf}} \approx 0\ ,\ D_S W\big|_{\text{inf}} \approx f(\Phi_0) \neq 0. \tag{2.12}$$

This implies that, as expected, ~~SUSY~~ during inflation is caused by the heavy sector (S). Hence the Goldstino during inflation (further eaten by the gravitino) is equal to the fermion from the S-sector (ψ_S) and not the inflatino (ψ_Φ).

The real scalar partner of the inflaton i.e. sinflaton $(\eta = \text{Re}(\Phi))$, has the following mass coming from its coupling to the SUSY-breaking curvature from (2.10):

$$m_\eta \approx \sqrt{6} H_{\text{inf}}. \tag{2.13}$$

This is within the favorable range of masses for observing it in primordial NG in the cosmological collider physics program. However, such a light sinflaton (i.e. $m_\eta \sim \mathcal{O}(H_{\text{inf}})$) is not guaranteed from this class of models. Indeed, a higher order term in the Kähler

potential with a direct coupling between S and Φ, respecting the shift symmetry of ϕ,

$$K \ni -\frac{c}{\Lambda^2}\left(\Phi+\bar{\Phi}\right)^2 \bar{S}S, \tag{2.14}$$

can give a large contribution to the sinflaton mass:

$$m_\eta^2 \approx 2V_{\text{inf}} + c\frac{V_{\text{inf}}}{\Lambda^2} \approx 6H_{\text{inf}}^2\left(1+\frac{c}{2\Lambda^2}\right). \tag{2.15}$$

Thus, $m_\eta \sim \mathcal{O}(H_{\text{inf}})$ for $\Lambda \approx \mathcal{O}(1)M_{\text{Pl}}$. But, $m_\eta \gg H_{\text{inf}}$ is also possible with $\Lambda \ll M_{\text{Pl}}$.

Even assuming $m_\eta \sim \mathcal{O}(H_{\text{inf}})$, in order for η to mediate observable primordial NG, there has to be sufficiently strong coupling between it and the inflaton (ϕ). The SUGRA scalar potential from (2.10) does have such couplings, but these are shift-symmetry violating and hence very small, e.g. $\mathcal{L} \ni m_\phi^2\eta^2\phi^2 \sim 10^{-10}\eta^2\phi^2$. However, higher order shift-symmetric terms in Kähler potential,

$$K \ni \frac{c'}{\Lambda^2}\left(\Phi+\bar{\Phi}\right)^4, \tag{2.16}$$

can generate derivative-interactions as

$$\mathcal{L} \ni \frac{c'}{\Lambda^2}(\partial\phi)^2\eta^2. \tag{2.17}$$

This sinflaton-inflaton interaction (with a non-zero VEV for η) along with $m_\eta \sim \mathcal{O}(H_{\text{inf}})$ can give rise to observable NG for sufficiently small Λ and large $\langle\eta\rangle$. However, in this chapter, we will not pursue the phenomenology of this model further.

The main drawback of this construction is that the origin of such a form of Lagrangian (2.10) is not explained within the model. Also, it suffers from the issue of trans-Planckian field displacement needed for ϕ, since a typical choice of $f(\Phi)$ in (2.10) gives a large-field inflation model subject to the Lyth bound [27].

2.3 SUSY bi-axion model

In this section, we develop the setup of supersymmetric inflation with the pseudo-Goldstone boson (or axion) nature of inflaton derived from a gauge symmetry in a compact extra dimension ("extranatural inflation" [42]). Firstly, we describe how we obtain the effective theory of a light axion supermultiplet starting from the $\mathcal{N} = 1$ 5D SUSY gauge theory. Then, we describe how to introduce two such axion supermultiplets in order to get $f_{\rm eff} > M_{\rm Pl}$ (for trans-Planckian field displacement satisfying the WGC). Finally, we also discuss how to take into account gravity, thus constructing our "SUSY bi-axion model".

As we will see later, this model has many common features with the KLR model described in Section 2.2. It however provides a more UV-complete and robust picture of inflationary dynamics where the central features are governed by the 5D SUSY gauge theory structure.

2.3.1 Light axion supermultiplet from 5D SUSY gauge theory

In this sub-section, we will show how a single light axion supermultiplet can emerge from 5D SUSY gauge theory. The extension to the more realistic case of two axion super-

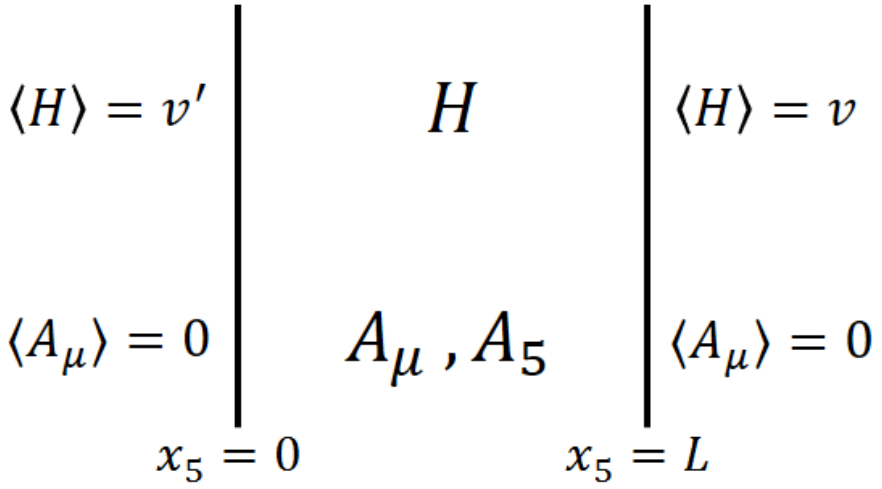

Figure 2.1: 5D gauge field and charged matter: non-SUSY version. See text and Table 2.1 for details.

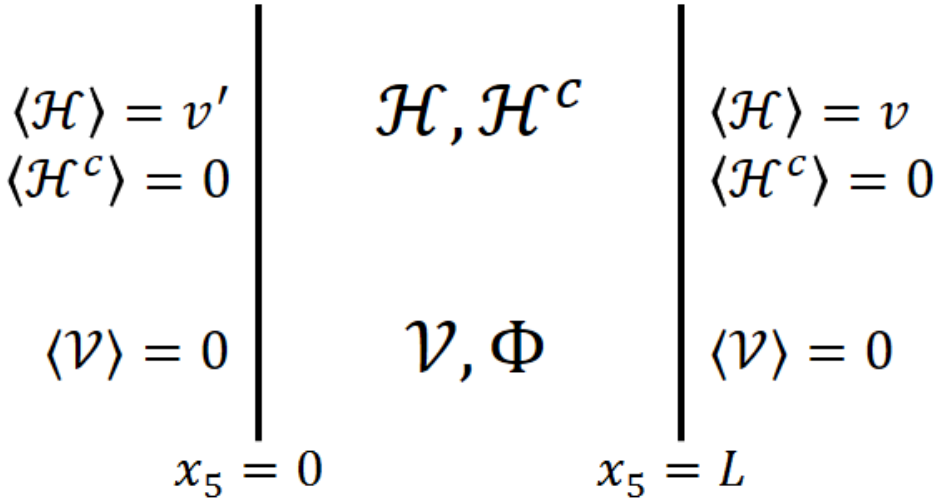

Figure 2.2: 5D gauge field and charged matter: SUSY version. See text and Table 2.1 for details.

multiplets follows in the next sub-section. Consider a flat extra dimension with boundaries, with a gauge field A_M and a charged scalar field H propagating in the bulk (see Figure 2.1). If A_μ and A_5 have, respectively, Dirichlet and Neumann boundary conditions at both the boundaries, then only A_5 has a zero-mode $\left(A_5^{(0)}\right)$. As mentioned in Section 2.1, if H has non-zero VEVs at both the boundaries, then it gives a tree-level

5D super-multiplet	5D fields	$\mathcal{N}=1$ 4D superfields
Gauge multiplet	$A_M, \chi_{\text{Dirac}}, \eta_{\text{real}}$	Vector superfields: $\mathcal{V}(x_5) \ni A_\mu(x_5), \chi_1(x_5)$ Chiral superfields: $\Phi(x_5) \ni \eta(x_5) + iA_5(x_5), \chi_2(x_5)$
Hypermultiplet	$H, H^c, \psi_{\text{Dirac}}$	Chiral superfields: $\mathcal{H}(x_5) \ni H(x_5), \psi(x_5)$ $\mathcal{H}^c(x_5) \ni H^c(x_5), \psi^c(x_5)$

Table 2.1: $\mathcal{N}=1$ 5D SUSY in the $\mathcal{N}=1$ 4D SUSY language

contribution to the effective potential of $A_5^{(0)}$.

Now, consider the full 5D supersymmetric version of this setup (see Figure 2.2). $\mathcal{N}=1$ 5D SUSY is equivalent to $\mathcal{N}=2$ 4D SUSY which can be written in the $\mathcal{N}=1$ 4D SUSY language as follows [135] (see Table 2.1). 5D SUSY gauge multiplet has a gauge field (A_M), Dirac gaugino (χ_{Dirac}) and a real scalar (η). These can be represented in $\mathcal{N}=1$ 4D SUSY language in terms of vector superfields $\mathcal{V}(x_5) \ni A_\mu(x_5), \chi_1(x_5)$ and chiral superfields $\Phi(x_5) \ni \eta(x_5) + iA_5(x_5), \chi_2(x_5)$, where the extra-dimensional coordinate x_5 is viewed as a mere continuous "label" from the $\mathcal{N}=1$ 4D viewpoint. Charged matter fields in 5D SUSY are part of a hypermultiplet which includes two complex scalars which are conjugates of each other under the respective gauge group (H, H^c) and a Dirac fermion (ψ_{Dirac}). These can be represented in $\mathcal{N}=1$ 4D SUSY language in terms of chiral superfields with conjugate representations: $\mathcal{H}(x_5) \ni H(x_5), \psi(x_5); \mathcal{H}^c(x_5) \ni H^c(x_5), \psi^c(x_5)$, again with the continuous "label" x_5.

As illustrated in [135], imposing 4D SUSY and 5D Poincare symmetry automatically generates an emergent 5D SUSY. Thus, the full 5D Lorentz-invariant, gauge-invariant and SUSY action for a gauge multiplet and a charged hypermultiplet, keeping manifest

only the $\mathcal{N}=1$ 4D SUSY, can be written as follows:

$$\mathcal{S}_5 = \int d^4x \int_0^L dx_5 \left[\int d^2\theta \, \frac{1}{4}\mathcal{W}_\alpha^2 + h.c. + \int d^4\theta \, \left\{ \partial_5 \mathcal{V} - \frac{1}{\sqrt{2}}(\Phi + \bar{\Phi}) \right\}^2 \right.$$
$$\left. + \int d^4\theta \, \left(\mathcal{H}^c e^{g_5 \mathcal{V}} \bar{\mathcal{H}}^c + \bar{\mathcal{H}} e^{-g_5 \mathcal{V}} \mathcal{H} \right) + \int d^2\theta \, \left\{ \mathcal{H}^c \left(m + \partial_5 - \frac{g_5}{\sqrt{2}}\Phi \right) \mathcal{H} \right\} + h.c. \right]. \tag{2.18}$$

As mentioned in Section 2.1, in the presence of SUSY, we need tree-level contributions from charged matter to the effective potential of A_5, which can be achieved by the charged matter taking non-zero VEVs at the boundaries. Such VEVs break gauge invariance, but this is allowed because we have already broken gauge invariance by the Dirichlet boundary conditions for the boundary components of the gauge fields. These VEVs can be achieved by adding the following boundary-localized superpotential terms to the action:

$$\delta\mathcal{S}_5 = \int d^4x \int_0^L dx_5 \left[\int d^2\theta \left\{ \lambda(\mathcal{H} - v)^2 \, \delta(x_5) + \lambda'(\mathcal{H} - v')^2 \, \delta(x_5 - L) \right\} + h.c. \right]. \tag{2.19}$$

Consider Dirichlet boundary conditions for $\mathcal{V}$ and $\mathcal{H}^c$ and Neumann boundary conditions for Φ and $\mathcal{H}$, at both the boundaries. We implement these boundary conditions via realizing the extra dimension with an interval as an "orbifold" of the circle. With the angular coordinate (θ) on the circle going from $-\pi$ to π, we identify the points θ with $-\theta$. Thus, half of the circumference of the extra-dimensional circle is the physical interval with x_5 going from 0 to $\pi R \equiv L$, where R is the radius of the circle. The Dirichlet and Neumann boundary conditions for the fields in an interval can be implemented by assigning, respectively, odd and even parity under orbifold $(\theta \to -\theta)$. (See [136] for a

review of this.)

Let us solve for the classical potential of this model. We need to integrate out the heavy fields (i.e. $\mathcal{H}, \mathcal{H}^c$ and the KK modes in $\mathcal{V}$) at tree-level to get an effective theory in terms of Φ. We search for a supersymmetric vacuum of the full theory where inflation happens at an excited state with ~~SUSY~~ vacuum energy V_{inf}. Considering the inflationary energy scale to be much less than the masses of the heavy fields $\left(V_{\text{inf}}^{1/4} \ll m_{KK}, m\right)$ [3], to the leading order in $\frac{V_{\text{inf}}^{1/4}}{m_{KK}}$, for the purpose of the dynamics of the heavy fields, their ground state can be approximated to be supersymmetric even during inflation. Thus, we can integrate them out by using their SUSY equations of motion.

Firstly, we can set $\mathcal{V}$ to zero since it contains only heavy fields and with zero VEVs. A_μ in $\mathcal{V}$ cannot have non-zero VEV due to Lorentz invariance. The D-scalar in $\mathcal{V}$ is an order parameter for SUSY and hence $\langle D \rangle = 0$ for SUSY ground state. Of course the fermions in $\mathcal{V}$ have vanishing VEVs. This leaves us with only the following terms in the action:

$$\mathcal{S}_5 = \int d^4x \int_0^L dx_5 \left[\int d^4\theta \left\{ \frac{1}{2}(\Phi + \bar{\Phi})^2 + \bar{\mathcal{H}}^c \mathcal{H}^c + \bar{\mathcal{H}} \mathcal{H} \right\} \right.$$
$$\left. + \int d^2\theta \left\{ \mathcal{H}^c \left(m + \partial_5 - \frac{g_5}{\sqrt{2}} \Phi \right) \mathcal{H} + \lambda (\mathcal{H} - v)^2 \, \delta(x_5) + \lambda' (\mathcal{H} - v')^2 \, \delta(x_5 - L) \right\} + h.c. \right]. \tag{2.20}$$

The heavy charged matter fields $\mathcal{H}$ and $\mathcal{H}^c$, with 5D bulk masses $m \gtrsim m_{KK}$, can now be

[3] As can be seen in Section 2.4.1, $\frac{V_{\text{inf}}^{1/4}}{m_{KK}} \sim \frac{vL}{\sqrt{f}} e^{-mL} \sim \frac{1}{\sqrt{g}} e^{-mL} v L^{3/2}$ which is small due to the smallness of e^{-mL} and the hypermultiplet boundary VEVs $\sim v$.

integrated out by imposing the following SUSY constraints:

$$\frac{\partial W}{\partial \mathcal{H}} = 0 = \frac{\partial W}{\partial \mathcal{H}^c}. \tag{2.21}$$

Thus, we obtain the following 4D effective action[4] for Φ,

$$\begin{aligned}\mathcal{S}_4 = \int d^4x \Bigg[& \int d^4\theta \, \frac{1}{2}(\Phi + \bar{\Phi})^2 \\ & + \int d^2\theta \left(W_0 + \lambda \frac{v^2 \, e^{-mL} \, e^{\frac{gL}{\sqrt{2}}\Phi} + v'^2 \, e^{mL} \, e^{-\frac{gL}{\sqrt{2}}\Phi} - 2vv'}{e^{mL} \, e^{-\frac{gL}{\sqrt{2}}\Phi} + e^{-mL} \, e^{\frac{gL}{\sqrt{2}}\Phi}} + h.c. \right) \Bigg],\end{aligned} \tag{2.22}$$

where we take $\lambda = \lambda'$ for technical simplicity. The derivatives on $\mathcal{H}$ and $\mathcal{H}^c$ at the boundaries in (2.20) are evaluated by taking into account their orbifold parity (even and odd, respectively).

The Kähler potential in (2.22) displays shift symmetry for A_5, which is the imaginary part of the scalar component of Φ. However, integrating out the charged hypermultiplet using (2.21) also generates shift symmetry violating terms in the Kähler potential. These corrections are however functions of $gL\Phi$ and suppressed by e^{-mL}, our modest expansion parameter. Thus, they contribute to the scalar potential only with $\frac{\Phi}{f}$-dependence $\left(f \equiv \frac{1}{gL}\right)$, not changing its qualitative form. Furthermore, the e^{-mL} suppression makes these corrections sub-dominant and hence we neglect them here.

The superpotential is the source of shift symmetry breaking for A_5 which is naturally suppressed by e^{-mL} for $mL \gtrsim 1$ (see e.g. for $v \sim v'$). This is a generic feature of extranatural inflation scenario where the compact extra dimension effectively acts as a

[4]Here, all the 4D fields are in canonical normalization. The 4D gauge coupling g is defined as: $\frac{1}{g^2} = \frac{L}{g_5^2}$.

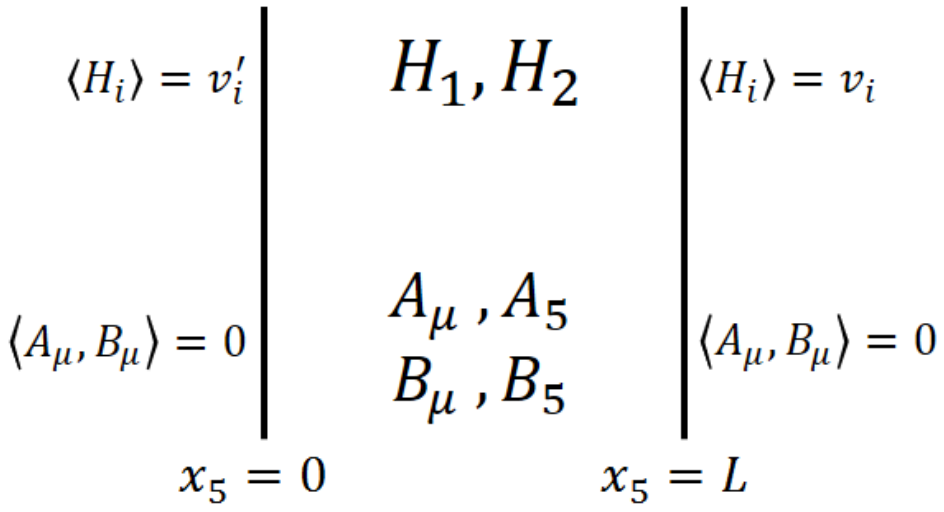

Figure 2.3: Bi-axion inflation field content: non-SUSY version. See text for details.

"filter" for any far-UV physics by suppressing its contribution by $e^{-M_{UV}L}$. W_0 is a constant term in the superpotential which is relevant only in the presence of gravity, as we will see in Section 2.3.3.

2.3.2 Bi-axion generalization to realize $f_{\text{eff}} > M_{\text{Pl}}$

As mentioned in Section 2.1, in order to have $f_{\text{eff}} > M_{\text{Pl}}$, we need to introduce two axions in such a way that one of their linear combinations has an effective super-Planckian field range. The non-SUSY version of bi-axion inflation has the setup as shown in Figure 2.3. There are two gauge fields (A_M, B_M) with only (A_5, B_5) having zero modes (by suitably assigning boundary conditions). The scalar fields H_1 and H_2 are charged under the gauge groups as $(0, 1)$ and $(1, N)$, respectively. This field content can now be embedded into the respective 5D SUSY multiplets, as shown in Figure 2.4. By extending the construction from Section 2.3.1, the full 5D action in this case can be

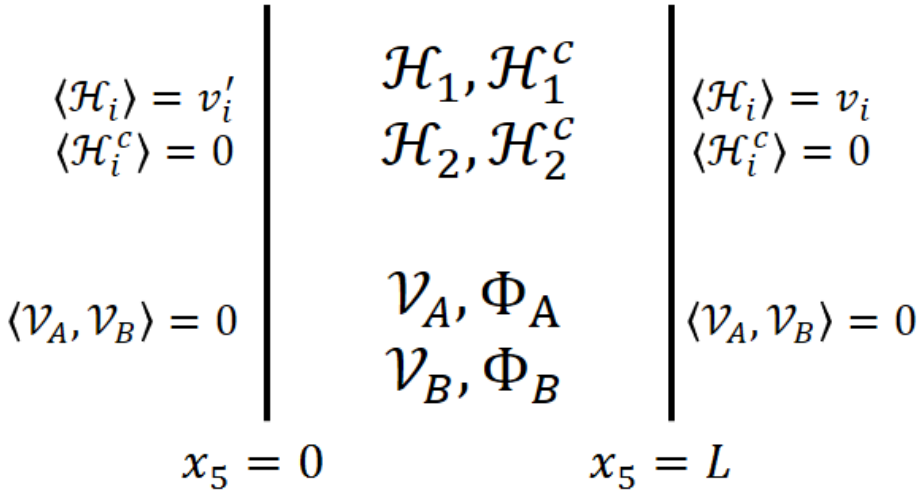

Figure 2.4: Bi-axion inflation field content: SUSY version. See text for details.

obtained as follows:

$$
\begin{aligned}
\mathcal{S}_5 = & \int d^4x \int_0^L dx_5 \left[\int d^2\theta \left(\frac{1}{4}\mathcal{W}_{A,\alpha}^2 + \frac{1}{4}\mathcal{W}_{B,\alpha}^2 \right) + h.c. \right. \\
& + \int d^4\theta \left\{ \partial_5 \mathcal{V}_A - \frac{1}{\sqrt{2}}(\Phi_A + \bar{\Phi}_A) \right\}^2 + \left\{ \partial_5 \mathcal{V}_B - \frac{1}{\sqrt{2}}(\Phi_B + \bar{\Phi}_B) \right\}^2 \\
& + \int d^4\theta \left\{ \left(\mathcal{H}_1^c e^{g_5 \mathcal{V}_B} \bar{\mathcal{H}}_1^c + \bar{\mathcal{H}}_1 e^{-g_5 \mathcal{V}_B} \mathcal{H}_1 \right) + \left(\mathcal{H}_2^c e^{g_5 (\mathcal{V}_A + N\mathcal{V}_B)} \bar{\mathcal{H}}_2^c + \bar{\mathcal{H}}_2 e^{-g_5 (\mathcal{V}_A + N\mathcal{V}_B)} \mathcal{H}_2 \right) \right\} \\
& + \int d^2\theta \left\{ \mathcal{H}_1^c \left(m + \partial_5 - \frac{g_5}{\sqrt{2}} \Phi_B \right) \mathcal{H}_1 + \mathcal{H}_2^c \left(m + \partial_5 - \frac{g_5}{\sqrt{2}} (\Phi_A + N\Phi_B) \right) \mathcal{H}_2 \right\} + h.c. \\
& + \int d^2\theta \left\{ \lambda_1 (\mathcal{H}_1 - v_1)^2 \, \delta(x_5) + \lambda_1' (\mathcal{H}_1 - v_1')^2 \, \delta(x_5 - L) \right\} + h.c. \\
& \left. + \int d^2\theta \left\{ \lambda_2 (\mathcal{H}_2 - v_2)^2 \, \delta(x_5) + \lambda_2' (\mathcal{H}_2 - v_2')^2 \, \delta(x_5 - L) \right\} + h.c. \right] .
\end{aligned}
\tag{2.23}
$$

Similarly to how (2.22) was obtained starting from (2.18) and (2.19) in the previous section, we can obtain the 4D effective Kähler potential and superpotential for the two

axion supermultiplets (Φ_A, Φ_B) as follows:

$$
\begin{aligned}
K &= \frac{1}{2}(\Phi_A + \bar{\Phi}_A)^2 + \frac{1}{2}(\Phi_B + \bar{\Phi}_B)^2, \\
W &= W_0 + \lambda_1 \frac{v_1^2\, e^{-mL}\, e^{\frac{gL}{\sqrt{2}}(\Phi_A + N\Phi_B)} + v_1'^2\, e^{mL}\, e^{-\frac{gL}{\sqrt{2}}(\Phi_A + N\Phi_B)} - 2v_1 v_1'}{e^{mL}\, e^{-\frac{gL}{\sqrt{2}}(\Phi_A + N\Phi_B)} + e^{-mL}\, e^{\frac{gL}{\sqrt{2}}(\Phi_A + N\Phi_B)}} \\
&\quad + \lambda_2 \frac{v_2^2\, e^{-mL}\, e^{\frac{gL}{\sqrt{2}}\Phi_B} + v_2'^2\, e^{mL}\, e^{-\frac{gL}{\sqrt{2}}\Phi_B} - 2v_2 v_2'}{e^{mL}\, e^{-\frac{gL}{\sqrt{2}}\Phi_B} + e^{-mL}\, e^{\frac{gL}{\sqrt{2}}\Phi_B}}.
\end{aligned}
\tag{2.24}
$$

We would like to highlight here that in (2.23), and hence also in (2.24), all the scales and field ranges are sub-Planckian.

2.3.3 Adding SUGRA and identifying the SUSY vacuum

We have not considered the effects of gravity so far in obtaining the $\mathcal{L}_{4,\text{eff}}(\Phi_A, \Phi_B)$ of (2.24). But now we can use this 4D effective K and W to compute the SUGRA scalar potential (V_{SUGRA}) directly in 4D (see Appendix A). With this strategy, from effective field theory perspective, we could only be missing M_{Pl}-suppressed terms e.g. $K \ni (\Phi_A + \bar{\Phi}_A)^4, (\Phi_B + \bar{\Phi}_B)^4$. In the case of SUSY bi-axion model, as highlighted below (2.24), the range (and hence also the VEVs) of fields in Φ_A and Φ_B is sub-Planckian, thus making the above-mentioned M_{Pl}-suppressed terms also sub-dominant. We would like to highlight here that in the case of a single axion (in Section 2.3.1), such M_{Pl}-suppressed terms in (2.22) are *not* sub-dominant due to the super-Planckian range of the fields. Hence the truncation of the Φ/M_{Pl} expansion is uncontrolled in this case. In Section 2.5, we will see that higher order Kähler interactions can have interesting observable effects if they are stronger than M_{Pl}-suppressed.

The W_0 parameter in (2.24) is now physical, due to the presence of gravity, and it

will contribute to the vacuum energy. We will consider a boundary-localized contribution to W_0 such that the net post-inflationary vacuum energy is (approximately) zero.

In order for the inflationary picture to be compatible with low energy SUSY (broken only at a scale somewhat above the EW scale) and approximately zero cosmological constant as observed today, the vacuum of post-inflationary dynamics should be SUSY-preserving and with zero vacuum energy. Thus, it seems that the inflation endpoint has to (approximately) satisfy the following three conditions: (1) unbroken SUSY ($\langle D_{\Phi_i} W \rangle = 0$), (2) zero vacuum energy ($\langle W \rangle = 0$), and (3) local minimum[5] of V_{SUGRA}. However, as shown below, (1) and (2) automatically imply (3), i.e. a point in the field space satisfying $D_{\Phi_i} W = 0$ and $W = 0$ implies that it is automatically at a local minimum of V_{SUGRA}, so we do not bother to check (3) further.

Consider, for simplicity, a single chiral superfield Φ for which V_{SUGRA} is

$$V = e^K \left(K^{-1}_{\Phi\bar{\Phi}} \ |D_\Phi W|^2 - 3 \, |W|^2 \right). \tag{2.25}$$

Now, for $D_\Phi W = 0$ and $W = 0$, one can clearly see that,

$$\partial_\Phi V = 0 = \partial_{\bar{\Phi}} V, \ \partial_{\bar{\Phi}} \partial_\Phi V = e^K K^{-1}_{\Phi\bar{\Phi}} \ |\partial_\Phi D_\Phi W|^2 \, , \ \partial^2_\Phi V = 0 = \partial^2_{\bar{\Phi}} V, \tag{2.26}$$

and for $\Phi = (\eta + i\phi)/\sqrt{2}$,

$$\partial_\eta V = 0 = \partial_\phi V, \ \partial^2_\eta V = \partial^2_\phi V = \frac{1}{2} e^K K^{-1}_{\Phi\bar{\Phi}} \ |\partial_\Phi D_\Phi W|^2 \, . \tag{2.27}$$

[5]Global minimum can be separated enough in the field space from this local minimum such that the decay via tunneling does not happen even on the cosmological timescales.

Thus, for $K^{-1}_{\bar{\Phi}\Phi} \geq 0$ and $K_{\bar{\Phi}\Phi\Phi}, K_{\bar{\Phi}\Phi\bar{\Phi}\Phi}$ finite, (2.27) implies a local minimum of V_{SUGRA}. The same proof can be applied for multiple chiral superfields Φ_i, with $K^{-1}_{\Phi_i\bar{\Phi}_i} \geq 0$ in the mass basis and no singularities in higher derivatives of K. These conditions are satisfied in our cases of interest, since we mostly have $K^{-1}_{\Phi_i\bar{\Phi}_i} \approx 1$ (see (2.24)) with corrections suppressed by high scales Λ and small field VEVs (see Section 2.5.1).

Furthermore, the conditions $D_{\Phi_i}W = 0$ and $W = 0$ are equivalent to the conditions

$$\partial_{\Phi_i}W = 0 \ , \ W = 0, \tag{2.28}$$

since $D_{\Phi_i}W = \partial_{\Phi_i}W + (\partial_{\Phi_i}K)\,W$. This hugely simplifies identifying the inflation end-point analytically. The conditions $\partial_{\Phi_A}W = 0 = \partial_{\Phi_B}W$ can be satisfied for the super-potential in (2.24) minimally by the following choice for the parameters[6] that govern the hypermultiplet VEVs at the boundaries (see (2.23)) :

$$v_1 = v_1' = v_2 \equiv v, v_2' \sim ve^{-mL}. \tag{2.29}$$

In order to avoid having significant fine-tuning for choosing $v_2' \sim ve^{-mL}$, we consider $e^{-mL} \sim \mathcal{O}(1)$, while still having $e^{-mL} < 1$ for valid perturbative expansion (e.g. $e^{-mL} \approx 1/3$ with $mL \approx 1.1$). With the choice of parameters v_i, v_i' as in (2.29), and after doing a change of basis from (Φ_A, Φ_B) to (Φ_h, Φ_l) as defined by

$$\Phi_h \equiv \Phi_B + \frac{1}{N}\Phi_A \ , \ \Phi_l \equiv \Phi_A - \frac{1}{N}\Phi_B, \tag{2.30}$$

[6]The simplest choice with $v_1 = v_1' = v_2 = v_2'$ does not admit a solution to $\partial_{\Phi_A}W = 0 = \partial_{\Phi_B}W$ when restricted to sub-Planckian field values.

the superpotential from (2.24) becomes

$$\begin{aligned}\frac{W}{v^2} = \frac{W_0}{v^2} + \lambda_1 \left[1 - \frac{1}{\cosh\left(mL - \frac{gL}{\sqrt{2}} N\Phi_h\right)}\right] \\ - 2\lambda_2\, e^{-2mL}\, e^{\frac{gL}{\sqrt{2}}\left(\Phi_h - \frac{\Phi_l}{N}\right)} \left[1 - \cosh\left(\frac{gL}{\sqrt{2}}\left(\Phi_h - \frac{\Phi_l}{N}\right)\right)\right] + \mathcal{O}\left(e^{-4mL}\right).\end{aligned} \tag{2.31}$$

Now, we can identify the required Minkowski SUSY endpoint of inflation. Firstly, we identify VEVs of all the scalars, $\Phi_k = \frac{1}{\sqrt{2}}(\eta_k + i\phi_k)$, at inflation end by solving $\partial_{\Phi_k} W = 0$ to obtain

$$\langle \phi_l \rangle = 0 = \langle \phi_h \rangle \,,\ \langle \eta_h \rangle \approx \frac{fmL}{N} \,,\ \langle \eta_l \rangle \approx fmL, \tag{2.32}$$

with $f \equiv \frac{2}{gL}$. Then, plugging these VEVs back into (2.31), we can enforce $\langle W \rangle = 0$. This self-consistently demands W_0 to be chosen to cancel the terms in (2.31) sub-dominant in e^{-mL}, i.e.

$$W_0 \sim v^2 \cdot \mathcal{O}\left(e^{-4mL}\right), \tag{2.33}$$

where, as mentioned below (2.29), e^{-mL} is our modest expansion parameter.

One can clearly see from (2.31) that $W \approx W\left(N\Phi_h, \Phi_l/N\right)$, for $N \gg 1$, and hence the scalar potential will be of the form

$$V \approx V\left(\frac{N\eta_h}{f}, \frac{N\phi_h}{f}, \eta_l, \frac{\phi_l}{Nf}\right). \tag{2.34}$$

Due to the e^K contribution from V_{SUGRA}, and that $K \ni \frac{1}{2}\left(\Phi_l + \bar{\Phi}_l\right)^2$ has η_l- but no ϕ_l-dependence, the potential along η_l varies over M_{Pl}, and not $Nf > M_{\text{Pl}}$. As we will

detail in Sec. 2.4.1, from (2.34) we can power-count $m_{\eta_h}, m_{\phi_h} \sim H_{\rm inf} \cdot \mathcal{O}\left(\frac{N^2}{f}\right) \gg H_{\rm inf}$ and $m_{\eta_l} \sim \mathcal{O}(H_{\rm inf})$, while only $m_{\phi_l} \ll H_{\rm inf}$. We will show in the Sec. 2.4.1 that after integrating out the heavy fields (η_h, ϕ_h, η_l), we get $V_{\rm eff}\left(\frac{\phi_l}{Nf}\right)$ such that ϕ_l has an effective super-Planckian field range: $f_{\rm eff} = Nf > M_{\rm Pl}$ with $f < M_{\rm Pl}$ and $N \gg 1$. Thus, we expect that the SUSY vacuum $\phi_l = 0$ can be approached from some $\phi_l^{\rm initial} \sim \mathcal{O}(Nf)$ along a slow-roll potential with the slow-roll parameters $\epsilon, \eta \sim \left(\frac{M_{\rm Pl}}{Nf}\right)^2 \ll 1$.

As in the case of single axion supermultiplet (see below (2.22)), integrating out the charged hypermultiplets in (2.23) also generates shift symmetry violating terms in the Kähler potential in (2.24). Similar to the case of single axion supermultiplet, these corrections are functions of $\frac{\Phi_l}{f_{\rm eff}}$ which maintain the form of the effective inflationary potential, $V_{\rm eff}\left(\frac{\phi_l}{f_{\rm eff}}\right)$, i.e. effective super-Planckian field range for ϕ_l. Furthermore, they are suppressed by powers of e^{-mL}, our modest expansion parameter, which makes them sub-dominant and hence we neglect them here.

2.4 Inflationary history

In this section, we describe various aspects of the inflationary history from our SUSY bi-axion model. Here we discuss the inflationary trajectory, SUSY breaking during inflation, accounting for the SUSY breaking vacuum that we occupy today, and the interplay of different fine-tunings within this model.

2.4.1 Inflationary trajectory

In order to identify the inflationary trajectory and the effective potential along it, we first consider the general problem where a potential depends on some heavy fields $\vec{H}$ and some light fields $\vec{L}$. We expand the potential to quadratic order in $\vec{H}$ while keeping it to all orders in $\vec{L}$:

$$V\left(\vec{H},\vec{L}\right) = V\left(\langle\vec{H}\rangle,\vec{L}\right) + A_i\left(\vec{L}\right)\cdot\delta H_i + \frac{1}{2}m_{ij}^2\left(\vec{L}\right)\cdot\delta H_i\cdot\delta H_j + \mathcal{O}(\delta H^3). \quad (2.35)$$

Here, $\langle\vec{H}\rangle$ are VEVs of the heavy fields at the post-inflationary SUSY vacuum, while $\delta\vec{H}$ are the fluctuations away from $\langle\vec{H}\rangle$ in the course of inflation. The expansion coefficients are

$$A_i\left(\vec{L}\right) \equiv \partial_{H_i}V\left(\langle\vec{H}\rangle,\vec{L}\right)\ ,\ m_{ij}^2\left(\vec{L}\right) \equiv \partial_{H_i}\partial_{H_j}V\left(\langle\vec{H}\rangle,\vec{L}\right), \quad (2.36)$$

which are functions of $\vec{L}$. We can now integrate out the heavy fields by extremizing (2.35) with respect to the heavy fluctuations $\delta\vec{H}$, for given light fields $\vec{L}$, thereby getting an effective potential for $\vec{L}$ as

$$V_{\text{eff}}\left(\vec{L}\right) \approx V\left(\langle\vec{H}\rangle,\vec{L}\right) + \frac{1}{2}\left[A_i\left(m^2\right)_{ij}^{-1}A_j\right]\left(\vec{L}\right). \quad (2.37)$$

In the case of our SUSY bi-axion inflation model, the heavy and light fields along the inflationary trajectory are, respectively,

$$\vec{H} = (\eta_h,\phi_h,\eta_l)\ ,\ \vec{L} = (\phi_l). \quad (2.38)$$

The coefficients A_i and mass matrix m_{ij}^2 in V_{SUGRA} (A.2), for the superpotential (2.31), scale parametrically as follows:

$$\begin{aligned} A_i\left(\vec{L}\right) &\sim \left(N^2, N^2, \frac{1}{N}\right) \frac{V\left(\langle\vec{H}\rangle, \vec{L}\right)}{f}, \\ m_{ij}^2\left(\vec{L}\right) &\sim \begin{pmatrix} N^4 & N^2 & N \\ N^2 & N^4 & 0 \\ N & 0 & f^2 \end{pmatrix} \frac{V\left(\langle\vec{H}\rangle, \vec{L}\right)}{f^2}, \end{aligned} \tag{2.39}$$

where the indices i, j run over $\vec{H}$ in the same order as in (2.38). We can now estimate the parametric size of the heavy fluctuations during inflation as

$$\left\langle \delta\vec{H} \right\rangle \sim \left(\frac{f}{N^2}, \frac{f}{N^2}, \frac{1}{Nf}\right). \tag{2.40}$$

This then implies that the $\mathcal{O}(\delta H^3)$ term that we dropped in (2.35) is sub-dominant, suppressed by the small parameters $\frac{1}{N}$ and $\frac{1}{Nf}$, and hence can be ignored along the inflationary trajectory.

The mass eigenvalues of the heavy fluctuations $\delta\vec{H}$ are as follows:

$$\begin{aligned} m_{1,2}^2 \approx m_{\eta_h,\phi_h}^2 &\sim N^4 \frac{V\left(\langle\vec{H}\rangle, \langle\vec{L}\rangle\right)}{f^2} \sim \frac{N^4}{f^2} H_{\text{inf}}^2, \\ m_3^2 \approx m_{\eta_l}^2 &\sim V\left(\langle\vec{H}\rangle, \vec{L}\right) \sim H_{\text{inf}}^2\left(\vec{L}\right). \end{aligned} \tag{2.41}$$

Thus, the heavy mass-squared eigenvalues are all positive and much larger than $m_{\phi_l}^2 \sim \frac{V\left(\langle\vec{H}\rangle, \vec{L}\right)}{N^2 f^2}$. Hence, we can integrate out the heavy fluctuations $\delta\vec{H}$ all along the inflationary

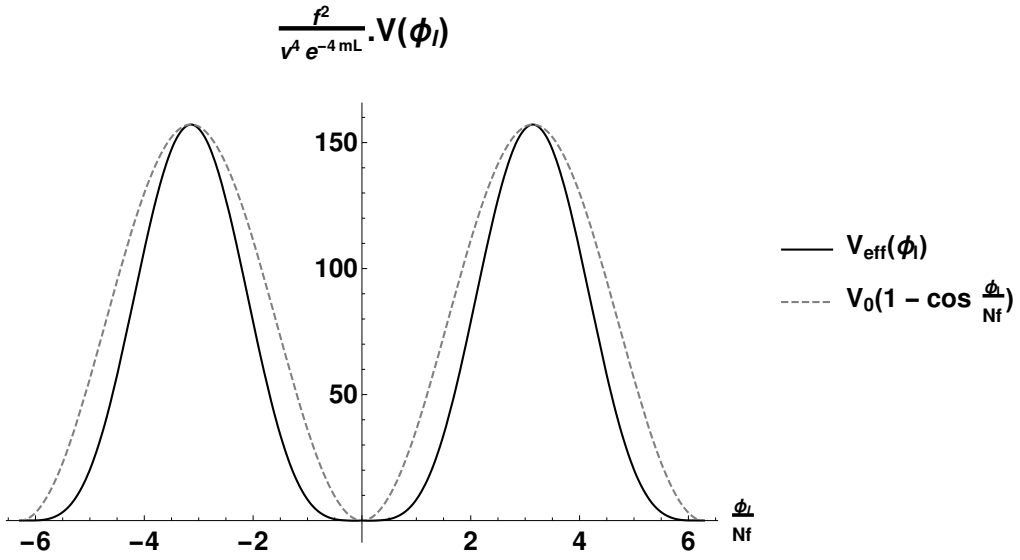

Figure 2.5: The dark line refers to the effective inflationary potential $V_{\text{eff}}(\phi_l)$ after numerically integrating out the heavy fields η_h, ϕ_h, η_l all along the inflationary trajectory. For comparison, a pure cosine potential with the magnitude matching to that of $V_{\text{eff}}(\phi_l)$ is plotted as the dashed line. Inflation can start close to the hilltop of $V_{\text{eff}}(\phi_l)$, with $V_{\text{inf}} \sim \frac{v^4 e^{-4mL}}{f^2}$.

trajectory yielding

$$V_{\text{eff}}\left(\phi_l\right) \approx V\left(\langle\vec{H}\rangle, \frac{\phi_l}{Nf}\right) \cdot \left[1 + \mathcal{O}(1) + \mathcal{O}\left(\frac{1}{N^2 f^2}\right)\right]. \tag{2.42}$$

Here, the second term comes from integrating out the mass eigenstates $(H_1, H_2) \approx (\eta_h, \phi_h)$ while the third term comes from integrating out $H_3 \approx \eta_l$. Since the contribution from (H_1, H_2) is of the same order as $V\left(\langle\vec{H}\rangle, \frac{\phi_l}{Nf}\right)$, we perform the integration out of $\delta\vec{H}$ numerically. Firstly, we verify that as suggested by the parametric estimates in (2.39) and (2.41), the heavy mass-squared eigenvalues are indeed much larger than $m_{\phi_l}^2$ all along the inflationary trajectory. The numerically computed $V_{\text{eff}}(\phi_l)$ is as shown in Fig. 2.5. It has the following approximate analytic form,

$$V_{\text{eff}}(\phi_l) \sim H_{\text{inf}}^2 \left(1 - \cos\frac{\phi_l}{Nf}\right) \ , \ H_{\text{inf}} \sim \lambda_2 \frac{v^2}{f}\, e^{-2mL}, \tag{2.43}$$

which is the leading contribution in terms of the small parameters $1/N$, f and e^{-mL}. Thus, the SUSY bi-axion model effectively provides an approximate Natural Inflation model with $f_{\text{eff}} = Nf > M_{\text{Pl}}$, where the best-fit values are [5]

$$f_{\text{eff}} = Nf \sim 10 M_{\text{Pl}} \ , \ V_{\text{inf}}^{1/4} \sim 10^{16} GeV. \tag{2.44}$$

The precise inflationary potential, $V_{\text{eff}}(\phi_l)$, does contain "higher harmonics" in $\frac{\phi_l}{Nf}$. Although, these do not affect the qualitative features as outlined above, they can play an important role in precision fitting to the CMB data which we will explore in a future work.

As can be seen from (2.41), the heavy fields η_h, ϕ_h are much heavier than H_{inf}:

$$m_{\eta_h}, m_{\phi_h} \sim H_{\text{inf}} \frac{N^2}{f}. \tag{2.45}$$

While sinflaton (η_l), the real scalar partner of the inflaton, has an intermediate mass,

$$m_{\eta_l} \sim \mathcal{O}(H_{\text{inf}}), \tag{2.46}$$

about which we will discuss more in Section 2.5.1.1.

2.4.2 SUSY breaking during inflation

As mentioned earlier in Section 2.2, the approximate de Sitter geometry during inflation requires it to be an excited state with spontaneous ~~SUSY~~ on top of the post-inflationary SUSY vacuum. The SUSY order parameters (see Appendix A) for Φ_h and Φ_l evaluated along the inflationary trajectory are

$$\begin{aligned} D_{\Phi_h} W\big|_{\langle\Phi_h\rangle,\langle\eta_l\rangle} &\sim \lambda_2 \frac{v^2}{f} e^{-2mL}\, e^{-i\frac{\phi_l}{Nf}} \left(1 - \cos\frac{\phi_l}{Nf}\right), \\ D_{\Phi_l} W\big|_{\langle\Phi_h\rangle,\langle\eta_l\rangle} &\sim \mathcal{O}\left(\frac{1}{N}\right) \cdot D_{\Phi_h} W\big|_{\langle\Phi_h\rangle,\langle\eta_l\rangle}. \end{aligned} \tag{2.47}$$

Here, we can clearly see that the SUSY order parameters are zero only at the vacuum (i.e. $\phi_l = 0$).

As described in Appendix A, the massless Goldstino of spontaneous ~~SUSY~~, which is "eaten" by gravitino to become massive, is given by the linear combination of all the fermions weighted by the respective SUSY order parameters: $\psi_{\text{Goldstino}} \propto \langle D_{\Phi_i} W\rangle \cdot \psi_i$. Hence, the SUSY order parameters during inflation (2.47) imply that,

$$\psi_{\text{Goldstino}} \sim \psi_h + \mathcal{O}\left(\frac{1}{N}\right) \cdot \psi_l, \tag{2.48}$$

i.e. the Goldstino during inflation belongs mostly to the heavy sector (Φ_h) and not to the inflaton sector (Φ_l). In other words, ~~SUSY~~ during inflation is caused mostly by the heavy sector (Φ_h). This feature of our SUSY bi-axion model is very similar to the KLR model discussed in Section 2.2 where the Goldstino during inflation belongs solely to the heavy sector (S) (see (2.12)).

2.4.3 SUSY breaking after inflation

We need to account for the post-inflationary ~~SUSY~~ vacuum that we occupy today which we have neglected so far. In this section, we look for any possibly significant effects of this ~~SUSY~~ vacuum on the inflationary dynamics. We consider a boundary-localized Polonyi-type sector with

$$\delta K_4 = \bar{X}X - \frac{(\bar{X}X)^2}{\Lambda^2}\ ,\ \delta W_4 = \Lambda_{\text{~~SUSY~~}}^2 X, \tag{2.49}$$

which undergoes spontaneous ~~SUSY~~ at a scale $\sim \Lambda_{\text{~~SUSY~~}}$. Consider the ~~SUSY~~ from this hidden sector to be minimally communicated to the Standard Model via M_{Pl} suppressed interactions which then implies an intermediate scale ~~SUSY~~ $\Lambda_{\text{~~SUSY~~}} \sim \sqrt{v_{\text{weak}} \cdot M_{\text{Pl}}} \sim 10^{11} GeV$. We expect that as long as $\Lambda_{\text{~~SUSY~~}} \ll H_{\text{inf}}$ or even $V_{\text{inf}}^{1/4}$, the effect of this ~~SUSY~~ X-sector on the inflationary dynamics will be negligible. (See also e.g. [137].) We show below that indeed this expectation is borne out here.

The scalar field X in the Polonyi sector gets $\mathcal{O}(H_{\text{inf}})$ mass during inflation, similar to that of η_l. Thus, X can be added to the "heavy" fields $\vec{H}$ of (2.38) and essentially the same procedure as described in Sec. 2.4.1 can be repeated to integrate them out along the inflationary trajectory. The tadpole and mass matrix terms (see (2.36)) involving X field scale as follows:

$$\begin{aligned} &A_X(\phi_l) \sim \Lambda_{\text{~~SUSY~~}}^2 H_{\text{inf}}(\phi_l) \cdot f\ ,\ m_{XX}^2(\phi_l) \sim H_{\text{inf}}^2(\phi_l), \\ &m_{\eta_h X}^2(\phi_l) \sim m_{\phi_h X}^2(\phi_l) \sim \Lambda_{\text{~~SUSY~~}}^2 H_{\text{inf}}(\phi_l) \cdot N\ ,\ m_{\eta_l X}^2(\phi_l) \sim \Lambda_{\text{~~SUSY~~}}^2 H_{\text{inf}}(\phi_l) \frac{1}{N}. \end{aligned} \tag{2.50}$$

The fluctuations of X during inflation can be estimated from (2.50) as

$$\delta X \sim \frac{\Lambda^2_{\cancel{\text{SUSY}}} f}{V^{1/2}_{\text{inf}}(\phi_l)}. \tag{2.51}$$

The $\mathcal{O}(\delta H^3)$ terms in (2.35) involving X are hence sub-dominant, suppressed by $\frac{\Lambda_{\cancel{\text{SUSY}}}}{V^{1/4}_{\text{inf}}}$. We can now integrate out X following (2.37) yielding

$$\delta V_{\text{eff}}(\phi_l) \sim \Lambda^4_{\cancel{\text{SUSY}}} \cdot f^2 \cdot \left[1 + \frac{1}{N^2} \frac{\Lambda^4_{\cancel{\text{SUSY}}}}{V_{\text{eff}}(\phi_l)}\right] \tag{2.52}$$

This $\delta V_{\text{eff}}(\phi_l)$ is much smaller than the $V_{\text{eff}}(\phi_l)$ of (2.42). Thus, as expected, for $\Lambda_{\cancel{\text{SUSY}}} \sim 10^{11} GeV$ and $V^{1/4}_{\text{inf}} \sim 10^{16} GeV$ (see (2.44)) satisfying $\Lambda_{\cancel{\text{SUSY}}} \ll V^{1/4}_{\text{inf}}$, the $\cancel{\text{SUSY}}$ X-sector gives a negligible contribution to $V_{\text{eff}}(\phi_l)$ and hence does not significantly affect the inflationary dynamics.

2.4.4 Interplay of electroweak, cosmological constant and superpotential tunings

In order to have (almost) vanishing vacuum energy after the end of inflation, as discussed in Section 2.3.3, we need to have $\langle W \rangle = 0$ which can be achieved by tuning the W_0 parameter in (2.24). We also need to account for the SUSY breaking vacuum that we occupy today. Here, we evaluate this combined fine-tuning which displays an interesting interplay with the electroweak (EW) and cosmological constant (CC) fine-tunings.

Consider the $\cancel{\text{SUSY}}$ hidden sector of Sec. 2.4.3 which minimally communicates to the Standard Model via gravity mediation (i.e. M_{Pl} suppressed interactions). In order for

it to address the electroweak hierarchy problem, this requires that $\frac{V_{\not{SUSY}}^{\text{today}}}{M_{\text{Pl}}^2} \sim v_{\text{weak}}^2$.[7] This implies the following fine-tuning in the EW sector,

$$T_{EW} \sim \frac{v_{\text{weak}}^2 M_{\text{Pl}}^2}{V_{\not{SUSY}}^{\text{today}}}, \tag{2.53}$$

which can be minimized with $\left(V_{\not{SUSY}}^{\text{today}}\right)^{1/4} \sim \sqrt{v_{\text{weak}} M_{\text{Pl}}}$, as is standard. This $\not{SUSY}$ sector and also $\Delta W_0 \neq 0$ in (2.24) give contributions to the CC today as below:

$$\text{CC} = -3\frac{\Delta W_0^2}{M_{\text{Pl}}^2} + V_{\not{SUSY}}^{\text{today}} \overset{\text{(obs.)}}{\sim} \text{meV}^4. \tag{2.54}$$

The two terms in the above equation have typical sizes of $\sim \frac{v^4}{M_{\text{Pl}}^2}$ (see (2.33)) and $\sim v_{\text{weak}}^2 M_{\text{Pl}}^2$, respectively, which consist of a priori different and unrelated scales. This implies that multiple contributions to ΔW_0, each of magnitude $\sim \frac{v^2}{M_{\text{Pl}}}$, must first cancel to within $\sqrt{V_{\not{SUSY}}^{\text{today}}}$. Hence, we have the following fine-tuning in the contributions to W_0:

$$T_{W_0} \sim \frac{\sqrt{V_{\not{SUSY}}^{\text{today}}} M_{\text{Pl}}}{v^2}. \tag{2.55}$$

Once the two terms on the right hand side of (2.54) are of the same order, they still have to cancel to give CC $\sim$ meV^4 as observed today. This amounts to having the following usual CC fine-tuning:

$$T_{CC} \sim \frac{\text{meV}^4}{V_{\not{SUSY}}^{\text{today}}}. \tag{2.56}$$

As can be seen from (2.53) and (2.56), the EW and CC fine-tunings favor $\not{SUSY}$ at

[7] $V_{\not{SUSY}}^{\text{today}} = \Lambda_{\not{SUSY}}^4$

low-scale. However, (2.55) shows that the W_0 fine-tuning displays preference for ~~SUSY~~ at high-scale! But, the net fine-tuning, assuming that these three are independent of each other, is

$$T_{\text{net}} = T_{EW} \times T_{W_0} \times T_{CC} \sim \frac{v_{\text{weak}}^2 M_{\text{Pl}}^3 \text{meV}^4}{v^2} \left(V_{\text{~~SUSY~~}}^{\text{today}}\right)^{-3/2}. \tag{2.57}$$

This shows a net preference for ~~SUSY~~ at low-scale, namely close to the EW scale.

Our considerations here are reminiscent of comparable tuning issues that arise in high-scale string-derived SUGRA theories, in particular the necessary existence of a high-scale W_0 which makes the tuning worse. See [138] for a review. For a sample choice of the parameters, $V_{\text{~~SUSY~~}}^{\text{today}} \sim v_{\text{weak}}^2 M_{\text{Pl}}^2$ and $v^2 \sim (0.1 M_{\text{Pl}})^3$, we see that the net tuning in (2.57) is considerable $(T_{net} \sim 10^{-100})$, predominantly because of the Cosmological Constant Problem. However, such a residual tuning is still acceptable in the context of the anthropic principle or some as yet unknown mechanism solving this problem. See [19, 20] for a review.

2.5 Observable signals

In this section we discuss the phenomenology of our SUSY bi-axion model. The observable signals from this model can come in the form of primordial non-Gaussianities mediated by heavy particles, sinflaton being the prime candidate for this. Also, "higher harmonic" terms in the inflaton potential can give rise to periodic modulations in the CMB.

2.5.1 Primordial non-Gaussianities

As first introduced in [107] and further illustrated in [108, 109, 110, 111, 112, 113, 114, 115, 116, 117], a particle X can mediate primordial non-Gaussianities of observable size if it (1) has $m_X \sim \mathcal{O}(H_{\text{inf}})$, (2) has sufficiently strong $X(\partial\phi)(\partial\phi)$ couplings, and (3) can give tree-level contribution to inflaton 3-point function which can come only from bosons.

2.5.1.1 Sinflaton

In the SUSY bi-axion model, mass of the sinflaton (η_l) during inflation is

$$m_{\eta_l} \approx \sqrt{6} H_{\text{inf}}, \tag{2.58}$$

which can be seen schematically from V_{SUGRA} as follows:

$$\begin{aligned} V_{\text{SUGRA}} &= e^K \left(|D_{\Phi_A} W|^2 + |D_{\Phi_B} W|^2 - 3 |W|^2 \right), \\ V(\eta_l) &\approx e^{\eta_l^2} V_{\text{inf}} \ni \eta_l^2 V_{\text{inf}} \approx 3 H_{\text{inf}}^2 \eta_l^2. \end{aligned} \tag{2.59}$$

This contribution to m_{η_l} comes from the coupling of η_l to the ~~SUSY~~ curvature during inflation which also shows up in the KLR model as described in Section 2.2 (see (2.13)). However, as in the case of the KLR model (see (2.15)), $m_{\eta_l} \sim \mathcal{O}(H_{\text{inf}})$ is not guaranteed in our SUSY bi-axion model too. A higher order term in Kähler potential of the form

$$K_5 \ni \delta(x_5) \frac{c_2}{\Lambda_2^2} (\Phi_A + \bar{\Phi}_A)^2 (\Phi_B + \bar{\Phi}_B)^2 \tag{2.60}$$

can give a contribution to the sinflaton mass as

$$m_{\eta_l}^2 \approx \frac{2V_{\rm inf}}{M_{\rm Pl}^2} + \frac{c_2 V_{\rm inf}}{\Lambda_2^2} = 6H_{\rm inf}^2\left(1 + \frac{c_2 M_{\rm Pl}^2}{2\Lambda_2^2}\right). \tag{2.61}$$

Thus, for $\frac{c_2}{\Lambda_2^2} \gg \frac{1}{M_{\rm Pl}^2}$, $m_{\eta_l} \gg H_{\rm inf}$ is possible.[8] The effective higher order coupling (2.60) between Φ_A and Φ_B can arise radiatively via the loops of hypermultiplet (H_2, H_2^c) which is charged under both the gauge groups as $(1, N)$. Naive dimensional analysis suggests that this loop contribution to (2.60) is

$$\left(\frac{c_2}{\Lambda_2^2}\right)_{\rm loop} \sim \frac{g^2 N^2}{16\pi^2}\frac{1}{m_{KK}^2}. \tag{2.62}$$

Considering $N \sim \mathcal{O}(100)$ and $m_{KK} \sim M_5 \sim 0.1 M_{\rm Pl}$ [9], we can have $\left(\frac{c_2}{\Lambda_2^2}\right)_{\rm loop} \lesssim \frac{1}{M_{\rm Pl}^2}$ with $g \lesssim 0.1$. Thus, with $g \lesssim 0.1$, the contribution from loop-induced term (2.60) to sinflaton mass is small, thus keeping $m_{\eta_l} \sim \mathcal{O}(H_{\rm inf})$, which is crucial to get observable NG mediated by it.

The references [139, 140] and [141] construct SUSY EFT of inflation with a minimal field content which does not include any scalar other than the inflaton, especially the sinflaton. This can be interpreted by the UV-completion of these EFTs having sinflaton with mass much greater than $H_{\rm inf}$. In our SUSY bi-axion model, as can be seen from (2.61), there exists a region of parameter space where $m_{\eta_l} \gg H_{\rm inf}$, which is consistent with the results of [139, 140, 141]. This parameter space corresponds to $\Lambda_2 \ll M_{\rm Pl}$ in

[8] One might worry that the sub-leading term (2.60) can have a dominant effect on the sinflaton mass and whether this signals breakdown of the EFT expansion. This is however not true. The sinflaton mass in (2.58) comes purely from $M_{\rm Pl}$-suppressed SUGRA contributions whereas the higher order Kähler term (2.60) gives a direct coupling with suppression scale (Λ_2) which can be below $M_{\rm Pl}$.

[9] $M_5 \sim M_{\rm Pl}\left(\frac{1}{M_{\rm Pl}L}\right)^{1/3}$ is the scale at which gravity becomes strong in 5D.

(2.61) or $g > 0.1$ in (2.62). This feature of having a region of parameter space allowing $m_{\text{sinflaton}} \gg H_{\text{inf}}$ is also present in the KLR model described in Section 2.2 (see (2.15)). However, in this case, the size of primordial NG suffers a severe exponential "Boltzmann-suppression" ($\sim e^{-\pi m_{\eta_l}/H_{\text{inf}}}$). Below, we focus on the region where $m_{\eta_l} \sim \mathcal{O}(H_{\text{inf}})$ which allows the sinflaton to be observable via primordial NG.

Even in the presence of $m_{\eta_l} \sim \mathcal{O}(H_{\text{inf}})$, η_l still needs to have sufficiently strong coupling with the inflaton to mediate NG of observable size. The V_{SUGRA} from (2.24) has the following coupling which violates the shift symmetry for ϕ_l and hence is very small:

$$V_{\text{SUGRA}} \ni 10^{-3} \frac{H_{\text{inf}}}{M_{\text{Pl}}} H_{\text{inf}} \eta_l \phi_l^2. \tag{2.63}$$

This coupling gives rise to the primordial NG of the following typical size [115, 117]:

$$f_{NL} \sim 10^{-2} \frac{H_{\text{inf}}}{M_{\text{Pl}}} \lesssim 10^{-6}. \tag{2.64}$$

This is much less than the sensitivity of the proposed experiments involving 21-cm cosmology, $f_{NL} \sim 10^{-2}$ [142, 143], or even from more futuristic surveys, $f_{NL} \sim 10^{-4}$ [144].

However, the following shift symmetry preserving, higher order, boundary-localized term in the Kähler potential,

$$K_5 \ni \delta(x_5) \frac{c_1}{\Lambda_1^2} (\Phi_A + \bar{\Phi}_A)^4, \tag{2.65}$$

can generate the following derivative coupling of sinflaton with inflaton:

$$\mathcal{L}_4 \ni \frac{c_1}{\Lambda_1^2}\eta_l^2 \left(\partial\phi_l\right)^2 . \tag{2.66}$$

The above coupling can give primordial NG of the size [115, 117]

$$f_{NL} \approx 0.03\, c_1^2\epsilon \left(\frac{M_{\rm Pl}}{\Lambda_1}\right)^4 \left(\frac{\langle\eta_l\rangle_{\rm inf}}{M_{\rm Pl}}\right)^2 \lesssim 10^{-6} \left(\frac{M_{\rm Pl}}{\Lambda_1}\right)^4 , \tag{2.67}$$

where the VEV of sinflaton during inflation is $\langle\eta_l\rangle_{\rm inf} \approx \frac{M_{\rm Pl}^2}{Nf} \approx 0.1 M_{\rm Pl}$, as can be calculated from $V_{\rm SUGRA}$ using (2.24). ϵ in the above expression is the slow roll parameter of inflation which is constrained to be $\lesssim 10^{-2}$ [5]. The suppression scale Λ_1 in (2.65), which would be the cutoff scale on the boundaries, has to be less than M_5. Considering $M_5 \sim \mathcal{O}(0.1) M_{\rm Pl}$, this implies that even for Λ_1 being very close to M_5, we can get $f_{NL} \sim \mathcal{O}(10^{-2})$. This signal can be observed at the proposed 21-cm experiments as described after (2.64). Furthermore, Λ_1 can be as low as the inflationary energy scale $V_{\rm inf}^{1/4} \lesssim 10^{-2} M_{\rm Pl}$, while maintaining EFT control, in which case $f_{NL} \sim \mathcal{O}(1)$ or even higher is also possible.

2.5.1.2 Boundary-localized gauge singlets

It is also possible to see boundary-localized fields via primordial NG. Consider, for example, a chiral superfield X localized at one of the boundaries and singlet under both the gauge groups A and B. If it has the following Kähler potential, i.e. a direct coupling

with Φ_A preserving its shift symmetry,

$$K_5 \ni \delta(x_5)\left[\frac{c_X}{\Lambda_X}(\Phi_A+\bar{\Phi}_A)^2(X+\bar{X})+\bar{X}X\right], \tag{2.68}$$

then it has the following derivative interaction between the real scalar part of X (η_X) and the inflaton:

$$\mathcal{L}_4 \ni \frac{c_X}{\Lambda_X}\eta_X\left(\partial\phi_l\right)^2. \tag{2.69}$$

Also, analogous to the case of sinflaton as in (2.59), mass of this gauge singlet during inflation is

$$m_X \approx \sqrt{3}H_{\text{inf}}. \tag{2.70}$$

(2.69) and (2.70) imply that the size of primordial NG mediated by η_X is as follows [115, 117]:

$$f_{NL} \approx 0.75\, c_X^2\epsilon\left(\frac{M_{\text{Pl}}}{\Lambda_X}\right)^2 \lesssim 10^{-2}\left(\frac{M_{\text{Pl}}}{\Lambda_X}\right)^2. \tag{2.71}$$

Similar to the case of Λ_1 as discussed below (2.67), $\Lambda_X \lesssim M_5 \sim 0.1M_{\text{Pl}}$ which can give $f_{NL} \gtrsim \mathcal{O}(1)$.

If the direct coupling in (2.68) is of the form $K_5 \ni \delta(x_5)\frac{c'_X}{\Lambda_X^2}(\Phi+\bar{\Phi})^2\bar{X}X$, then it gives the interaction $\mathcal{L}_4 \ni \frac{c'_X}{\Lambda_X^2}|X|^2\left(\partial\phi_l\right)^2$. In this case, the f_{NL} mediated by X has an additional suppression factor due to its VEV during inflation: $f_{NL} \sim c_X^2\epsilon\left(\frac{M_{\text{Pl}}}{\Lambda_X}\right)^2\left(\frac{\langle X\rangle}{\Lambda_X}\right)^2$. Hence, in order to get f_{NL} of an observable size, we need to have $\langle X\rangle$ during inflation to be sufficiently large as compared to Λ_X.

2.5.2 Periodic modulations in the CMB

Extra-dimensional realization of Natural Inflation gives the leading slowly varying inflaton potential with super-Planckian field range ($\sim f_{\text{eff}} = Nf > M_{\text{Pl}}$), while also generically giving sub-leading "higher harmonic" terms oscillating over a much shorter range ($\sim f, f/N \ll M_{\text{Pl}}$). Although these higher harmonics in $V(\phi_{\text{inf}})$ are suppressed by factors of e^{-ML}, they can still give observable effects in the form of primordial features with periodic modulations in the CMB power spectrum. These features, being motivated from various theoretical constructions, have been searched for in the Planck CMB data [44, 118, 119, 120, 121, 122, 123, 124, 125, 126].

In our SUSY bi-axion model, there exist such higher harmonics in $V(\phi_l)$ arising from within the model, but they are small. These can come from the sub-dominant terms in the superpotential (2.31), $\delta W = \delta W \left(e^{-mL} \cdot e^{\frac{gL}{\sqrt{2}N}\Phi_l}\right)$, suppressed by powers of e^{-mL}. This gives corrections to the inflaton potential of the form

$$\frac{\delta V}{V_{\text{inf}}} \sim e^{-2nmL} \cos\left(n\frac{\phi_l}{Nf}\right). \tag{2.72}$$

However, contributions to the periodic modulations in the CMB come only from the harmonics with $n \gg 1$ i.e. $n \sim \mathcal{O}(N)$. But, such $\cos\left(\mathcal{O}(N) \cdot \frac{\phi_L}{Nf}\right)$ terms in the potential are hugely suppressed by $\sim e^{-2mL\cdot\mathcal{O}(N)}$. Thus, the higher harmonics from within the SUSY bi-axion model cannot give rise to observable CMB periodic modulations.

But, let us now consider contribution from a generic heavy hypermultiplet beyond our minimal model $(\mathcal{H}_3, \mathcal{H}_3^c)$, with mass M and charges (n_A, n_B) under the gauge groups

A and B. This will give an additional term in the superpotential (2.31) as

$$\delta W \approx 2v^2 e^{-ML}\left[1 - e^{\frac{gL}{\sqrt{2}}(n_A\Phi_A + n_B\Phi_B)}\right], \tag{2.73}$$

where we have taken the parameters governing boundary VEVs of H_3, H_3^c to be equal: $v_3 = v_3' = v$. As expected, this is suppressed by e^{-ML} which is "filtered" out by the extra dimension for $M \gg 1/L$. However, as discussed below, the precision CMB observables can be sensitive to the contributions to periodic modulations sourced by such a hypermultiplet if it is not too heavy. The contribution to the inflaton potential from (2.73) is

$$\frac{\delta V}{V_{\rm inf}} \approx n_B e^{2mL} e^{-ML} \cos\left[(Nn_B - n_A)\frac{\phi_l}{Nf}\right]. \tag{2.74}$$

The observational constraint on the size of CMB periodic modulations is $\left|\frac{\delta V}{V_{\rm inf}}\right| \lesssim 10^{-5}$, also depending upon the higher harmonic frequency [125]. Considering $n_B \sim \mathcal{O}(N) \sim 100$ and $e^{-mL} \sim 1/3$, we can get $\left|\frac{\delta V}{V_{\rm inf}}\right| \sim 10^{-5}$ from $M \sim 20 \times \frac{1}{L}$. This shows sensitivity of CMB periodic modulations to the charged matter much heavier than the KK scale!

The 5D gauge theory being non-renormalizable has a cutoff which is given by $\Lambda_{5D} \sim \frac{c}{g^2}\frac{1}{L}$. As discussed below (2.62), we require $g \lesssim 0.1$ in order to have $m_{\eta_l} \sim \mathcal{O}(H_{\rm inf})$ for getting observable primordial NG mediated by sinflaton. Hence, for $g \lesssim 0.1$ and $c \sim \mathcal{O}(1)$, the cutoff is $\Lambda_{5D} \gtrsim 100 \times \frac{1}{L}$. Thus, charged matter beyond the minimal model with

$$M \lesssim \frac{1}{5}\Lambda_{5D} \tag{2.75}$$

can generate observable periodic modulations in the CMB power spectrum with $\left|\frac{\delta V}{V_{\rm inf}}\right| \sim$

10^{-5}. Of course, some such heavy states are expected near the cutoff of 5D gauge theory as part of a UV-completion of our non-renormalizable effective field theory.

2.6 Discussion

In the present work, we demonstrated the compatibility of low-energy SUSY (i.e. SUSY broken only at somewhat above the EW scale) with high-scale axionic inflation where the axionic nature of inflaton is derived from extra-dimensional gauge symmetry. The inflaton potential, in the presence of SUSY, can be generated at tree-level by charged matter in the 5D bulk with gauge symmetry breaking at the 5D boundaries. We also required that this robust gauge-theoretic origin for the inflaton satisfy the Weak Gravity Conjecture quantum gravity constraints, which are especially tight given the super-Planckian inflaton field range required by the data (Lyth bound). But we showed that this can be achieved by introducing two axion supermultiplets, containing a light inflaton direction having $f_{\text{eff}} > M_{\text{Pl}}$. The heavy sector, apart from stabilizing the inflationary trajectory, also contributes dominantly to SUSY breaking (~~SUSY~~) during inflation. The Goldstino of spontaneous ~~SUSY~~ during inflation lies mostly in this heavy sector.

Our SUSY bi-axion model displays an interesting interplay of electroweak (EW), cosmological constant (CC) and superpotential (W_0) fine-tunings after considering the ~~SUSY~~ vacuum we occupy today. The fine-tuning for EW and CC, as usual, prefer low-scale ~~SUSY~~. The W_0 fine-tuning, however, shows preference for high-scale ~~SUSY~~. We showed that the net fine-tuning is dominated by EW and CC fine-tunings and hence prefers low-scale ~~SUSY~~ i.e. somewhat above the EW scale.

The observable signals in our model can come in the form of primordial non-Gaussianities (NG) and periodic modulations in the CMB. The sinflaton can naturally have $\mathcal{O}(H_{\text{inf}})$ mass via its coupling to the ~~SUSY~~ curvature during inflation. It can also naturally have sufficiently strong couplings with inflaton such that it can be seen via primordial NG in future 21-cm experiments, with the measure of NG, f_{NL}, being $\gtrsim 10^{-2}$. The sinflaton mass can receive large contributions from higher order Kähler terms which, however, can be kept sub-dominant with small enough gauge coupling. Similarly, a boundary-localized gauge singlet can have $\mathcal{O}(H_{\text{inf}})$ mass during inflation and strong enough coupling with inflaton, via higher order Kähler couplings, thus allowing it to mediate large primordial NG with even $f_{NL} \gtrsim \mathcal{O}(1)$.

Although the extra dimension acts as a "filter" for the unknown UV-completion of our non-renormalizable model, with e^{-ML} suppression, the precision observables in the CMB can still probe modulating features imprinted by such heavy physics. We showed that charged matter, not far below the effective field theory cutoff of our model, can generate modulations in the inflationary potential, $\left|\frac{\delta V}{V_{\text{inf}}}\right| \sim 10^{-5}$, which lie within the sensitivity of ongoing searches [123, 125].

As mentioned in Section 2.1, the recent Planck 2018 CMB data [5] puts tight constraints on Natural Inflation. The bi-axionic inflation studied here, while very roughly giving a Natural Inflation potential, can have significant differences at precision level that can be used to better agree with the data, as exemplified in [127]. We hope to further explore SUSY axionic inflation models in the future for the best fit to the precision data.

Chapter 3: TwInflation: natural low-scale inflation via discrete symmetry

3.1 Introduction

As we discussed in the previous chapter, cosmic inflation can be implemented minimally by the slow rolling of a single real scalar field, the inflaton (ϕ), along its nearly flat potential ($V(\phi)$). But, this requires the inflaton to be significantly lighter than the Hubble scale, which gives rise to a hierarchy problem known as the "$\eta-$problem" (see e.g. [36]).

Furthermore, the observations so far [5] seem to rule out or strongly constrain some of the simplest forms of $V(\phi)$, originating from straightforward and natural microscopic models explaining the lightness of the inflaton. They typically predict a large tensor-to-scalar ratio, $r \gtrsim 0.01$, and hence a high scale of inflation. But, with the non-observation of primordial tensor fluctuations to date, the data seems to hint towards lower-scale inflation. The upcoming and near-future proposed experiments like BICEP Array [28], Simons Observatory [29], CMB-S4 [30], LiteBIRD [31], and PICO [32], will be able to measure $r \gtrsim 10^{-3}$, corresponding to $H \gtrsim 5 \times 10^{12}$ GeV. It is therefore interesting to reconsider the structure of inflationary dynamics, especially keeping the $\eta-$problem in mind, to see whether observable r is a robust prediction or whether extremely small r can be readily achieved.

Indeed, inflation may well take place at a much lower scale than above, i.e. with

$H \ll 10^{12}$ GeV, with unobservably small tensor fluctuation at these near-future experiments, although, realizing such low-scale inflation with a simple single-field model is typically fine-tuned. This fine-tuning can come in the form of the potential, the model parameters, and also the initial conditions (see e.g. [145, 146, 147, 148, 149]). On the other hand, multi-field inflation, i.e. with the field(s) orthogonal to inflaton playing an important dynamical role in (ending) inflation, can help in the model building for low-scale inflation. The classic example of this is Hybrid Inflation [51]. Here, the inflaton couples to a "waterfall" field (σ) in such a way that σ has a ϕ-dependent mass term. During inflation, the much heavier σ is fixed at 0, while ϕ performs the slow roll. As the inflaton rolls past a critical field value, σ becomes tachyonic and rapidly rolls down to the global minimum of the potential. This fast rolling along the "waterfall" on the inflationary trajectory ends inflation by releasing the vacuum energy in the σ field. Hybrid inflation exhibits a separation of roles with the space-time expansion during inflation dominantly driven by vacuum energy in σ, and the slow-roll "clock" provided by ϕ, which helps in realizing low-scale inflation as we will review in Sec. 3.2. This provides a mechanism generating an effective inflationary trajectory with an abrupt drop in vacuum energy, which is difficult to realize from a single-field perspective. However, as we will review in Sec. 3.2, hybrid inflation needs fine-tuning in the model parameters to achieve radiative stability and EFT control. We will address this issue in the present work and build an EFT-controlled and natural low-scale inflationary model.

The primary challenge offered by the hybrid inflation paradigm towards building a microscopic model is the following: ϕ needs to be a light real scalar, but with sufficiently strong non-derivative coupling with the heavy σ field as required for the waterfall effect.

Even if ϕ is modeled as a pseudo-Nambu Goldstone boson (pNGB) of a global symmetry, its coupling with σ explicitly breaks the symmetry and induces quadratic sensitivity in the effective inflationary potential to the ultra-violet (UV) physics. Hence, we need some extra ingredient to achieve naturalness in hybrid inflation. This issue is similar to the case of the light Higgs boson as required in the Standard Model (SM) in the presence of its Yukawa and gauge couplings. This, hence, motivates one to apply different particle physics mechanisms explored in the literature to address the hierarchy problem of the SM Higgs boson, to the case of hybrid inflation mentioned above. There are various supersymmetric constructions of hybrid inflation, see e.g. [150, 151, 152, 153, 154]. Little Inflaton [155, 156] is also one such proposal addressing the issue of naturalness in hybrid inflation based on the Little Higgs mechanism [157]. This makes use of "collective symmetry breaking" to protect the inflaton potential from the radiative contributions sourced by its coupling with the waterfall field. See also [158, 159, 160, 161] for more proposals aimed at building such a radiatively stable, EFT-controlled and viable model for hybrid inflation.

Twin Higgs [52] is another mechanism proposed to address the (little) hierarchy problem of the SM Higgs boson. Here, the light scalar is protected from radiative corrections sourced by its non-derivative couplings by using a discrete symmetry, with a symmetry-based cancellation of 1-loop quadratic divergences. Inspired by this, in the present work, we make use of a $\mathbb{Z}_2$-symmetry structure to build a quite simple, natural and EFT-controlled model of hybrid inflation, which we will call "Twinflation".[1] As we

[1] We thank N. Craig, S. Koren and T. Trott for giving us permission to re-use this name, first used by them in the different setting of Ref. [162].

will see in Sec. 3.5, Twinflation can naturally give rise to a viable model of inflation, with a red tilt in the primordial scalar fluctuations consistent with the observations [5], and with the inflationary Hubble scale as low as $\sim 10^7$ GeV.

Low-scale inflation and the consequent reheating, apart from explaining the smallness of yet-unobserved primordial tensor fluctuations, can also be motivated from other particle physics considerations. For example, if QCD axions or axion-like particles constitute (a significant fraction of) cold dark matter (CDM) and if Peccei-Quinn (PQ) symmetry is broken during inflation, low-scale inflation is favored to avoid CDM isocurvature constraints (see e.g. [5, 45, 46]). Such inflationary scenarios are also often invoked so that heavy, unwanted relics e.g. monopoles, moduli, gravitino, which might be generated by the UV physics (see e.g. [47, 48, 49, 50]) are diluted away/not reheated.[2] Furthermore, for sufficiently low inflationary scales, we can have complementary terrestrial particle physics probes of inflation and reheating, such as at current and future collider experiments, see e.g. [163, 164, 165, 166].

The paper is organized as follows. In Sec. 3.2, we review the basic mechanism of hybrid inflation, also reviewing that it requires fine-tuning of parameters to achieve radiative stability and EFT control, the criteria of which we also explain. In Sec. 3.3, we present a simple variant of hybrid inflation with a *soft* (dimensionful) waterfall coupling, and show that even this suffers from a similar naturalness problem as before. In Sec. 3.4, we describe the effective single-field inflation with the massive waterfall field integrated out. Here, we also introduce a simplifying notation for the effective inflationary potential

[2] We note that it is also possible to avoid reheating heavy relics just by requiring a low reheating temperature while still having a high-scale inflation.

that arises quite generically from hybrid inflation (irrespective of its naturalness) using which we can estimate the inflationary observables and constrain some model parameters. In Sec. 3.5, we construct the Twinflation model, starting with a simple renormalizable version, analysing its radiative stability and EFT consistency, and then presenting a more complete version realizing the pNGB structure of the inflaton. In Sec. 3.6, we discuss a simple way to address the cosmological domain wall problem related to the spontaneous breaking of a (simplifying but non-essential) σ-parity at the end of inflation, via a small explicit breaking. We conclude in Sec. 3.7.

3.2 Hybrid inflation and naturalness

The basic mechanism of hybrid inflation can be described by the following simple variant [167] of the original potential in [51]:

$$V(\phi,\sigma) = V_{\rm inf} + v(\phi) + \frac{1}{2}M_\sigma^2\sigma^2 + \frac{1}{4}\lambda_\sigma\sigma^4 - \frac{1}{2}g\phi^2\sigma^2 + \dots . \tag{3.1}$$

Here, ϕ is the slowly rolling inflaton and σ is the "waterfall" field whose dynamics ends inflation. Inflation starts at small ϕ, with $0 < g\phi^2 < M_\sigma^2$, such that the minimum in the σ direction is at $\sigma = 0$. The ellipsis in Eq. (3.1) includes higher-dimensional interaction terms ensuring global stability of the potential at large field values. A crucial ingredient of the hybrid inflation mechanism is that during inflation the σ-mass is bigger than both the ϕ-mass and the Hubble scale. This ensures that σ remains localized at $\sigma = 0$, and does not play any role until the end of inflation. Therefore, during inflation, i.e. for $g\phi^2 < M_\sigma^2$,

$V(\phi,\sigma)$ in Eq. (3.1) effectively reduces to

$$V_{\text{eff}}(\phi) \approx V_{\text{inf}} + v(\phi). \tag{3.2}$$

For $|v(\phi)| \ll V_{\text{inf}}$, this implies that the detailed dynamics of the inflaton is governed by $v(\phi)$, while the vacuum energy V_{inf} dominantly drives the spacetime expansion. We will see that the relaxation of V_{inf} to zero, as needed at the end of inflation, can be triggered by σ dynamics, rather than purely the single-field rolling of ϕ. The crucial separation of roles between v and V_{inf} is one of the primary reasons why the waterfall mechanism allows for consistent low-scale models of inflation.

As inflation progresses, ϕ slowly rolls down its potential $v(\phi)$, i.e. towards larger ϕ. As it crosses a critical value $\phi_* = \frac{M_\sigma}{\sqrt{g}}$ (assumed to be smaller than the minimum of $v(\phi)$), the effective mass-squared for σ switches sign. Consequently, the now-tachyonic σ rapidly rolls down to its new minimum. This *fast* rolling of the waterfall field violates the *slow*-roll conditions and ends inflation by releasing the inflationary vacuum energy, V_{inf}. The two fields finally settle into the global minimum which can be characterized by some ϕ_{min} with $\sigma_{\text{min}} = \sqrt{\frac{g\phi_{\text{min}}^2 - M_\sigma^2}{\lambda_\sigma}}$. Demanding a negligible vacuum energy in the post-inflationary era fixes

$$V_{\text{inf}} = 3H^2 M_{\text{Pl}}^2 \approx \frac{\left(g\phi_{\text{min}}^2 - M_\sigma^2\right)^2}{4\lambda_\sigma} = \frac{\left(1 - \phi_{\text{min}}^2/\phi_*^2\right)^2}{4}\frac{M_\sigma^4}{\lambda_\sigma} \sim \mathcal{O}(1)\frac{M_\sigma^4}{\lambda_\sigma}. \tag{3.3}$$

In the last step above, we have considered that the ellipsis in Eq. (3.1) fixes the global minimum in ϕ only $\mathcal{O}(1)$ away from ϕ_*, i.e. $\phi_* \sim \mathcal{O}(\phi_{\text{min}})$. This is also so that there

is no tuning required in the initial inflaton field location (see also Sec. 3.4). As we will see in Sec. 3.5.4, all these aspects can be easily realized with ϕ being a pNGB of a global symmetry and consequently its couplings taking trigonometric forms.

In the original hybrid inflation model [51], $v(\phi) = +\frac{1}{2}m_\phi^2\phi^2$ along with an opposite choice of signs in the potential in Eq. (3.1) for the M_σ^2 and g terms, allowing inflation to start at large ϕ. This convex form of $v(\phi)$ in hybrid inflation, however, leads to blue tilt in the power spectrum of the primordial scalar perturbations (after respecting the constaint on tensor-to-scalar ratio) which is strongly disfavored by the Planck data [5]. In order to get the observed red tilted spectrum, we will consider a hilltop-like $v(\phi)$ [167] with inflation happening somewhat near its maximum. In Sec. 3.4, we will see that no tuning is required in the initial inflaton field value to achieve this. A simple example of such a potential is

$$v(\phi) = -\frac{1}{2}m_\phi^2\phi^2 + \frac{\lambda_\phi}{4}\phi^4 + \dots, \tag{3.4}$$

which has a hilltop at $\phi = 0$. The ellipsis above refers to sub-dominant higher-dimensional terms in ϕ.

3.2.1 Naturalness considerations

In high-scale models of inflation, the inflaton field typically traverses super-Planckian field distances [27], requiring special UV structures to ensure the consistency of the inflationary effective field theory, e.g. as in [41]. Here, for our lower-scale inflation, we will aim to have a more straightforward EFT consistency. In particular, we will be aiming to construct a low-scale model of hybrid inflation where

- all the parameters take natural (or bigger) values,
- all the relevant mass scales and field values are smaller than the respective EFT cutoff(s),
- the EFT cutoff(s) is (are) sub-Planckian.

In the following, we will examine the naturalness of hybrid inflation, in light of the above requirements, first for the original model in Eq. (3.1) (with a hilltop structure of $v(\phi)$) and then in Sec. 3.3 for our simple modification with a *soft* waterfall coupling.

The non-derivative coupling with the waterfall field in Eq. (3.1) badly breaks shift symmetry of the inflaton and radiatively generates quadratic sensitivity in m_ϕ^2 to the UV cutoff scale[3] Λ:

$$\left(\delta m_\phi^2\right)_{\text{1-loop}} \sim \frac{g\Lambda^2}{16\pi^2}. \tag{3.5}$$

In order to satisfy naturalness in m_ϕ^2, we require

$$\left(\delta m_\phi^2\right)_{\text{1-loop}} \lesssim \left(m_\phi^2\right)_{\text{tree}} \quad \text{i.e.} \quad \Lambda^2 \lesssim \left(16\pi^2\eta\right)\frac{H^2}{g}, \tag{3.6}$$

implying that the UV cutoff Λ cannot be arbitrarily large. Here $\eta \equiv M_{\text{Pl}}^2 \frac{\partial_\phi^2 V(\phi,\sigma)}{V(\phi,\sigma)} \ll 1$ is the slow-roll parameter during inflation, with $(m_\phi^2)_{\text{tree}} \sim \eta H^2$. Furthermore, the requirement that σ is not dynamical during inflation, i.e. it being frozen at $\sigma = 0$, implies its effective mass should be bigger than the Hubble scale,

$$M_{\sigma,\text{eff}}^2 \equiv M_\sigma^2 - g\phi_0^2 \sim \mathcal{O}(1)\cdot g\phi_0^2 \gtrsim H^2, \tag{3.7}$$

[3]More precisely, Λ should be thought of as a placeholder for the mass of some heavy field.

where ϕ_0 denotes a typical inflaton field value during inflation and $M^2_{\sigma,\text{eff}} \sim M^2_\sigma \sim \mathcal{O}(1) \cdot g\phi_0^2$. To satisfy conditions in Eq. (3.6) and (3.7), we need

$$\phi_0^2 \gtrsim \frac{\Lambda^2}{16\pi^2\eta}. \tag{3.8}$$

Since the observed tilt of the primordial perturbations gives $\eta \sim 10^{-2}$, this demands inflaton field displacement bigger than the UV scale, i.e.

$$\phi_0 \gtrsim \Lambda. \tag{3.9}$$

However, this is only marginally consistent with our requirements above, and we cannot take $\phi_0 \ll \Lambda$ as desired.

Furthermore, even marginally satisfying validity of the EFT, i.e. $\phi_0 \sim \Lambda$ in Eq. (3.9), we need to satisfy $M^2_{\sigma,\text{eff}} \sim H^2$ in Eq. (3.7). However, using Eq. (3.3), this then requires the post-inflationary σ-VEV to be $\sim M_{\text{Pl}}$:

$$\langle\sigma\rangle^2_{\text{post-inf.}} \sim \frac{M^2_\sigma}{\lambda_\sigma} \sim M^2_{\text{Pl}}\frac{H^2}{M^2_\sigma} \sim M^2_{\text{Pl}}, \tag{3.10}$$

which is against our EFT requirements of sub-Planckian field values mentioned earlier. In detail, $\langle\sigma^2\rangle_{\text{post-inf.}} = \frac{g\phi^2_{\text{min}} - M^2_\sigma}{\lambda_\sigma} = \frac{M^2_\sigma}{\lambda_\sigma}\left(\frac{\phi^2_{\text{min}}}{\phi^2_*} - 1\right)$, and hence $\langle\sigma^2\rangle_{\text{post-inf.}} < \frac{M^2_\sigma}{\lambda_\sigma}$ is possible implying a slightly sub-Planckian σ-VEV. However, this is only marginal, and we will have a greater confidence in the EFT-control if the σ-VEV is *parametrically* lower than M_{Pl}.

Thus, the only way to construct a consistent hybrid inflation model with Eq. (3.1),

which is under EFT control, is with fine-tuning in m_ϕ^2, i.e. with fine cancellations between $m^2_{\phi,\text{tree}}$ and $\delta m^2_{\phi,1-\text{loop}}$. Only at the cost of such a tuning, can we satisfy $\phi_0 < \Lambda$.

3.2.2 Allowing for different cutoff scales

Since the quadratic sensitivity of m_ϕ^2 at 1-loop comes due to the σ field running in the loop, another solution one may try is allowing for different cutoff scales for ϕ and σ, i.e. Λ_ϕ and Λ_σ, respectively. This can come about if ϕ and σ belong to two different sectors with different physical scales involved in their UV completions. A familiar but dramatic example is given by the chiral Lagrangian description of composite pions of QCD, cut off by the GeV hadronic scale, while light leptons and gauge fields interacting with these pions have a much higher cutoff.

With a choice

$$\Lambda_\phi \gtrsim \phi_0 \gtrsim \Lambda_\sigma, \tag{3.11}$$

one may evade Eq. (3.9) while still ensuring EFT control in the $\phi-$sector. Now, we examine if hybrid inflation satisfies naturalness for all couplings, all scales being sub-Planckian and also smaller than the respective cutoffs, i.e. $m_\phi, \phi_0 \lesssim \Lambda_\phi$ and $M_\sigma, \langle\sigma\rangle \lesssim \Lambda_\sigma$. The radiative corrections to m_ϕ^2 now are

$$\left(\delta m_\phi^2\right)_{1-\text{loop}} \sim \frac{g\Lambda_\sigma^2}{16\pi^2} \gtrsim \frac{g\langle\sigma\rangle^2}{16\pi^2} \sim \frac{H^2 M_{\text{Pl}}^2}{16\pi^2\phi_0^2}, \tag{3.12}$$

where we use $\Lambda_\sigma \gtrsim \langle\sigma\rangle$ and $\langle\sigma\rangle \sim \frac{HM_{\text{Pl}}}{\sqrt{g}\phi_0}$ following Eq. (3.10). Now, we can see that

1-loop naturalness in m_ϕ^2, i.e. $\left(\delta m_\phi^2\right)_{1-\text{loop}} \lesssim m_\phi^2 \sim \eta H^2$, can only be satisfied with

$$\phi_0 \gtrsim M_{\text{Pl}}, \tag{3.13}$$

which is against our requirements to realize a truly low-scale hybrid inflation model.

Thus, even allowing for separate cutoffs, hybrid inflation is still not naturally in EFT control.

3.3 Hybrid inflation with a soft "waterfall" coupling

The naturalness problem described in Sec. 3.2 stems from the quadratic UV scale sensitivity in m_ϕ^2. One of the simplest solutions is to have only a soft shift symmetry breaking for ϕ, i.e. a dimensionful $\phi - \sigma$ interaction, e.g.

$$V(\phi,\sigma) = V_{\text{inf}} + \left(-\frac{m_\phi^2}{2}\phi^2 + \frac{\lambda_\phi}{4}\phi^4 + \dots\right) + \left(\frac{M_\sigma^2}{2}\sigma^2 + \frac{\lambda_\sigma}{4}\sigma^4\right) - \frac{\mu\phi}{2}\sigma^2 + \dots . \tag{3.14}$$

Here, during inflation, i.e. for $\mu\phi < M_\sigma^2$, σ remains localized at $\sigma = 0$, thus giving the same effective inflationary potential as Eq. (3.2). The ellipsis after the last term in Eq. (3.14) above, as in Eq. (3.1), includes higher-dimensional interaction terms which ensure that the global minimum in ϕ is only $\mathcal{O}(1)$ away from the critical value $\phi_* = \frac{M_\sigma^2}{\mu}$. As ϕ rolls down past ϕ_*, the waterfall in σ is triggered, thus ending inflation by releasing the inflationary vacuum energy $V_{\text{inf}} \sim \mathcal{O}(1)\frac{M_\sigma^4}{\lambda_\sigma}$, similarly to Eq. (3.3). As mentioned before, this parametric form of V_{inf} along with $\phi_{\text{min}} \sim \mathcal{O}(\phi_*)$ can be explicitly realized in the pNGB realization of the inflaton which we detail in Sec. 3.5.4.

3.3.1 Naturalness considerations

The soft coupling μ generates only a logarithmic cutoff sensitivity in m_ϕ^2:

$$(\delta m_\phi^2)_{1-\text{loop}} \sim \frac{\mu^2 \ln \Lambda}{16\pi^2}. \tag{3.15}$$

As in the previous case, demanding that the loop-induced inflaton mass is smaller than its tree-level mass, i.e. $\frac{\mu^2}{16\pi^2} \lesssim \eta H^2$ (taking $\ln \Lambda \sim \mathcal{O}(1)$), and that σ is non-dynamical during inflation, i.e. $M_{\sigma,\text{eff}}^2 \sim \mu\phi_0 \gtrsim H^2$, we get

$$\frac{H}{\phi_0} \lesssim \frac{\mu}{H} \lesssim 4\pi\sqrt{\eta} \sim \mathcal{O}(1). \tag{3.16}$$

Therefore, at the first sight, there is no constraint such as $\phi_0 \gtrsim \Lambda$ as before. However, the μ term in Eq. (3.14) also generates a quadratically divergent ϕ-tadpole:

$$V(\phi, \sigma) \ni \frac{\mu\Lambda^2}{16\pi^2}\phi. \tag{3.17}$$

Indeed, the soft waterfall coupling breaks $\phi \to -\phi$ symmetry allowing for a tadpole like above. Although it is possible for the theory to have a larger tadpole, e.g. $\Lambda^3\phi$, but it is *natural* for it to have the above radiatively generated value. We take $\mu \ll \Lambda$ to characterize the small breaking of $\phi \to -\phi$ symmetry in any coupling of the model. The tadpole in Eq. (3.17) can be absorbed in Eq. (3.14) with a large shift in the ϕ field:

$$\delta\phi \sim \frac{\mu\Lambda^2}{16\pi^2 m_\phi^2} \sim \frac{\mu\Lambda^2}{16\pi^2\eta H^2} \sim \frac{\mu\Lambda^2}{H^2}. \tag{3.18}$$

Such a large shift in ϕ, however, also gives large contributions to other terms in Eq. (3.14), e.g.

$$\frac{\delta M_\sigma^2}{M_{\sigma,\text{eff}}^2} \sim \frac{\delta\phi}{\phi_0} \sim \frac{\mu\Lambda^2}{H^2\phi_0} \sim \frac{M_{\sigma,\text{eff}}^2}{H^2}\frac{\Lambda^2}{\phi_0^2}. \tag{3.19}$$

We can see from above that, in order for naturalness in M_σ^2 (and also to allow for waterfall transition), i.e. for $\delta M_\sigma^2 \lesssim M_{\sigma,\text{eff}}^2$, we need

$$\frac{\phi_0^2}{\Lambda^2} \gtrsim \frac{M_{\sigma,\text{eff}}^2}{H^2} \gtrsim 1. \tag{3.20}$$

This again implies $\phi_0 \gtrsim \Lambda$, which is in contradiction with the EFT requirements stated earlier.

3.3.2 Allowing for different cutoff scales

Allowing even for different cutoff scales in this hybrid inflation model with soft coupling, we get a similar result as Eq. (3.13). The radiative corrections to M_σ^2 here are

$$\left(\delta M_\sigma^2\right)_{1-\text{loop}} \sim \frac{\lambda_\sigma\Lambda_\sigma^2}{16\pi^2} + \frac{\mu^2\Lambda_\sigma^2}{16\pi^2 m_\phi^2}. \tag{3.21}$$

Naturalness for the first term on the right hand side above, as before, demands $\langle\sigma\rangle \lesssim \Lambda_\sigma \lesssim 4\pi\langle\sigma\rangle$, now with $\langle\sigma\rangle \sim \frac{HM_\text{Pl}}{\sqrt{\mu\phi_0}}$. In order to satisfy naturalness for the second term (sourced by quadratically divergent ϕ-tadpole), i.e.

$$1 \gtrsim \frac{\mu^2\Lambda_\sigma^2}{16\pi^2 m_\phi^2 M_\sigma^2} \gtrsim \frac{\mu\langle\sigma\rangle^2}{H^2\phi_0} \sim \frac{M_\text{Pl}^2}{\phi_0^2}, \tag{3.22}$$

we again need

$$\phi_0 \gtrsim M_{\rm Pl}. \tag{3.23}$$

Thus, we see that with either marginal or soft $\phi - \sigma$ coupling, even with different cutoffs for the inflaton and the waterfall field, if we demand EFT control (i.e. all scales being smaller than the respective cutoffs) and sub-Planckian physics, the only way to have a consistent hybrid inflation model is with fine-tuning of the relevant parameters, m_ϕ^2 or M_σ^2 as discussed in this and the previous section. This suggests that in order to build a natural model for hybrid inflation, we need some significant new mechanism to entirely get rid of the quadratic UV-sensitivity in the inflaton potential coming from its necessarily non-derivative coupling to the waterfall field.

3.4 Effective single-field inflation

The models described in Sec. 3.2 and 3.3 cannot give rise to consistent hybrid inflation under EFT control without fine-tuning of parameters. Before we propose such a natural model for hybrid inflation in Sec. 3.5, in this section we first focus on effective single-field inflation with the massive waterfall field integrated out. We also introduce here a simplifying notation for the effective inflationary potential that arises quite generically from hybrid inflation. As we will see, this simplified single-field analysis allows us to easily estimate the inflationary observables and use them to constrain the effective model parameters, even without knowing the detailed form of the full potential. This "satellite view" will be helpful later in Sec. 3.5 by simply identifying the realistic parts of parameter space deserving a fuller analysis.

The waterfall field, although with a ϕ-dependent mass, still remains heavier than H throughout inflation, except at the end of inflation when $M_\sigma^2(\phi)$ passes through zero. Thus, prior to the end of inflation we can integrate it out and get an effective single-field description in terms of ϕ. Hybrid inflation quite generically gives this effective single-field inflationary potential in the form of Eq. (3.2), which varies as some function $v(\phi)$ with a large vacuum energy offset V_{inf}. In this section, we introduce a simplifying notation with

$$v(\phi) = V_0 \cdot F\left(\frac{\phi}{f}\right), \tag{3.24}$$

where V_0 controls the magnitude, while the shape is specified by a dimensionless function F. The effective inflationary potential then has the following form:

$$V_{\text{eff}}(\phi) = V_{\text{inf}} + V_0 \cdot F\left(\frac{\phi}{f}\right) \quad ; \quad V_{\text{inf}} \gg V_0. \tag{3.25}$$

The hilltop-like $v(\phi)$ that we considered earlier in Eq. (3.4) has the form as in Eq. (3.24). We will also show later how this simple form arises generically from a more complete hybrid inflation model in Sec. 3.5 where the inflaton is realized as a pNGB, and where $F\left(\frac{\phi}{f}\right)$ takes a trigonometric form.

The main benefit of using this simplifying notation is that, assuming the function F and its derivatives are $\sim \mathcal{O}(1)$ during inflation, which is also the case in the model that we discuss later in Sec. 3.5, we can obtain general expressions for inflationary observables as shown below, even without specifying the explicit form of F. We assume that inflation starts[4] at ϕ_i which is somewhat near the hilltop of $F\left(\frac{\phi}{f}\right)$ as preferred by the data [5],

[4]More precisely, when the largest scales observable today exit the horizon during inflation.

and ends at ϕ_e by a waterfall transition along the σ field. Then, the slow-roll inflation parameters are[5]

$$\eta \equiv \frac{V''}{V} M_{\rm Pl}^2 \sim \frac{V_0}{V_{\rm inf}} \frac{M_{\rm Pl}^2}{f^2} \ , \ \epsilon \equiv \frac{1}{2} \left(\frac{V'}{V} \right)^2 M_{\rm Pl}^2 \sim \eta^2 \frac{f^2}{M_{\rm Pl}^2},$$
$$A_s \equiv \frac{1}{8\pi^2} \frac{H^2}{M_{\rm Pl}^2} \frac{1}{\epsilon} \sim \frac{10^{-2}}{\eta^2} \frac{H^2}{f^2} \ , \ \mathcal{N}_e \equiv \int_{\phi_i}^{\phi_e} \frac{d\phi}{M_{\rm Pl}\sqrt{2\epsilon(\phi)}} \sim \frac{1}{\eta} \int_{\theta_i}^{\theta_e} \frac{d\theta}{F'(\theta)} \sim \frac{\mathcal{O}(1)}{\eta}. \tag{3.26}$$

The last relation above involving the number of observable e-foldings $\mathcal{N}_e$ uses the notation $\theta \equiv \phi/f$. First line of Eq. (3.26) shows that quite generically the slow-roll parameter ϵ is parametrically suppressed compared to η (for $f \ll M_{\rm Pl}$), thereby naturally explaining the smallness of the yet-unobserved primordial tensor fluctuations [5]. The observables—spectral tilt of the primordial scalar fluctuations $(1 - n_s)$, tensor-to-scalar ratio (r), and the scalar power spectrum amplitude (A_s)—as per the Planck CMB data [5, 22] are

$$1 - n_s = 6\epsilon - 2\eta \approx -2\eta \approx 0.04 \ , \ r = 16\epsilon < 0.06 \ , \ A_s \approx 2 \times 10^{-9}, \tag{3.27}$$

where, in the first part above, we assume $\epsilon \ll \eta$ as is the case preferred by the data. Also, as the spectral tilt constraint above shows, $\eta < 0$ is strongly preferred, especially for the low-scale models we are considering (i.e. for small ϵ). A convex form of $F\left(\frac{\phi}{f}\right)$ in Eq. (3.25), or more generally convex $v(\phi)$ in Eq. (3.2), e.g. $v(\phi) = +\frac{1}{2}m_\phi^2\phi^2$ as mentioned earlier, gives $\eta > 0$ and hence a blue spectral tilt which is strongly disfavored. Hence, we

[5]The slow roll parameters ϵ, η as defined above are, in general, functions of ϕ. However, unless an explicit functional argument is shown, they refer to the parameters evaluated at an epoch when the largest scales observable today exit the horizon during inflation, normally ∼50-60 e-folds before the end of inflation.

consider a hilltop-like $F\left(\frac{\phi}{f}\right)$ with inflation happening somewhat close to its maximum. Eq. (3.27) constrains the parameters of the effective single-field inflation as described by Eq. (3.25), i.e. (V_{inf}, V_0, f), as[6]

$$\frac{f}{H} \sim \frac{0.1}{\eta\sqrt{A_s}} \sim 10^6 \ , \ \frac{V_0}{f^4} \sim 10^2\eta^3 A_s \sim 10^{-12} \ , \ \frac{V_0}{V_{\text{inf}}} \sim \frac{\epsilon}{\eta} \sim \mathcal{O}(10)\ r. \tag{3.28}$$

Hilltop inflation models, in order to satisfy the slow roll conditions, typically require inflation to happen very close to the hilltop. However, with a large offset in the vacuum energy as in Eq. (3.25), this tuning in the initial inflaton field location is not required. Here, the potential generically satisfies slow-roll conditions for all values of ϕ and not just near its extrema. As can be seen in Eq. (3.26), $\mathcal{N}_e \propto 1/\eta \sim \mathcal{O}(100)$. Hence, the dimensionless integral there needs only to be $\mathcal{O}(1)$ to get $\mathcal{N}_e = 50 - 60$ which can be easily satisfied with $\phi_i, \phi_e \sim \mathcal{O}(f)$.

3.5 Hybrid "Twinflation"

In the present section, we propose a natural model for hybrid inflation, "Twinflation", which satisfies naturalness for all parameters, all mass scales and field values being smaller than the respective UV cutoff scales, and sub-Planckian physics. We will also make use of the estimates in Sec. 3.4, since the effective inflationary potential here has the same form as in Eq. (3.25), as we will see later.

In order to get rid of the quadratic sensitivity of the inflaton potential $V_{\text{eff}}(\phi)$ to-

[6] We will do a better job of estimating these parameters, especially $\frac{f}{H}$, in Sec. 3.5.4, taking the $\sim \mathcal{O}(1)$ factors in F and its derivatives from Eq. (3.25) into account.

wards the UV physics, we consider mirroring the σ-field with a $\mathbb{Z}_2$ exchange symmetry. Considering the original structure of hybrid inflation, Eq. (3.1), one could try $g\phi^2\sigma^2 \to g\phi^2\left(\sigma_A^2 - \sigma_B^2\right)$, such that the quadratic sensitivity of the inflaton mass to the UV scale is canceled between σ_A and σ_B. However, no symmetry protects this structure and hence it is not radiatively stable. Instead, we consider twinning the σ-field in our variant hybrid inflation, Eq. (3.14), i.e.

$$\mu\phi\sigma^2 \to \mu\phi\left(\sigma_A^2 - \sigma_B^2\right). \tag{3.29}$$

Here, m_ϕ^2 has already only log-sensitivity to the UV scale. Now the twinning in σ prevents a quadratically divergent ϕ-tadpole, and thereby removing the associated issues as discussed in Sec. 3.3. Also, there exists a symmetry protecting this structure: $\sigma_A \to \sigma_B, \phi \to -\phi$; along with σ-parity i.e. $\sigma_i \to -\sigma_i$ $(i = A, B)$ for simplicity.[7] So, this structure is radiatively stable. This can also be realized by a UV completion where ϕ is a pNGB of a $U(1)$ global symmetry with soft explicit breaking (see Sec. 3.5.4).

A similar model construction to the one presented in the Sec. 3.5.1, i.e. Eqs. (3.30) and (3.31), was considered in Ref. [168] but in the context of mirror-world models to achieve asymmetric reheating of the mirror sector so as to avoid the $\Delta N_{\rm eff}$ constraints. However, here our primary goal is to point out the utility of the twin symmetry in Eq. (3.30) to address the $\eta-$problem for the inflaton, by constraining inflaton radiative corrections, while reheating can proceed as in standard hybrid inflation.

[7] In the next section we will softly break the $\sigma-$parity in a controlled manner to address the cosmological domain wall problem while ensuring naturalness.

3.5.1 Basic model

We now consider the symmetry structure described above, namely,

$$\sigma_A \to \sigma_B \ , \ \phi \to -\phi \tag{3.30}$$

under the twin symmetry, and also $\sigma_i \to -\sigma_i$ for simplicity. The most general potential consistent with the above symmetry is given by

$$\begin{aligned} V(\phi, \sigma_{A,B}) = \ & V_{\text{inf}} + \left(-\frac{1}{2} m_\phi^2 \phi^2 + \frac{\lambda_\phi}{4} \phi^4 + \dots \right) \\ & + \left(\left(\frac{1}{2} M_\sigma^2 \sigma_A^2 + \frac{\lambda_\sigma}{4} \sigma_A^4 \right) + (A \to B) \right) + \frac{\bar{\lambda}_\sigma}{4} \sigma_A^2 \sigma_B^2 \\ & + \frac{\mu}{2} \phi \left(\sigma_A^2 - \sigma_B^2 \right) + \kappa \phi^2 \left(\sigma_A^2 + \sigma_B^2 \right) + \dots , \end{aligned} \tag{3.31}$$

where ellipsis after the last term includes higher-dimensional interaction terms, as in Eq. (3.14). Approximate shift symmetry for the inflaton ϕ then requires

$$\mu, m_\phi \ll M_\sigma \ \text{ and } \ \kappa, \lambda_\phi \ll \lambda_\sigma, \bar{\lambda}_\sigma \ , \tag{3.32}$$

which ensures that ϕ is much lighter and weakly coupled as compared to σ_i.

Let us first analyze the effective inflationary dynamics at tree-level. During inflation, i.e. for $\mu\phi < M_\sigma^2$, both the σ fields remain heavy and with vanishing VEVs. Then, integrating them out at tree-level is simply dropping σ_i in Eq. (3.31). This gives

$$V_{\text{eff}}(\phi) = V_{\text{inf}} + \left(-\frac{1}{2} m_\phi^2 \phi^2 + \frac{\lambda_\phi}{4} \phi^4 + \dots \right) = V_{\text{inf}} + \frac{\lambda_\phi}{4} (\phi^2 - f^2)^2 + \dots , \tag{3.33}$$

where $f \sim m_\phi/\sqrt{\lambda_\phi}$ and the ellipsis includes sub-dominant higher-dimensional terms in ϕ. This potential is of the form of Eq. (3.25) and hence all the results of Sec. 3.4, in particular Eq. (3.28), apply here. We will consider inflationary trajectory somewhat close to the hilltop of $V_{\rm eff}(\phi)$ (i.e. $\phi = 0$), but still with a typical inflaton field value of $\sim \mathcal{O}(f)$ to avoid any considerable initial location tuning. As ϕ rolls down its potential, $M^2_{\sigma_i}$ change as

$$M^2_{\sigma_{A,B}}(\phi) = M^2_\sigma \pm \mu\phi. \tag{3.34}$$

In order for the waterfall effect to take place, we need

$$M^2_\sigma \sim \mathcal{O}(\mu f). \tag{3.35}$$

Since $M^2_{\sigma_A}$ always stays positive along the inflationary trajectory, σ_A has no dynamical role in the model. But σ_B, which is the true waterfall field here, turns tachyonic at $\phi_* = \frac{M^2_\sigma}{\mu} \sim \mathcal{O}(f)$ and rapidly rolls down to its new minimum. The global minimum can be characterized by

$$\sigma_{B,\rm min} = \left(\frac{\mu\phi_{\rm min} - M^2_\sigma}{\lambda_\sigma}\right)^{1/2} = \frac{M_\sigma}{\sqrt{\lambda_\sigma}}\left(\frac{\phi_{\rm min}}{\phi_*} - 1\right)^{1/2}, \ \sigma_{A,\rm min} = 0. \tag{3.36}$$

This fast rolling to the global minimum ends inflation by releasing the vacuum energy given by

$$V_{\rm inf} = \frac{M^4_\sigma}{4\lambda_\sigma}\left(\frac{\phi_{\rm min}}{\phi_*} - 1\right)^2 \sim \mathcal{O}(1)\frac{\mu^2 f^2}{\lambda_\sigma}. \tag{3.37}$$

In the last step above, as also alluded to before in Sec. 3.3, we have set $\phi_{\rm min} \sim \mathcal{O}(\phi_*) \sim$

$\mathcal{O}(f)$ assuming that the higher-dimensional interaction terms in the ellipsis in Eq. (3.31) fix the global minimum in ϕ at $\sim \mathcal{O}(f)$. As we will see later in Sec. 3.5.4, this can be easily realized in a more complete model with ϕ as pNGB of a $U(1)$ global symmetry.

3.5.2 Radiative stability and naturalness

In order for the tree-level analysis of the Twinflation model from the previous section to be valid even at loop-level, we need the radiative corrections in Eq. (3.31) to be sufficiently small which we explore in this section. The effect of loops is two-fold: renormalizing tree-level parameters, and giving non-analytic field-dependence via logarithmic terms in the Coleman-Weinberg (CW) potential. First, we require that renormalization of tree-level parameters respects radiative stability and naturalness, and get the resulting constraints on the model parameters. Then, in Sec. 3.5.3, we also consider the effects of the full CW potential, but we will show that they can have significant effects only at the boundary of the allowed parameter space, i.e. when naturalness in $V_{\rm eff}(\phi)$ is saturated, which we examine numerically and show in Fig. 3.1. In this section, we will therefore defer the full CW analysis in order to first identify the bulk of the viable parameter space.

Here we look for the constraints in the parameter space required to achieve naturalness of the tree-level parameters. In the σ-sector, quadratic divergence in M_σ^2 is induced by the σ self-quartic couplings as

$$\delta M^2_{\sigma,1-\text{loop}} \sim \frac{\lambda_\sigma \Lambda_\sigma^2}{16\pi^2} + \frac{\bar{\lambda}_\sigma \Lambda_\sigma^2}{16\pi^2}. \tag{3.38}$$

Hence, naturalness in M_σ^2 demands the cutoff in σ-sector to be

$$\frac{M_\sigma}{\sqrt{\lambda_\sigma}} \lesssim \Lambda_\sigma \lesssim 4\pi \frac{M_\sigma}{\sqrt{\lambda_\sigma}}. \tag{3.39}$$

The first constraint above is obtained by demanding that the VEV of σ is smaller than the UV scale, which is one of our EFT consistency requirement. We also consider $\bar{\lambda}_\sigma \lesssim \lambda_\sigma$ such that the upper bound on Λ_σ is controlled by λ_σ as above. Since both $\bar{\lambda}_\sigma$ and λ_σ get the same radiative contributions as mentioned below in Eq. (3.40), this is justified.

In the ϕ-sector, for simplicity, first we consider an exact shift symmetry, which is then only softly broken by the μ term in Eq. (3.31). Then, the loop-level one-particle irreducible (1PI) effective potential has contributions as follows (here we track only the μ-dependent corrections):

$$\begin{aligned}
\delta m^2_{\phi,1-\text{loop}} &\sim \frac{\mu^2}{16\pi^2} \ln \Lambda_\sigma \ , \\
\delta \left(\lambda_\phi, \lambda_\sigma, \bar{\lambda}_\sigma\right)_{1-\text{loop}} &\sim \frac{\mu^4}{16\pi^2 M_\sigma^4} \sim \frac{\mu^2}{16\pi^2 f^2} \ , \\
\delta \kappa_{1-\text{loop}} &\sim \frac{\lambda_\sigma \mu^2}{16\pi^2 M_\sigma^2} \sim \frac{\lambda_\sigma \mu}{16\pi^2 f} \ .
\end{aligned} \tag{3.40}$$

Here, we first note that there is no quadratic sensitivity to the UV cutoff scales as in Eq. (3.17), due to cancellations induced by the twin symmetry, and only a log-sensitivity in m_ϕ^2. Now, we will consider even tree-level hard breaking of ϕ-shift symmetry, i.e. tree-level λ_ϕ and κ couplings, which are comparable to the loop contributions above. We will take tree-level values for the other parameters to be at least comparable or bigger than

their loop contributions. This gives

$$m^2_{\phi,\text{tree}} \gtrsim \frac{\mu^2}{16\pi^2} \ , \quad \left(\lambda_\sigma, \bar{\lambda}_\sigma\right)_{\text{tree}} \gtrsim \frac{\mu^2}{16\pi^2 f^2} \ , \quad \lambda_{\phi,\text{tree}} \sim \frac{\mu^2}{16\pi^2 f^2} \ , \quad \kappa_{\text{tree}} \sim \frac{\lambda_\sigma \mu}{16\pi^2 f} \ , \tag{3.41}$$

taking $\ln \Lambda_\sigma \sim \mathcal{O}(1)$. We note that with the above choice for m^2_ϕ and λ_ϕ, the ϕ-transit scale is indeed $\mathcal{O}(f)$. But, the tree-level λ_ϕ and κ hard breaking terms now induce quadratic UV-sensitivity in $V_{\text{eff}}(\phi)$. However, their values satisfying the above constraints are sufficiently small so that naturalness in m^2_ϕ can still be maintained as below:

$$\begin{aligned} \delta m^2_{\phi,1-\text{loop},(\lambda_\phi)} &\sim \frac{\lambda_\phi \Lambda^2_\phi}{16\pi^2} \sim \frac{\mu^2}{16\pi^2} \frac{\Lambda^2_\phi}{16\pi^2 f^2} \lesssim \frac{\mu^2}{16\pi^2} \lesssim m^2_{\phi,\text{tree}} \ , \\ \delta m^2_{\phi,1-\text{loop},(\kappa)} &\sim \frac{\kappa \Lambda^2_\sigma}{16\pi^2} \sim \frac{\mu^2}{16\pi^2} \frac{\Lambda^2_\sigma}{16\pi^2 M^2_\sigma/\lambda_\sigma} \lesssim \frac{\mu^2}{16\pi^2} \lesssim m^2_{\phi,\text{tree}} . \end{aligned} \tag{3.42}$$

As can be seen above, this requires cutoffs in the two sectors to be bounded as

$$\Lambda_\phi \lesssim 4\pi f \ , \quad \Lambda_\sigma \lesssim 4\pi \frac{M_\sigma}{\sqrt{\lambda_\sigma}} \ , \tag{3.43}$$

where the σ-cutoff also satisfies Eq. (3.39). We note that these cutoffs can still be bigger than the respective field values.

Getting a consistent inflationary model:

In order to get a consistent single-field inflation model, we need to satisfy

$$m^2_\phi \sim \eta H^2 \ , \ M_\sigma \gtrsim H \ , \ V_{\text{inf}} \sim H^2 M^2_{\text{Pl}} \sim \frac{M^4_\sigma}{\lambda_\sigma} . \tag{3.44}$$

The first condition above, along with Eq. (3.41), requires $\mu \lesssim \mathcal{O}(H)$. The second condition, i.e. the σ fields being at least heavier than the Hubble scale, combined with $M_\sigma^2 \sim \mu f$ (see Eq. (3.35)) and $f \sim 10^6 H$ (see Eq. (3.28)), requires $\mu \gtrsim 10^{-6} H$. Together, these constrain the model parameter μ as

$$10^{-6} \lesssim \frac{\mu}{H} \lesssim \mathcal{O}(1). \tag{3.45}$$

The lower bound on μ above also satisfies $\langle\sigma\rangle \lesssim M_{\rm Pl}$ following Eq. (3.37) and Eq. (3.39). A stronger requirement of $\Lambda_\sigma \sim 4\pi\langle\sigma\rangle \lesssim M_{\rm Pl}$ implies $\frac{\mu}{H} \gtrsim 10^{-3}$.

Lower bound on the Hubble scale:

The third condition in Eq. (3.44), which relates the inflationary Hubble scale to the model parameters, implies

$$\lambda_\sigma \sim \frac{M_\sigma^4}{H^2 M_{\rm Pl}^2} \sim \frac{\mu^2 f^2}{H^2 M_{\rm Pl}^2} \sim 10^{22} \frac{\mu^2}{f^2} \frac{H^2}{M_{\rm Pl}^2}, \tag{3.46}$$

using Eq. (3.28) in the last step. Hence naturalness in λ_σ, i.e. $\lambda_\sigma \gtrsim \frac{\mu^2}{16\pi^2 f^2}$ (see Eq. (3.41)), combined with Eq. (3.46) gives a lower bound on the inflationary Hubble scale within our Twinflation model as

$$H \gtrsim 10^6 \text{GeV}. \tag{3.47}$$

This also implies a lower bound on the tensor-to-scalar ratio as $r \gtrsim 10^{-16}$.

As we can see above, naturalness in λ_σ also implies $H^2 M_{\rm Pl}^2 \lesssim 16\pi^2 f^4$ i.e. $V_{\rm inf} \lesssim \Lambda_\phi^4$, with the ϕ-cutoff $\Lambda_\phi \lesssim 4\pi f$. Also, perturbativity of λ_σ combined with Eq. (3.37) and

(3.39) implies $V_{\rm inf} \lesssim \Lambda_\sigma^4$. Thus, the inflationary energy scale being smaller than the UV scales ensures good EFT control in this model.

Thus, our Twinflation model of Eq. (3.31), with the parameters satisfying the constraints in Eq. (3.41), exhibits naturalness and EFT control. All the mass scales and the field values are less than the corresponding UV cutoff scales, especially $f \lesssim \Lambda_\phi$ and $\langle\sigma\rangle \lesssim \Lambda_\sigma$. As we will see later in Sec. 3.5.4, there is a significant parameter space available satisfying $\Lambda_\phi, \Lambda_\sigma \lesssim M_{\rm Pl}$ (see Fig. 3.1) such that we have a truly low-scale, sub-Planckian hybrid inflation model under EFT control, satisfying all of our naturalness requirements as mentioned in Sec. 3.2.

3.5.3 One-loop Coleman-Weinberg effective potential

As we noted earlier, the σ fields are always heavy before the end of inflation, and hence can be integrated out to give a 1-loop Coleman-Weinberg (CW) potential:

$$\begin{aligned} V_{\rm CW}(\phi) &= \sum_{i=A,B} \frac{M_{\sigma_i}^4(\phi)}{64\pi^2} \ln \frac{M_{\sigma_i}^2(\phi)}{\Lambda_\sigma^2} \\ &= \frac{\mu^2 f^2}{64\pi^2} \left[\left(2\frac{\phi^2}{f^2} + \cdots \right) \ln \frac{\mu f}{\Lambda_\sigma^2} + \frac{(\phi_* + \phi)^2}{f^2} \ln \frac{\phi_* + \phi}{f} + \frac{(\phi_* - \phi)^2}{f^2} \ln \frac{\phi_* - \phi}{f} \right] . \end{aligned} \tag{3.48}$$

The first term above renormalizes $m_{\phi,\rm tree}^2$ as in Eq. (3.40). Parameterizing the tree-level inflaton mass as

$$m_{\phi,\rm tree}^2 \equiv c_\phi \frac{\mu^2}{16\pi^2} , \tag{3.49}$$

the naturalness constraint in Eq. (3.41) requires $c_\phi \gtrsim \mathcal{O}(1)$. Then, $V_{\rm CW}(\phi)$ in Eq. (3.48) is comparable to tree-level $V_{\rm eff}(\phi)$ in Eq. (3.33) only when $c_\phi \approx 1$, while giving subdominant effects for the bulk of the natural parameter space ($c_\phi \gg 1$). Nevertheless, in our full numerical analysis in Sec. 3.5.4, we will incorporate the logarithmic effects in the inflaton that distinguish the 1-loop potential, but they are so modest as to be difficult to resolve by eye, as we will see in Fig. 3.1.

3.5.4 Pseudo-Nambu-Goldstone inflaton realization

In this section, we discuss a simple and more complete extension of the model in Eq. (3.31), realizing the inflaton as a pNGB of a global $U(1)$ symmetry, with soft explicit breaking. The Lagrangian is given by,

$$\begin{aligned}\mathcal{L}_{\rm UV} =& |\partial\Phi|^2 - V_\Phi(|\Phi|^2) \\ &+ \left(\left(\frac{1}{2}(\partial\sigma_A)^2 - \frac{1}{2}M_\sigma^2\sigma_A^2 - \frac{\lambda_\sigma}{4}\sigma_A^4\right) + (A \to B)\right) - \frac{\bar{\lambda}_\sigma}{4}\sigma_A^2\sigma_B^2 \\ &+ \left(\frac{\mu\Phi}{2\sqrt{2}}(\sigma_A^2 - \sigma_B^2) + \frac{c_\phi}{64\pi^2}(\mu\Phi)^2 + \text{h.c.}\right) - g|\Phi|^2\left(\sigma_A^2 + \sigma_B^2\right) - V_{\rm inf}. \end{aligned} \tag{3.50}$$

Similar to the symmetry structure in Eq. (3.30), we demand

$$\Phi \to -\Phi, \quad \sigma_A \to \sigma_B \tag{3.51}$$

under the twin symmetry, and also for simplicity a $\mathbb{Z}_2$-symmetry under which $\sigma_i \to -\sigma_i$ for $i = A, B$. Furthermore, we treat μ as a $U(1)$ "spurion" with charge -1 that compensates the $+1$ charge of Φ under the $U(1)$. This spurion analysis, along with the symmetry

structure in Eq. (3.51), uniquely fixes the Lagrangian in Eq. (3.50) at the dimension-4 level. There are two dimensionless coupling constants c_ϕ and g, with $\mu, M_\sigma, \lambda_\sigma, \bar{\lambda}_\sigma$ being the same as in Eq. (3.31).[8] The potential V_Φ is such that it allows for a spontaneous breaking of $U(1)$ with the inflaton (ϕ) being the corresponding Nambu-Goldstone boson (NGB). The $\mu-$term in the third line of Eq. (3.50) then gives mass to the inflaton, as we will see below, making it a pseudo-NGB. We parametrize the inflaton ϕ as $\Phi = \frac{f+\chi}{\sqrt{2}} e^{i\phi/f}$, where χ is the radial mode and $\langle \Phi \rangle = f$ is the VEV. Integrating out χ and redefining $\frac{\phi}{f} \to \frac{\phi}{f} + \pi/2$, we get an effective Lagrangian from Eq. (3.50) as

$$\begin{aligned}\mathcal{L}_{\rm IR} = &\left(\left(\frac{1}{2}(\partial\sigma_A)^2 - \frac{1}{2}\widetilde{M}_\sigma^2 \sigma_A^2 - \frac{\lambda_\sigma}{4}\sigma_A^4 \right) + (A \to B) \right) - \frac{\bar{\lambda}_\sigma}{4}\sigma_A^2\sigma_B^2 \\ &+ \frac{1}{2}(\partial\phi)^2 - \frac{\mu f}{2}\sin\left(\frac{\phi}{f}\right)\left(\sigma_A^2 - \sigma_B^2\right) - c_\phi \frac{\mu^2 f^2}{64\pi^2}\cos\left(\frac{2\phi}{f}\right) - V_{\rm inf}. \end{aligned} \tag{3.52}$$

Here we have defined $\widetilde{M}_\sigma^2 \equiv M_\sigma^2 + g f^2$. For the waterfall mechanism to work, we need both $M_\sigma^2 \sim \mu f$, which was discussed earlier, and $g \lesssim \mu/f$, which then implies $\widetilde{M}_\sigma^2 \sim M_\sigma^2 \sim \mu f$. Hence, in what follows, we will drop the tilde over M_σ^2. This value of g is technically natural since loop-contributions in the 1PI effective potential include

$$\delta g_{1-\rm loop} \sim \frac{\lambda_\sigma \mu^2}{16\pi^2 M_\sigma^2} \sim \frac{\lambda_\sigma \mu}{16\pi^2 f} \ll \frac{\mu}{f}. \tag{3.53}$$

[8] To simplify the notation, we keep using the same parameter μ as before, although now it has a spurion charge.

Inflation starts somewhat near the hilltop along ϕ i.e. close to $\phi = 0$. Expanding for $\phi/f \ll 1$ in Eq. (3.52), we get[9]

$$\mathcal{L}_{\rm IR} \approx \left(\left(\frac{1}{2}(\partial\sigma_A)^2 - \frac{1}{2}M_\sigma^2\sigma_A^2 - \frac{\lambda_\sigma}{4}\sigma_A^4\right) + (A \to B)\right) - \frac{\bar{\lambda}_\sigma}{4}\sigma_A^2\sigma_B^2 + \frac{1}{2}(\partial\phi)^2 - \frac{\mu\phi}{2}\left(\sigma_A^2 - \sigma_B^2\right) - V_{\rm inf} + c_\phi\frac{\mu^2}{16\pi^2}\left(\frac{\phi^2}{2} - \frac{\phi^4}{6f^2} + \dots\right). \tag{3.54}$$

For $c_\phi \gtrsim \mathcal{O}(1)$, as required by technical naturalness in Eq. (3.50), this reproduces all the interactions relevant for hybrid inflation as was studied earlier in Eq. (3.31) for $c_\phi > 0$.

During inflation, i.e. with $\sin\left(\frac{\phi}{f}\right) < \frac{M_\sigma^2}{\mu f}$, both $\sigma_{A,B}$ remain heavy and with vanishing VEVs. Thus, integrating them out at tree-level, which is dropping them in Eq. (3.52), gives an effective inflationary potential

$$V_{\rm eff}(\phi) \approx V_{\rm inf} + c_\phi\frac{\mu^2 f^2}{64\pi^2}\cos\left(\frac{2\phi}{f}\right). \tag{3.55}$$

This is of the form of Eq. (3.25) with the function $F\left(\frac{\phi}{f}\right)$ taking trigonometric form as above, and hence all the results of Sec. 3.4 apply here too. As inflaton rolls past a critical value ϕ_* such that

$$\sin\left(\frac{\phi_*}{f}\right) = \frac{M_\sigma^2}{\mu f}, \tag{3.56}$$

waterfall is triggered along σ_B. The fields then rapidly roll down to the global minimum

[9]The size of the cosine potential in ϕ ($\sim \mu^2 f^2/16\pi^2$) is much smaller than $V_{\rm inf} \sim \mu^2 f^2/\lambda_\sigma$, as we will see later in Eq. (3.58), and hence the constant term from the cosine can be neglected here.

which is situated at

$$\frac{\phi_{\rm min}}{f} = \frac{\pi}{2}, \;\; \sigma_{A,\rm min} = 0,$$
$$\sigma_{B,\rm min} = \sqrt{\frac{1}{\lambda_\sigma}\left(\mu f \sin\left(\frac{\phi_{\rm min}}{f}\right) - M_\sigma^2\right)} = \sqrt{\frac{\mu f}{\lambda_\sigma}\left(1 - \sin\left(\frac{\phi_*}{f}\right)\right)} \sim \mathcal{O}(1)\sqrt{\frac{\mu f}{\lambda_\sigma}}. \tag{3.57}$$

The inflationary vacuum energy released during this waterfall transition is given by

$$V_{\rm inf} \approx \frac{\mu^2 f^2}{4\lambda_\sigma}\left(1 - \sin\left(\frac{\phi_*}{f}\right)\right)^2 \sim \mathcal{O}(1)\frac{\mu^2 f^2}{\lambda_\sigma}. \tag{3.58}$$

Thus, as mentioned earlier in Sec. 3.5.1, once ϕ is realized as a pNGB of a $U(1)$ global symmetry as in this section, the global minimum in ϕ is fixed only $\sim \mathcal{O}(1)$ away from the critical point triggering waterfall, i.e. $\phi_{\rm min} \sim \mathcal{O}(\phi_*) \sim \mathcal{O}(f)$. Consequently, the parametric dependence of $V_{\rm inf}$ (and hence H) on the model parameters is obtained as in Eq. (3.58), which is as expected in Eq. (3.37).

Integrating out the heavy σ fields at 1-loop level, similar to Eq. (3.48), gives rise to the following logarithmic dependence from the Coleman-Weinberg potential:

$$V_{\rm CW}\left(\theta \equiv \frac{\phi}{f}\right) = \frac{\mu^2 f^2}{64\pi^2}\left[(\sin\theta_* + \sin\theta)^2 \ln\left(\sin\theta_* + \sin\theta\right)\right. \\ \left. + \left(\sin\theta_* - \sin\theta\right)^2 \ln\left(\sin\theta_* - \sin\theta\right)\right]. \tag{3.59}$$

As mentioned earlier in Sec. 3.5.2, this can give considerable effects only when naturalness is saturated for m_ϕ^2, i.e. for $c_\phi \approx 1$. These effects, numerically computed in Fig. 3.1, are however so modest as to be difficult to resolve by eye.

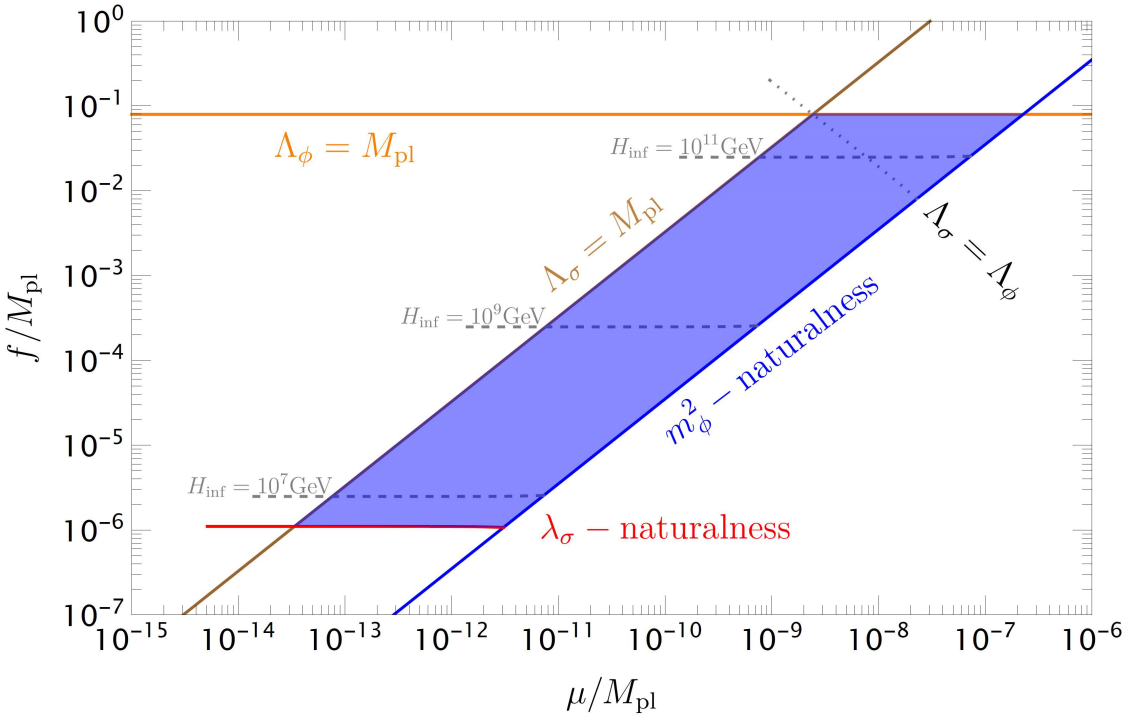

Figure 3.1: Available parameter space in the $U(1)$ version of our Twinflation model (see Sec. 3.5.4) exhibiting naturalness and EFT-control: $\phi_*/f = \pi/5$ for concreteness. The right and bottom edges of the shaded region correspond to naturalness constraints on m_ϕ and λ_σ, respectively. The top and left edges correspond to the cutoffs Λ_ϕ and Λ_σ being sub-Planckian, respectively. $\Lambda_\phi \approx \Lambda_\sigma$ on the dotted line. The parameter c_ϕ varies from 1 to $\sim 10^4$ as we move from right to left edge, which makes the loop contributions to inflaton potential smaller and smaller as compared to the tree-level term. The dashed lines show contours for $H = 10^7, 10^9, 10^{11}$ GeV, corresponding to $r \approx 10^{-15}, 10^{-11}, 10^{-7}$, respectively. n_s is fixed to 0.9649, its central value from the Planck CMB constraints [5]. Varying its value up or down by a percent shifts the entire blue region slightly to the left or right, respectively, by about a percent which is hardly resolvable by eye.

Fig. 3.1 shows the available parameter space in our Twinflation model described by Eq. (3.52), satisfying the requirements of naturalness and EFT control, and giving a viable hybrid inflation model. Here we have fixed $\frac{\phi_*}{f} = \frac{\pi}{5}$ for concreteness. This then gives the initial field value[10] $\frac{\phi_i}{f} \approx 0.1\pi$ to get 60 e-foldings, using the effective potential in Eq. (3.55) and the analysis in Sec. 3.4. This gives the trigonometric functions $\sim \mathcal{O}(1)$ for both $\frac{\phi_i}{f}$ and $\frac{\phi_*}{f}$, as alluded to before in Sec. 3.4. The other essential parameters M_σ^2 and λ_σ

[10]This value changes slightly for different c_ϕ values, i.e. including the CW potential from Eq. (3.59).

are then fixed by the model requirements in Eqs. (3.56), (3.58), and (3.28). The right and bottom edges of the allowed parameter space correspond to naturalness constraints on m_ϕ (see Eq. (3.45)) and λ_σ (see Eq. (3.41)), respectively. The top and left edges correspond to the cutoffs in the ϕ and σ sectors being sub-Planckian, respectively. Here we consider $\Lambda_\phi \approx 4\pi f, \Lambda_\sigma \approx 4\pi \frac{M_\sigma}{\sqrt{\lambda_\sigma}}$ saturating the constraints in Eq. (3.43). Thus, the shaded region satisfies our naturalness and EFT consistency requirements. n_s is fixed to 0.9649, its central value from the Planck CMB constraints [5]. Varying its value up or down by a percent shifts the entire allowed region slightly to the left or right, respectively, by about a percent. The dashed lines show contours for H which are mostly horizontal (i.e. constant f/H, see Eq. (3.28)), but bending slightly upwards close to the right edge due to the CW potential contribution. As we can see in the figure, Λ_ϕ being sub-Planckian restricts the model to realize $H \lesssim 10^{11}$ GeV, while the λ_σ-naturalness gives a lower bound on H as $\sim 10^6$ GeV as expected from Eq. (3.47). The two cutoffs $\Lambda_\phi, \Lambda_\sigma$ are approximately equal on the dotted line. Thus, as the figure shows, demanding $\Lambda_\phi \approx \Lambda_\sigma$ can only realize H bigger than $\sim 10^{10}$ GeV. Only a small part of the parameter space lying above this dotted line corresponds to $\Lambda_\phi > \Lambda_\sigma$, while a majority of the allowed region has $\Lambda_\sigma > \Lambda_\phi$.

The Lagrangian of the $U(1)$ model in Eq. (3.50) contains terms only up to dimension-4. This will also include higher-dimensional terms respecting the symmetry in Eq. (3.51) and the spurion analysis mentioned thereafter, and thus will be of the form

$$\delta\mathcal{L}_{\text{UV,non-ren.}} \ni c_{nm} \frac{(\mu\Phi)^n \left(\sigma_i^2\right)^m}{\left(\Lambda^2\right)^{n+m-2}} \quad . \tag{3.60}$$

Here, the exponents n, m and the combinations of $\sigma_{A,B}$ in σ_i^2 will be such that they respect

the symmetry in Eq. (3.51). Also, for simplicity, we consider here a single UV cutoff scale Λ suppressing these non-renormalizable terms.[11] In order to satisfy naturalness in the σ-potential, it suffices to have $c_{0m} \lesssim (16\pi^2)^{m-2}\,\lambda_\sigma$. This mild requirement on the coefficients c_{nm} in Eq. (3.60), i.e. $c_{nm} \sim c_{0m} \lesssim (16\pi^2)^{m-2}\,\lambda_\sigma$, is sufficient to render the entire model natural, even at the non-renormalizable level, as illustrated below. The most vulnerable terms would be the super-renormalizable terms in Eq. (3.50), i.e. the bare and $\Phi-$dependent σ mass terms, which we collectively refer to as $M_\sigma^2(\Phi)$. The higher-dimensional terms in Eq. (3.60) can contribute to $M_\sigma^2(\Phi)$ at loop- or tree-level (i.e. after setting some fields to their VEVs) as

$$\frac{\delta M_\sigma^2(\Phi)}{M_\sigma^2} \sim \frac{c_{nm}(\mu\Phi)^n \cdot \langle\sigma\rangle^{2(m-1)}}{M_\sigma^2 \cdot \Lambda^{2(n+m-2)}} \lesssim \frac{(16\pi^2)^{m-2}(\mu\Phi)^n \cdot \langle\sigma\rangle^{2(m-2)}}{\Lambda^{2(n+m-2)}} \sim \left(\frac{\mu\Phi}{\Lambda^2}\right)^n \lesssim \left(\frac{\mu}{\Lambda}\right)^n, \tag{3.61}$$

which is negligible due to the suppression from $\frac{\mu}{\Lambda} \lesssim \frac{H}{4\pi f} \lesssim 10^{-6}$. Also, any higher-dimensional terms in Eq. (3.50) involving $|\Phi|^2$ will be sub-dominant since they will come with suppression factors of at least $\frac{|\Phi|^2}{\Lambda^2} \sim \frac{1}{16\pi^2}$.

3.6 Addressing the cosmological domain wall problem

Spontaneous breaking of an exact discrete symmetry, in our model $\sigma_i \to -\sigma_i$, during cosmological evolution, will lead to the formation of domains (with $\langle\sigma_B\rangle > 0$ or < 0) after the end of inflation, separated by cosmologically stable domain walls (DW). The energy density in these domain walls redshifts slower than both matter and radiation.

[11] It can be shown that even with different cutoff scales for ϕ and σ fields, analogous to what is shown here for $\Lambda_\phi \sim \Lambda_\sigma$, these non-renormalizable terms do not pose any danger to our model.

This gives rise to a late-time universe dominated by domain walls contrary to what is observed during Big-Bang Nucleosynthesis. This is the so called "cosmological domain wall problem" [169], which our Twinflation model faces for an exact $\sigma_i \to -\sigma_i$ symmetry. The σ fields could be charged under a $U(1)$ gauge symmetry, which then may not give rise to domain walls, but instead forms the much less constrained cosmic strings (see e.g. [170, 171, 172]). However, this approach requires additional fields and structures. Here we will consider a simple solution to the domain wall problem via small explicit breaking of the discrete symmetry.

We first note that $\sigma_i \to -\sigma_i$ symmetry is not an essential ingredient of our model and is used so far only for simplicity. We can hence add a small soft breaking of this symmetry in Eq. (3.31) or (3.52) via

$$V(\phi, \sigma_i) \ni M\sigma_i^3, \tag{3.62}$$

where M is a dimensionful spurion of this σ-parity breaking. This leads to a bias between the previously degenerate vacua as

$$\frac{\Delta V_{\rm bias}}{V_{\rm inf}} \sim \frac{M}{M_\sigma \sqrt{\lambda_\sigma}}, \tag{3.63}$$

where in the denominator we have $V_{\rm inf}$ which is also the typical size of the σ-potential. This bias provides a pressure force acting against the surface tension of the walls, eventually leading to their annihilation. Then, demanding that this annihilation of domain walls

happens before their cosmological energy domination, we need [173, 174, 175]

$$\mathcal{O}(1) \gtrsim \frac{\Delta V_{\rm bias}}{V_{\rm inf}} \gtrsim \frac{M_\sigma^2}{\lambda_\sigma M_{\rm Pl}^2}, \tag{3.64}$$

which can be realized in our model, using Eq. (3.63), by having

$$M_\sigma \sqrt{\lambda_\sigma} \gtrsim M \gtrsim \frac{M_\sigma^3}{\sqrt{\lambda_\sigma} M_{\rm Pl}^2}. \tag{3.65}$$

However, the cubic term in Eq. (3.62) radiatively generates the following σ-tadpole:

$$V(\phi, \sigma_i) \ni M \frac{\Lambda_\sigma^2}{16\pi^2} \sigma_i \sim M \frac{M_\sigma^2}{\lambda_\sigma} \sigma_i. \tag{3.66}$$

Tadpole terms of this order shift the minimum in σ_i in a ϕ-dependent way as

$$\delta\sigma_i(\phi) \sim \frac{M M_\sigma^2}{\lambda_\sigma M_{\sigma_i}^2(\phi)} \sim \frac{M}{\lambda_\sigma} \left(1 \pm \frac{\sin(\phi/f)}{\sin(\phi_*/f)}\right)^{-1}, \tag{3.67}$$

where $M_{\sigma_i}^2(\phi) = M_\sigma^2 \pm \mu f \sin(\phi/f)$ is the ϕ-dependent mass-squared for σ_i (see Eq. (3.52)). This shift contributes to the effective inflaton potential as[12]

$$\delta V_{\rm eff}(\phi) \sim \sum_{i=A,B} \frac{M^2 M_\sigma^4}{\lambda_\sigma^2 M_{\sigma_i}^2(\phi)} \sim \frac{M^2 M_\sigma^2}{\lambda_\sigma^2} \left(1 - \frac{\sin^2(\phi/f)}{\sin^2(\phi_*/f)}\right)^{-1}. \tag{3.68}$$

Demanding that this contribution is sub-dominant to the inflaton potential implies

[12] As $\phi \to \phi_*$, i.e. towards the end of inflation, the expressions in Eqs. (3.67), (3.68) seem to diverge. However, this is because the effective mass for σ_B vanishes at ϕ_*, and hence we have to balance the σ-tadpole with σ-cubic which will modify these expressions close to ϕ_*.

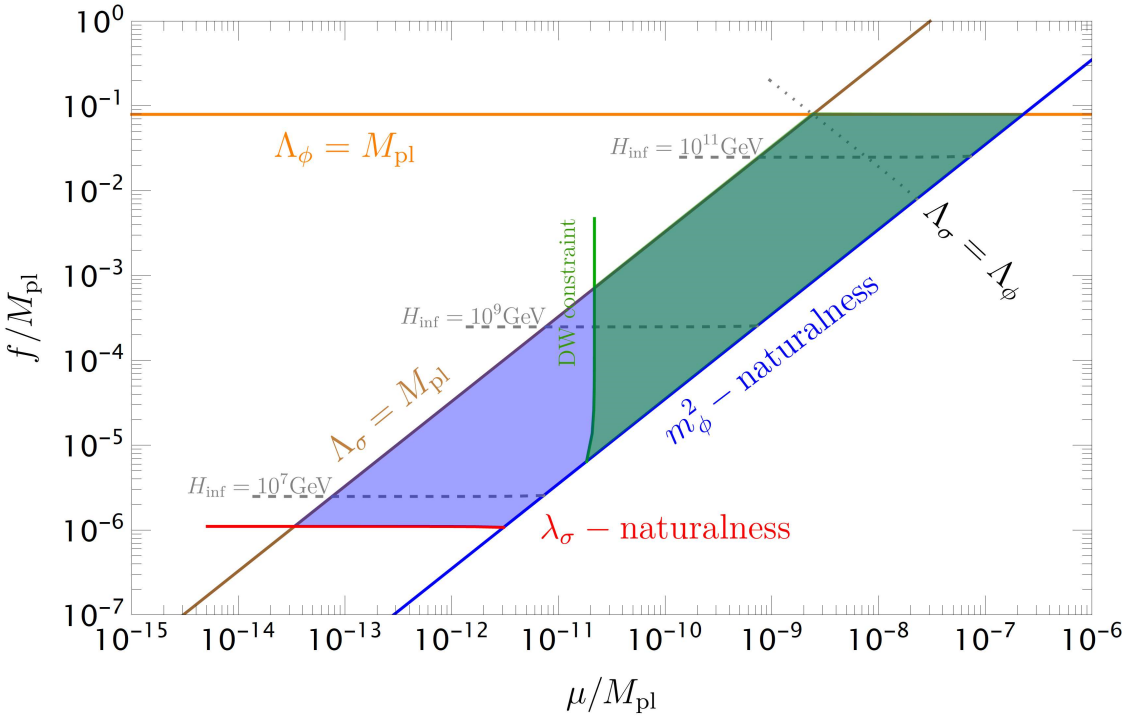

Figure 3.2: Addressing the cosmological domain wall problem in Twinflation: The blue region (same as in Fig. 3.1) satisfies our naturalness and EFT consistency requirements. Small explicit breaking of σ-parity (see Eq. (3.62)) solves the domain wall problem. Its contribution to $V_{\rm eff}(\phi)$, via the natural value of σ-tadpole, is sub-dominant in the green region shown above.

$$1 \gtrsim \frac{\delta V_{\rm eff}(\phi)}{V_{\rm eff}(\phi)} \sim \frac{16\pi^2 M^2}{c_\phi \lambda_\sigma^2 M_\sigma^2} \gtrsim \frac{16\pi^2 M_\sigma^4}{c_\phi \lambda_\sigma^3 M_{\rm Pl}^4}, \tag{3.69}$$

where in the last step we have used Eq. (3.65). Then, using our model requirements – $\lambda_\sigma \sim \frac{M_\sigma^4}{H^2 M_{\rm Pl}^2}$, $M_\sigma^2 \sim \mu f$, $\frac{f}{H} \sim 10^6$ – we get the constraint for the allowed parameter region as

$$\sqrt{c_\phi}\frac{\mu^2}{f M_{\rm Pl}} \gtrsim 10^{-17}. \tag{3.70}$$

This is evaluated numerically and shown in Fig. 3.2 as the green region. We can also note

here that this now gives a lower bound on the Hubble scale as

$$H \gtrsim 10^7 \text{GeV}, \tag{3.71}$$

which is $\sim \mathcal{O}(10)$ bigger than that obtained in Eq. (3.47).

Thus, the cosmological domain wall problem can be solved in our model by introducing a small explicit breaking of σ-parity at the cost of some reduction in the allowed parameter space as shown in Fig. 3.2. One might explore more general ways of explicit σ-parity breaking than the simple one we considered here via Eq. (3.62), possibly allowing for viable hybrid inflation in the entire blue region. We leave this exploration for a future study.

3.7 Discussion

In the present work, we build a viable, natural, and EFT-controlled model of low-scale hybrid inflation, "Twinflation". Here, inflation happens somewhat near the hilltop of the effective inflaton potential, although without any fine-tuning of the initial position. This gives rise to the red tilt in the scalar perturbations, consistent with the observations. The quadratic sensitivity to the UV cutoff scales in the inflaton potential, induced by its necessarily non-derivative coupling with the waterfall field, is removed by a twin symmetry. All the parameters take (technically) natural values, without any fine-tuning. All the mass scales and field values are below the respective UV cutoff scales and also the Planck scale, thus rendering the model under (straightforward) EFT control. This model can realize low-scale inflation with the Hubble scale as low as $\sim 10^6$ GeV (see Fig. 3.1).

It is therefore easily consistent with the smallness of the yet-unobserved primordial tensor fluctuations, which could be unobservably small ($r \sim 10^{-16}$) for the lowest Hubble scales realized in our model.

Spontaneous breaking of the discrete symmetry $\sigma_i \to -\sigma_i$ towards the end of inflation will lead to cosmic domain wall formation in the post-inflationary universe. One simple way to be compatible with our universe on the large scales at late times, is to demand that such domain walls should annihilate before they start dominating the cosmic energy density. As discussed in Sec. 3.6, we show that this can be easily implemented in our model with a small explicit breaking of the σ-parity, which we only considered for technical simplification in any case. This, however, can be achieved only in the parameter space as shown in Fig. 3.2, allowing for the smallest inflationary Hubble scale to be $\sim 10^7$ GeV. We expect that allowing for more general ways of explicit σ-parity breaking can possibly relax this constraint, which we leave for a future study. It is also interesting that the domain wall dynamics can give rise to a stochastic gravitational wave (GW) background observable in future GW experiments. See [175] for a review.

Hybrid inflation models typically require fine-tuned couplings. However, our model does not require any fine-tuning in the parameters to achieve radiative stability. With regards to the initial conditions, we also showed that there is no tuning required in the initial inflaton field location, i.e. it need not start very close to the hilltop and can have a transit of $\sim \mathcal{O}(f)$. A large initial inflaton velocity can be compensated by starting more uphill along the potential, up to the hilltop. However, demanding that it first damps to the terminal slow-roll velocity, then gives the required number of e-foldings of slow-roll inflation before entering the waterfall phase, we see that the initial velocity has to be sufficiently

small: $\frac{\dot{\phi}}{f^2} \lesssim \frac{H}{f} \sim 10^{-6}$. (See also [176] for similar constraints.) Furthermore, there is the question of whether inflation can begin in an inhomogeneous spacetime. Numerical simulations show that whereas large-field inflation models are less susceptible to inhomogeneities preventing the onset of inflation, small-field inflation models may be more so [145, 177, 178, 179, 180, 181]. These issues can however be addressed, for example, by invoking tunneling from a prior metastable vacuum in the landscape of the theory, which naturally gives rise to a state with small field velocity and inhomogeneity (see e.g. [182, 183, 184, 185]).

It would obviously be very interesting if we could directly observe the waterfall field(s) (σ_i) via their mediation of primordial non-Gaussianity (NG), using the idea of "Cosmological Collider Physics" [108, 115]. Ordinarily such signals would be strongly "Boltzmann"-suppressed by $e^{-\pi M_\sigma/H}$, since $M_\sigma \gg H$. However, the recently discussed "scalar chemical potential" mechanism [186] may eliminate this suppression and be compatible with our twin symmetry structure. We leave an exploration of this to future work.

As discussed in the Introduction, a variety of UV physics scenarios may give rise to unwanted defects or relics like monopoles, moduli, gravitino (see e.g. [47, 48, 49, 50]). Different UV scenarios can also exhibit a meta-stable high temperature phase in which the universe can remain stuck if the phase transition to the familiar low temperature phase fails to complete [187]. Reheating of the universe at a low temperature, following inflation with a low Hubble scale, might help to address these issues in a straightforward way. Another motivation towards low-scale inflation can come from the constraints on isocurvature perturbations sourced by (QCD) axionic dark matter (see e.g. [5, 45, 46]). If

the Peccei-Quinn symmetry is broken during inflation, axions source dark matter isocurvature perturbations which are stronger for higher H (for any given axion decay constant, f_a), the non-observation of which thus prefers low-scale inflation. Furthermore, with current and future collider experiments, such as a future $\sim \mathcal{O}(100)$ TeV collider, we might have the opportunity to investigate the physics during and after such a low-scale inflation in laboratory searches too, along with the cosmological ones!

Chapter 4: New physics opportunities for long-lived particles at electron-proton colliders

4.1 Introduction

Progress in high energy physics relies on designing new experiments to explore ever higher mass scales and smaller interactions [188]. This is vital both to understand the Standard Model (SM) at new energy regimes, as well as for the discovery of Beyond SM (BSM) physics. As the Large Hadron Collider (LHC) makes impressive progress exploring of the TeV scale, it is therefore a high priority to look ahead and identify the most important physics opportunities presented by the next round of proton and electron colliders.

Lessons learned from the LHC era provide important context for any future collider program (see e.g. ref. [189]). When the LHC experiment was designed more than two decades ago, the main focus was the discovery of the Higgs boson and searches for BSM theories like supersymmetry (SUSY) [34]. This meant that identification of high energy final states, copiously produced in prompt decays of intermediate particles with masses around the TeV scale, was paramount. The exploration of this canonical "High Energy Frontier" will be an important goal for future experiments, but the ab-

sence (to date) of any such BSM signatures at the LHC presents us with an important puzzle: How do we reconcile LHC null results with the fact that motivation for BSM theories is as strong as ever? The hierarchy problem has been sharpened by the discovery of the Higgs and explicitly calls for TeV-scale new physics, while dark matter, baryogenesis and neutrino masses continue to beg for explanations. An important lesson of the last decade is that these fundamental mysteries can be addressed by theories which have signatures very unlike the high energy SUSY signals of the canonical high energy frontier. Hidden valleys [59, 60, 61, 62, 63, 64], Hidden Sectors connected to Dark Matter [65, 66, 67, 68, 69, 70], Neutral Naturalness [52, 71, 72], WIMP baryogenesis [73, 74, 75, 76], many varieties of SUSY [53, 54, 55, 56, 57, 58], and right-handed neutrinos [77, 78, 79, 80, 81, 82, 83] might only show up in "exotic channels" like Long-Lived Particle (LLP) signatures. It is important that future colliders can explore this "Lifetime Frontier" as well as the High Energy or High Intensity Frontiers.

Future colliders: Most proposals fall into two categories: lepton or hadron colliders. The proposed e^+e^- colliders, namely the ILC in Japan [190, 191], the CEPC in China [192], and the FCC-ee (formerly known as TLEP) [193] and CLIC at CERN [194] are ideal for precision measurements of the Higgs boson properties due to their exquisitely clean experimental environment. The sensitivity of the Higgs to the existence of new physics (see e.g. [195]) makes this an endeavor of the highest priority, but direct discovery of new BSM states at such machines is generally less likely, since their center of mass energy is below that of the present LHC.

On the other hand, presently discussed future pp colliders like the FCC-hh at CERN [196, 197, 198] or the SppC in China [199] would offer enormous center of mass energies at

the 100 TeV scale as well as huge event rates for many weak-scale processes like Higgs Boson production. This would enable them to probe very high mass scales and very rare processes, provided the final states can be identified in such an extremely high-energy high-rate environment.

There is a hybrid of these two approaches which is less often discussed: electron-proton colliders. HERA was the only such machine ever built, and it was instrumental to establish the inner structure of the proton via deep inelastic scattering (DIS) measurements. The resulting information about Parton Distribution Functions (PDFs) is now part of textbooks and Monte Carlo generators. This was HERA's primary objective, and its successes are of foundational importance for high energy measurements and BSM searches at pp colliders like the Tevatron and the LHC. HERA's direct contributions to BSM searches, however, were much more limited. The electron-proton initial state does not give rise to large cross sections for many BSM processes, and HERA's center-of-mass energy of $\sqrt{s} = 320\ \mathrm{GeV}$ and integrated luminosity of $\sim 500\ \mathrm{pb}^{-1}$ was far below the Tevatron's $1.96\ \mathrm{TeV}$ and $10\ \mathrm{fb}^{-1}$. As a result, HERA was outclassed in mass reach for almost all BSM signatures, with the exception of some leptoquark scenarios [200, 201].

Beyond HERA: Plans for electron-proton colliders have evolved considerably since HERA. Modern proposals envision them an "add-on" or "upgrade" to an existing high-energy pp collider, at a cost that is roughly an order of magnitude below that of the pp machine alone. The LHeC proposal [6, 86, 87] consists of a 60 GeV high-intensity linac supplying the electron beam to meet the 7 TeV proton beam at a collision point in the LHC tunnel. This includes a dedicated detector, with a geometry that accommodates the asymmetric nature of the collision. The LHeC would have a center of mass energy of

1.3 TeV and is planned to deliver up to 1 ab^{-1} of collisions over its approximately 10-year lifetime, a drastic increase of energy and especially luminosity compared to HERA. An analogous proposal, FCC-eh, exists for a future 100 TeV pp collider at CERN [88], but one could just as easily imagine such an extension for the HE-LHC [202] or the SppC [199].

Future machines like the LHeC or the FCC-eh would greatly advance our knowledge of the proton [203] with many important benefits for the main pp program, but the physics potential does not stop there. Future e^-p machines can access mass scales beyond the energies of lepton colliders, while maintaining a clean experimental environment and delivering high luminosity, all for a fraction of the cost. This explains their perhaps surprising ability to support a strong precision Higgs program [204, 205, 206, 207, 208]: LHeC measurements of Higgs couplings relying on Vector Boson Fusion (VBF) production might be competitive with electron colliders (albeit without the important model-independent measurement of the Higgs width via Zh production).

Could we harness this unique experimental setup to explore hitherto inaccessible BSM signatures as well? Previous studies exploring the BSM reach of future e^-p colliders mostly focused on *production modes* that allowed for large signal rates from the asymmetric initial state: leptoquarks [6], 4^{th} generation quarks [209] or excited leptons [210], right-handed (RH) neutrinos [84, 210, 211, 212, 213], and left-right symmetric models with new gauge bosons in the t-channel [214, 215]. However, in all of those cases, with the exception of RH neutrino models (which include LLP signals [84]), the LHC or HL-LHC has higher mass reach [216, 217, 218, 219, 220, 221, 222]. This is a familiar echo of the HERA-Tevatron interplay. One might think naïvely that this puts

a damper on the BSM motivation for electron-proton colliders, but we argue that this conclusion is premature.

In fact, we argue that e^-p colliders are uniquely suited to discover new physics, with strengths that are truly complementary to both pp and e^+e^- programs. Given the unknown nature of new physics signatures in light of the LHC puzzle, this makes e^-p colliders a vital component of a future high energy physics program.

Focusing on the final state: Rather than focusing on BSM scenarios with large production rates, we suggest focusing on BSM scenarios which give rise to *final states that look like hadronic noise* in the pile-up-rich environment of pp colliders. The clean environment of the e^-p collider allows for their unambiguous reconstruction, while their large center-of-mass energies allow them to access higher mass scales than lepton colliders. This view is tentatively backed up by the encouraging results of the initial precision Higgs and RH neutrino studies, which relied heavily on the clean experimental environment. The shifted focus from initial to the final state also allows us to consider more general BSM production modes like VBF, which are present in any theory with new electroweak charged states. We consider LLP signatures to demonstrate the utility of this new paradigm.

Long lived particles: New states with macroscopic lifetime are extremely broadly motivated. They often emerge as result from basic symmetry principles of Quantum Field Theory and are highly generic in BSM theories, where states can be long-lived due to approximate symmetries, modest mass hierarchies, or sequestration of different sectors in a UV completion. As outlined above, they are ubiquitous in theories of hidden valleys and general hidden sectors, and are the smoking gun signal of Neutral Naturalness, certain

varieties of SUSY, theories explaining the origin of neutrino masses, as well as many baryogenesis and dark matter scenarios.

LLPs can be detected directly via their passage through the detector material if they are charged or colored (and long-lived enough), or by reconstruction of a *displaced vertex* (DV) if they decay in the detector. They are not picked up by most standard searches focusing on prompt signals, making them consistent with recent LHC null results. However, the spectacular nature of these signals means that *dedicated* LLP searches typically have very low backgrounds, often allowing for discovery with just a few observed events at the LHC or future colliders [78, 83, 84, 223, 224, 225, 226] There are, however, important regions of LLP signature space which are very difficult for pp colliders to probe, due to low signal acceptance, trigger thresholds, or sizable backgrounds. This includes (i) invisible LLPs with very long lifetimes that escape the main detectors, (ii) LLPs with very soft decay products, and (iii) LLPs with very short lifetimes $\lesssim$ mm, making them difficult to distinguish from hadronic backgrounds. Recent proposals for dedicated external LLP detectors near an LHC collision point, like MATHUSLA [227, 228], milliQan [229], CODEX-b [230] and FASER [231], aim to address the first of these shortcomings. The second and third class of signals are prime targets for $e^- p$ colliders.

We examine two important BSM signatures at $e^- p$ colliders after briefly reviewing the salient details of these proposals in Section 4.2. We study Higgsinos in Section 4.3. If the winos are decoupled, the charged Higgsino can have a lifetime of up to several mm, decaying to often just a single soft pion via a small mass splitting to the neutral Higgsino. This decay cannot be reconstructed at pp colliders, forcing searches to rely on monojet or disappearing track signals. In the clean environment of $e^- p$ colliders, these

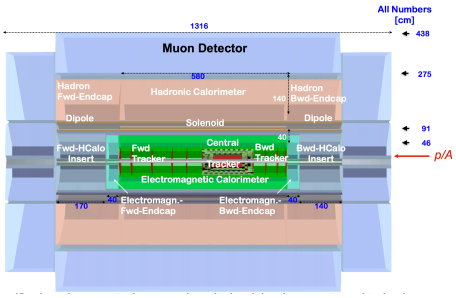

Figure 4.1: Possible layout of the LHeC detector, figure from [6].

soft displaced final states can be explicitly reconstructed, and lifetimes many orders of magnitude shorter than those accessible by pp colliders can be probed at masses far beyond the reach of lepton colliders. To demonstrate the utility of e^-p colliders for general LLP signals with very short lifetime, we also consider LLP production in exotic Higgs decays in Section 4.4. Again, the e^-p searches outperform searches for pp colliders by orders of magnitude for very short lifetimes. We conclude in Section 4.5.

4.2 Electron-proton collider basics

Electron-proton colliders are hybrids between e^-e^+ and pp colliders. Today's proposals consider electron beams from a linac that intersect with the hadron beam from an existing pp collider (though using an electron beam from a circular collider would also be possible). Such machines allow for a clean collision environment with very little pile-up, center-of-mass energies of $\mathcal{O}(1)$ TeV and luminosities of $1\ \mathrm{ab}^{-1}$ or more.

The Large Hadron electron Collider (LHeC) [6, 86, 87] is a proposed upgrade for the high luminosity phase of the LHC. It foresees the construction of a high-intensity electron accelerator adjacent to the main rings. The resulting 60 GeV e^- beam would

meet the 7 TeV proton beam from the LHC at a dedicated interaction point in the HL-LHC tunnel, with an envisaged total luminosity of $1\ \mathrm{ab}^{-1}$ at a 1.3 TeV center-of-mass energy over the lifetime of the program. We remark that higher electron beam energies are also discussed [6]. The collisions would be analyzed in a general-purpose detector, with an adjusted geometry to accommodate the asymmetric collision.

An even more powerful electron-proton collider is discussed as part of the Future Circular Collider design study, namely the Future Circular electron-hadron Collider (FCC-eh) [88]. The FCC-eh is based on the electron beam from the LHeC facility, colliding with the 50 TeV proton beam from the hadron-hadron mode of the FCC. The final integrated luminosity is currently assumed to be $\sim 1\ \mathrm{ab}^{-1}$, at center-of-mass energies up to 3.5 TeV [203]. In the following, we will refer to this experimental setup as the FCC-eh (60) to indicate the electron beam energy.

The goal of our study is to assess the BSM potential of $e^- p$ colliders, which should be a major design driver for the electron accelerator and detector. The FCC-eh specifications are much less finalized than the LHeC, and it is instructive to consider alternatives to the existing proposal, and how they differ in BSM reach. We will therefore also discuss a version of the FCC-eh which represents a less realistic setup, which might be feasible *in principle*: an electron beam with energy 240 GeV meeting the 50 TeV proton beam, to generate center-of-mass energies of 6.9 TeV. We refer to this scenario as the FCC-eh (240). Such a high energy electron beam would be challenging to implement, but there are several options, including a nearby ILC or CLIC-like facility. [1] Morevoer, since the

[1] One could also consider to make use of a high-energy circular electron-positron collider in the same tunnel (as is planned in the CEPC/SppC project in China). In this case, however, it is unlikely that comparable luminosities to the FCC-eh(60) can be achieved.

benchmark luminosity of the FCC-hh program is $\sim$10 times higher than foreseen for the HL-LHC, we also allow for the analogous possibility of $10\ \mathrm{ab}^{-1}$ at the FCC-eh (60) and FCC-eh (240).

The LHeC detector layout from the technical design report is shown in Fig. 4.1 [6]. Precise details of the detector are not relevant for our benchmark studies, and we only focus on the most salient features. For concreteness, and also to be somewhat conservative, we assume the same detector capabilities for the FCC-eh as for the LHeC (though this does not affect our qualitative conclusions).

Notable is the tracker coverage to very high rapidity of 4.7 in the forward and backward direction with respect to the proton beam, starting at a distance of about 3cm from the beams. The detector has a magnetic field of ~ 3.5 T, and the nominal tracking resolution is 8 μm. Studies for ILC detectors show that impact parameter resolutions down to $\sim$5 μm may be possible [232, 233, 234]. To assess the importance of tracking resolution on LLP reach, we therefore consider resolutions of 5, 8 and 16 μm. The elliptical interaction point has rms dimensions of 7 μm in the transverse plane and 0.6 mm along the longitudinal beam direction. Charged hadronic tracks with energies above few GeV are generally accepted by the calorimeters. However, since we will be considering LLPs that decay to soft low-multiplicity hadrons, precise energy thresholds will be important. To assess their impact on LLP reach we consider p_T thresholds of 50, 100 and 400 MeV for reliable reconstruction of a single charged particle track. The trigger capabilities of the tracking system are not yet completely defined [6], but since DIS measurements are a major design driver, we assume that single jets with $p_T > 20\ \mathrm{GeV}$ can be triggered on with high efficiency. This means trigger considerations will not play a major role in our

analyses.

With the above specified performance parameters, the corresponding $e^- p$ collider concepts offer center-of-mass energies larger than all but the most ambitious lepton collider proposals, while maintaining a very clean experimental environment. In comparison to pp colliders, the various hadronic backgrounds have very different distributions and are strongly suppressed. At the LHeC, the pile-up is expected to be ~ 0.1 per event, while for the FCC-eh (60) it may rise to ~ 1. We will consider analysis strategies which take advantage of, but are robust with respect to, these low pile-up levels.

4.3 Long-lived Higgsinos

The electroweakinos (EWinos) of the MSSM are well-motivated candidates for LLPs. The mixing of the Bino, Wino and Higgsino fields gives rise to four neutralino and two chargino mass eigenstates.

If the mixing of these particles is significant they can be detected at hadron colliders via searches for high energy leptons and missing energy [235, 236].

In the following we consider the challenging limit of small mixing. In that case, the masses of the lightest Higgsino (Wino) chargino and the lightest neutralino are only slightly split due to electroweak symmetry breaking loop effects.[2] The difference between these two masses, referred to as the 'mass splitting' (Δm) in the following, is $\mathcal{O}(100)$ MeV which corresponds to a lifetime $c\tau \sim 7\mathrm{mm}$ (~ 6 cm). Charged LLPs with this lifetime, decaying into a massive neutral particle, can be searched for at the

[2]These cases are often referred to in the literature as 'pure' limits. We note that a 'pure Bino' that is stable on cosmological time scales and thus a viable dark matter candidate needs to be lighter than 100 GeV not to overclose the universe, which is ruled out by LEP searches[237].

LHC via so-called 'disappearing-track searches'. Owing to the larger lifetime and four times larger production cross section,[3] Wino searches have significant mass reach at the LHC and FCC-hh [238, 239]. Searches for Higgsinos are much more challenging, and a customized tracker with sensitivity to shorter lifetimes is needed, as shown in ref. [7] (see also ref. [240]). Due to the almost-degenerate mass spectrum, the leptons and jets from the chargino decay have very small momenta and thus largely fail to pass reconstruction thresholds of the LHC analyses. Depending on the value of Δm, searches that include an ISR jet and additional 'soft' leptons can yield relevant constraints [241, 242, 243, 244, 245, 246, 247, 248, 249]. In scenarios where the mass splitting of the electroweakinos is given by the loop effects only, the relevant signature at the LHC is the missing energy, which is included in the so-called mono-jet searches.

There are important incentives to study Higgsino signatures beyond their role in supersymmetry. Neutral Higgsinos are thermal DM relics that can yield the observed relic density if their masses m_χ is around 1.1 TeV [250] or below (depending on mixing). Furthermore, the lessons learned from studying pure Higgsinos can easily be transferred to theories with similar phenomenology, for instance models with inert multiplets [251, 252, 253] and vector-like leptons (see e.g. [254, 255, 256, 257, 258, 259]), which are also interesting in the context of minimal models for gauge unification [260, 261]. This makes the 'pure-Higgsino' case very theoretically compelling, even as their low production cross section, soft decay products, and short lifetime make them the most experimentally challenging electroweakino scenario at proton-proton colliders.

In the remainder of this section we review the main phenomenological features,

[3] The Casimir group factor is given simply by T_3^2.

branching ratios and lifetimes of Higgsinos. After setting the stage by summarizing current and projected constraints from cosmology and pp colliders, we show how $e^- p$ colliders can fill in crucial gaps in coverage.

4.3.1 Higgsino Phenomenology

The spectrum and interactions of EWinos in the MSSM has been studied in depth [34, 262], and we only focus on the aspects relevant for our analysis here. In the decoupled Wino limit where $\mu \ll M_2$ and $\mu < M_1$ there is one charged state $\chi^\pm$ and three neutral $\chi_i^0, i = 1, 2, 3$. The mass of the charged state receives the 1-loop correction from EW gauge bosons, $\Delta_{1-\text{loop}}$. In the neutral sector the two lighter states are at about the scale μ split by Δ_0 and the third one at the heavy scale M_1. The latter does not impact directly on the phenomenology, but rather dictates Δ_0. One can thus trade the Lagragian parameters $\mu, M_1, \tan\beta$ for the mass of the lightest neutralino $m_{\chi_1^0}$ and the mass splitting with respect to the chargino ($\Delta m \equiv m_{\chi^\pm} - m_{\chi_1^0}$) and to the second neutralino ($\Delta_0 \equiv m_{\chi_2^0} - m_{\chi_1^0}$). The relevant expressions read

$$\begin{aligned} m_{\chi_1^0} &= |\mu| - \frac{m^2(1+\text{sign}(\mu)s_{2\beta})}{2M_1(1-|\mu|/M_1)}\,, \\ \Delta m &= \Delta_{1-\text{loop}} + \frac{m^2(1+\text{sign}(\mu)s_{2\beta})}{2(M_1-|\mu|)}\,, \\ \Delta_0 &= \frac{m^2}{M_1}\Big(\frac{1+\text{sign}(\mu)s_{2\beta}\mu/M_1}{1-\mu^2/M_1^2}\Big)\,, \end{aligned} \tag{4.1}$$

where $\tan\beta = v_u/v_d$, and the above results assume $m = m_Z s_W \approx 44\ \text{GeV} \ll |M_1 - \mu|$. We consider M_1 to be real and positive, while μ is real with either sign. $\Delta_{1-\text{loop}} \sim 300\ \text{MeV}$ has very modest dependence on $m_{\chi^\pm}$, and one can see from the above expres-

sions that the dependence on $\tan\beta$ is modest as well. For concreteness, we take in our analysis $\tan\beta = 15$. The choice of $m_{\chi^\pm}$ and Δm then determines the spectrum. Note that $\Delta m = m_{\chi^\pm} - m_{\chi_1^0} > \Delta_{1-\text{loop}} > m_{\chi^\pm} - m_{\chi_2^0}$. Upscattering in direct detection experiments [263, 264] forces $\Delta_0 \gtrsim 0.1$ MeV, which implies an upper bound on $M_1 \lesssim 20$ PeV.

The neutralino couplings to the gauge bosons follow from the EW charges. The three particles with masses $\sim |\mu|$ are 'almost-doublets', and hence the Z-current couples χ_1^0 and χ_2^0 with 'almost-full' strength. Both the Z and Higgs interactions with the DM candidate χ_1^0 arise from doublet-singlet mixing, and hence they are suppressed by powers of $m_Z/|\mu|, m_Z/M_1$, which also suppresses the direct detection cross section, see section 4.3.2 below.

The decay modes of the long-lived chargino are computed using the expressions in refs. [265, 266] and shown in Fig. 4.2. Chargino decays to χ_1^0 are always allowed with a mass splitting greater than $\Delta_{1-\text{loop}}$, which sets the maximum possible lifetime in this model (though longer lifetimes can be considered in more general scenarios). If M_1 is much larger than $|\mu|$, the lifetime gets reduced by a factor of 2, as the chargino decays with a similar width to each neutralino. Note that this is unlike the Wino case, where there is only one neutralino in the low energy spectrum. For lower values of M_1, the chargino decays to χ_2^0 become smaller. The hadronic decay widths require some care due to the small mass splitting. For $\Delta m \lesssim 1$ GeV, one must compute partial widths to exclusive hadron final state like $\pi^+\chi_1^0$. For $\Delta m \gg 1$ GeV, quarks are the relevant degrees of freedom, and hadronic decays give rise to jets which shower and hadronize.

In practice, we compute hadronic final states both in the exclusive hadron picture

and the inclusive quark picture, and define Δm_* as the mass splitting where $\sum \Gamma(\chi^\pm \to \text{hadrons} + \chi_1^0) = \sum \Gamma(\chi^\pm \to \text{quarks} + \chi_1^0)$. For $\Delta m < \Delta m_*$ we then use the hadron picture and for $\Delta m > \Delta m_*$ we use the quark picture, which is responsible for the sharp turn-over at $\Delta m \approx 1.75$ GeV in Fig. 4.2. This unphysical sharp turn-over between the two regimes is sufficient at the level of detail of our study. To capture the effect of hadronization uncertainties, we follow ref. [265] and compute the partial decay widths to quarks assuming $m_d = 0.5$ GeV and $m_d = 0$ GeV, with different Δm_* for each case.

We note a few important features of the branching ratios in Fig. 4.2. At small mass splitting, decays to both χ_1^0 and χ_2^0 are kinematically allowed while for larger mass splittings all decays are to χ_1^0. Our region of interest for displaced searches is $c\tau \gtrsim \mu m$, corresponding to $\Delta m \lesssim 2.5$ GeV. The branching fractions have some quantitative (but not qualitative) dependence on $\text{sign}(\mu)$, but very little dependence on $m_{\chi^\pm}$ itself. As mentioned above, the minimal mass splitting is given by $\Delta_{1-\text{loop}}$ and larger mass splittings are possible when M_1 is closer to μ, although for our region of interest M_1 is still several TeV to tens of TeV.

On our scenario, LEP excludes χ^+ masses below 104 GeV [237]. The existing LHC searches for soft leptons [267] are currently only sensitive to $\Delta \sim 20$ GeV. The prospects of the HL-LHC and of future colliders are summarized below.

4.3.2 Probing Higgsinos with pp colliders and cosmology

To understand the unique role $e^- p$ colliders could play in the exploration of Higgsino parameter space, we briefly review the reach of future pp colldiers, as well as

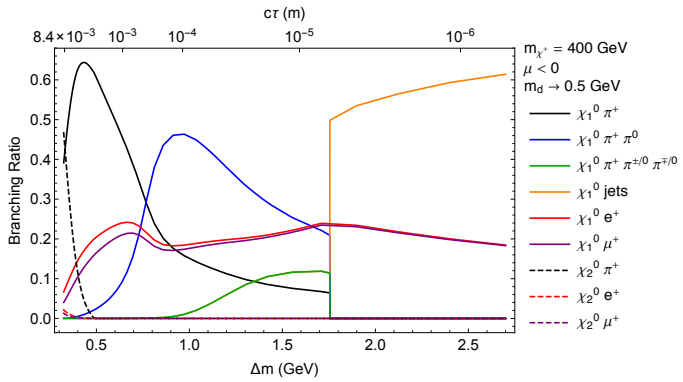

Figure 4.2: Decay branching ratios for a 400 GeV charged Higgsino as a function of $\Delta m = m_{\chi_1^\pm - \chi_1^0}$ and $\mu < 0$. Note the chargino lifetime on the upper vertical axis. Hadronic decay widths are computed assuming $m_d = 0.5$ GeV. The switch from an exclusive hadronic final state description to an inclusive jet final state description occurs at around $\Delta m \approx 1.75$ GeV, which decreases to 1.3 GeV if the assumed m_D is taken to zero. The $\mu > 0$ case is qualitatively very similar, and there is very little dependence on the Higgsino mass.

projected cosmological bounds from dark matter direct and indirect detection. This is summarized in Fig. 4.3.

Searches at future pp colliders

The dominant production mode for EWinos at pp colliders are s-channel Drell-Yan-like processes. The cross section is much larger than at $e^- p$ colliders, which offers opportunities to search for pure Winos with large decay lengths. A challenge in the high-energy environment of pp collisions is that the SM final state from the chargino decays are often very soft (sometimes just a single pion) which cannot be reliably reconstructed. It is therefore difficult to find the corresponding displaced secondary vertex in this environment: the signal gets swamped by the surrounding hadronic activity, and becomes part of the "hadronic noise".

One promising search strategy is the so-called "disappearing track search", which

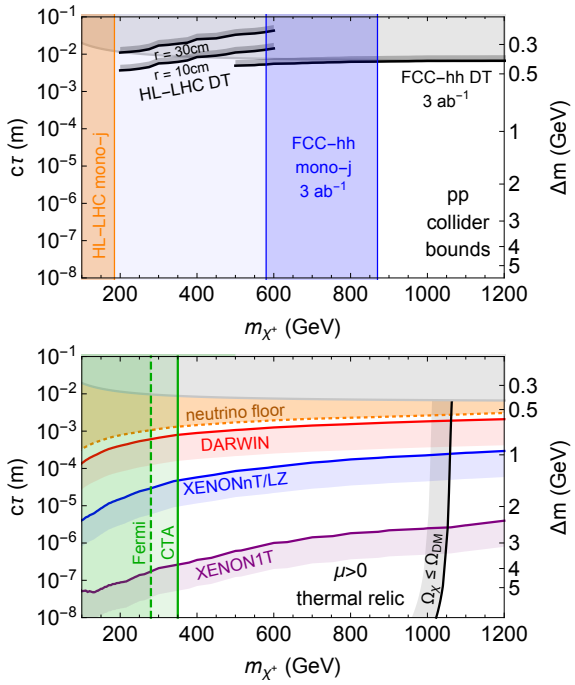

Figure 4.3: Projected Higgsino bounds from future pp colliders (top) and cosmology (bottom). *Top:* Vertical bands indicate the approximate projected mass reach of monojet searches, with darker shading indicating the dependence of reach on the assumed systematic error. Regions above black contours can be excluded by disappearing track searches [7] at the HL-LHC (optimistic and pessimistic) and FCC-hh. See text for details. *Bottom*: Longer lifetimes indicate smaller direct detection signal, hence the bounds from XENON1T [8], XENONnT [8]/LZ [9] and DARWIN [10] are sensitive to the region *below* the colored contours. The orange region lies below the neutrino floor for direct detection. Also shown is the approximate mass exclusion of Fermi (existing) and CTA (projected). The black line indicates the maximum mass for the Higgsinos such that their relic abundance is at most $\Omega_{\rm DM}$. The $\mu < 0$ case is nearly identical. Relic density and direct detection bounds are taken from [11]. Grey upper region indicates lifetimes corresponding to smaller mass splittings than the minimal electroweak contribution.

targets the traces that the long-lived chargino leaves in the tracker of the detector. This strategy relies on the chargino to reach the first few inner tracking layers, which severely limits the sensitivity for short lifetimes. At the HL-LHC the disappearing track searches have a mass reach up to $\sim$ 200 GeV with standard tracking if $c\tau \sim$ 7mm ($\Delta m = \Delta_{1-\text{loop}}$) [7, 238, 240]. Hypothetical upgrades to the HL-LHC trackers in the high-rapidity region could increase mass reach to about 380 GeV. We show these two scenarios in Fig. 4.3 (top), using the results from [7]. (This study examined Higgsinos heavier than 200 GeV, but the proposed search would have sensitivity to lower masses as well.) The pessimistic HL-LHC disappearing track reach projection assumes that the Higgsino must reach a transverse distance of 30cm, while the optimistic projection only requires 10cm. The realistic reach likely lies between these estimates, but we point out that recent ATLAS tracker upgrades should allow for the reconstruction of Higgsinos that travel 12 cm [268].

At future 100 TeV colliders like the FCC-hh or the SppC with 3 ab^{-1} of luminosity,[4] disappearing track searches can probe $m_\chi \sim 1.1$ TeV if $\Delta m \sim \Delta_{1-\text{loop}}$ assuming a chargino traveling 10cm can be reconstructed, but the reach disappears for shorter lifetimes [7, 240].[5] These sensitivity projections are also shown in Fig. 4.3 (top).

Another strategy is the search for the missing mass that is carried away by the neutral heavy final state. Studies show that such so-called "monojet searches" can probe pure Higgsinos with masses up to $\sim 100 - 200$ GeV at the HL-LHC [238, 243, 249, 269], depending on assumptions about systematic errors. At future 100 TeV collider (see e.g. refs. [238, 270, 271, 272, 273]), significantly higher masses of $\sim 600 - 900$ GeV [238]

[4] Since many recent benchmarks assume 30 ab^{-1} luminosity for future 100 TeV colliders [196, 198], these reach estimates may be conservative.

[5] The reach can be improved considering improved forward tracking close to the beam pipe compared to current benchmark detector proposals.

can be probed for the loop-induced mass splitting. We show bounds from [238] in Fig. 4.3 (top). The darker shading indicates how the mass reach changes when background systematic errors are varied between 1% and 2%.[6]

In general, the direct detection of the chargino LLP yields more information than a monojet missing energy signal. Both of the above search strategies suffer significant limitations. Monojet (or mono-X) searches have modest mass reach and reveal no information as to the nature of the produced BSM state beyond the invisibility of the new final states.[7] It would therefore be impossible to diagnose the signal as coming from a Higgsino-like state. Disappearing track searches can have slightly higher mass reach, but only if the lifetime is near the theoretically motivated maximum for this scenario.

Lifetimes below a few mm are in general extremely challenging to probe in these environments. It is clear, that the pure Higgsinos with their extremely small mass splitting and relatively short decay length are something of a night-mare scenario for searches at proton-proton colliders.

Cosmology

EWinos make natural candidates for thermal Dark Matter if they are stable on cosmological time scales. Thus, cosmological considerations may serve as general motivator for our theoretical setup and provide constraints for specific models. It is important to keep in mind, however, that these constraints are dependent on the universe's cosmological history, and are therefore not as robust as collider searches.

[6] For larger mass splittings, a soft lepton search can increase Higgsino mass reach [238], but $\Delta m < 5$ GeV in our region of interest.

[7] The prospects of the mono-Z searches at the FCC are currently under investigation [11].

Assuming that the lightest neutralino contributes to the thermal relic density provides us with additional bounds from cosmological observation. The abundance from Higgsinos with masses above $\sim$ 1.1 TeV [250] is larger than the observed dark matter relic density. This makes 1.1 TeV an obvious target for collider searches, see Fig. 4.3 (bottom)

Direct dark matter detection experiments are sensitive to Higgsinos with mass splittings in the GeV range or above, see e.g. ref. [249]. Sensitivity projections are summarized in Fig. 4.3 (bottom), and notably constrain short lifetimes but not long ones. This is due to the coupling to the Higgs boson, which mediates nuclear scattering and depends on the Higgsino-Bino mixing angle, or, equivalently, $\Delta m - \Delta_{1-\text{loop}}$ and only becomes appreciable for mass splittings $\sim$ GeV. Hence, the lack of signals in direct detection strongly favors a highly compressed spectra.[8] The most sensitive of these future experiments is DARWIN [10], which will be able to probe DM-nucleon cross sections very close to the so-called *neutrino floor*, where backgrounds from solar, cosmic and atmospheric neutrinos become relevant. For thermal Higgsino DM, this scattering rate corresponds to mass splittings of about 0.5 GeV.[9] Probing cross sections below the neutrino floor will be much more challenging.

Indirect detection experiments search for signs of dark matter annihilation in the cosmic ray spectra. Assuming a thermal relic abundance, current bounds from Fermi disfavor masses below 280 GeV, with proposed CTA measurements being sensitive to $m_\chi \sim 350$ GeV [275]. AMS antiproton data might exclude somewhat higher masses

[8] It is also possible to have an accidentally small (or null) coupling of Higgs to dark matter in the so called blind-spots [274]. We will not consider this option further in this work.

[9] This implies a lower bound on the singlet mass of 10 TeV. The singlet might then be well outside the reach of both the present and future generation of collider experiments.

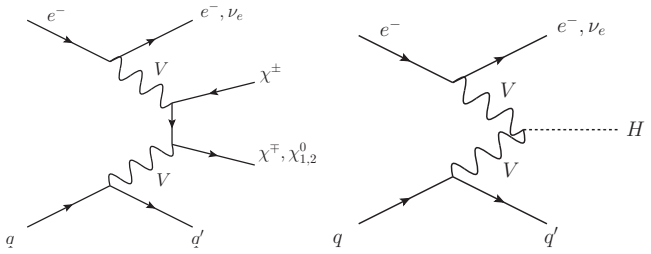

Figure 4.4: Example of dominant Higgsino (left) and Higgs (right) production processes at e^-p colliders. $V = W^\pm$ or Z as required.

[276], but that bound is subject to very large uncertainties.

While these cosmological bounds complement collider searches, they are much more model-dependent. One can imagine a Higgsino-like inert doublet scenario which does not give rise to a stable dark matter candidate (e.g. the lightest neutral state could decay to additional hidden sector states), making colliders the only direct way to probe their existence. Even if the assumptions about cosmology hold, collider searches are vital to fill in the blind spots below the neutrino floor. If a direct detection signal is found, the precise nature of dark matter would then have to be confirmed with collider searches. Finally, even with the most optimistic projections there are regions of parameter space at intermediate mass splitting (lifetimes $\lesssim$ mm) that are difficult to probe using both direct detection and current strategies at pp colliders.

4.3.3 Higgsino search at e^-p colliders

At e^-p colliders, Higgsinos are produced dominantly in VBF processes as shown in Fig. 4.4 (left). Since the production process is $2 \to 4$ it suffers significant phase space suppression and has a rather small cross section, as shown in Fig. 4.5. Fortunately, the spectacular nature of the LLP signal, and the clean experimental environment, still allows

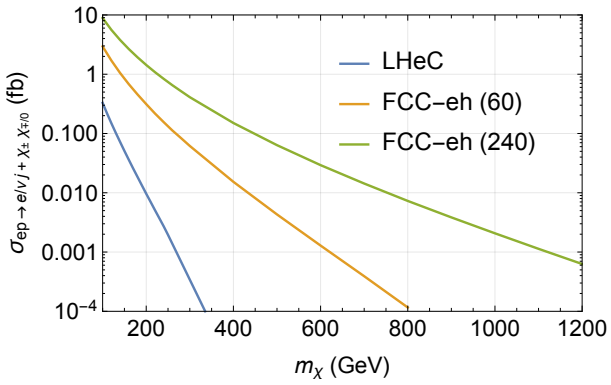

Figure 4.5: Production rate of Higgsinos at $e^- p$ colliders. The fraction of events with two charged Higgsino LLPs is $\sim 40 - 50\%$.

for significant improvements in reach compared to the existing search strategies outlined in the previous subsection.

LLP signature

We first consider searches at the LHeC. Weak-scale Higgsinos are produced in association with a recoiling, highly energetic jet with $p_T > 20$ GeV. This jet alone will ensure that the event passes trigger thresholds and is recorded for offline analysis. Crucially, the measurement of this jet will also determine the position of the primary vertex (PV) associated with the Higgsino production process.

Due to the asymmetric beams the center-of-mass frame of the process is boosted by $b_{\rm com} \approx \frac{1}{2}\sqrt{E_q/E_e} = \sqrt{x_q\, E_p/E_e} \approx 5.5\sqrt{x_q}$ with respect to the lab frame, where q and x_q are a parton and its Bjorken variable, respectively. Subsequently, the long lived charginos are typically significantly boosted along the proton beam direction, which increases their lifetime in the laboratory frame.

For small mass splittings $\lesssim 1$ GeV considered here, the dominant decay modes of

the Higgsinos are to single $\pi^{\pm}, e^{\pm}, \mu^{\pm}$ + invisible particles. The single visible charged particle typically has transverse momenta in the $\mathcal{O}(0.1\ \mathrm{GeV})$ range. In the clean environment (i.e. low pile up) of the $e^{-}p$ collider, such single low-energy charged tracks can be reliably reconstructed.

Analysis strategy

The following offline analysis strategy is sketched out in Fig. 4.6. One or two charginos are produced at the PV, which is identified by the triggering jet (A). A chargino decaying to a single charged particle is depicted in Fig. 4.6 (B). The charged track has an impact parameter with respect to the PV. If the impact parameter with respect to the PV is greater than a given r_{min}, we assume that this track can be tagged as originating from an LLP decay. Since the triggering jet provides the location of the PV, this LLP identification also holds if the chargino decays inside the interaction region. Therefore, this analysis explicitly takes advantage of the clean environment of the ep collider, with pile-up being either absent or controllable (that is, clearly distinguishable from the harder LLP production events). If the chargino decays to two or more charged particles, a conventional displaced vertex can be reconstructed (C). In that case, the PV-DV distance has to be greater than r_{min} to identify an LLP decay.[10]

The most relevant parameter of our search strategy is thus r_{min}. While we do not explicitly include detector resolution in our simulations, we implicitly take it into account by choosing r_{min} to be 5 detector resolutions. As such, our nominal benchmark assumes

[10] In a realistic analysis, r_{min} can be different for displaced tracks and vertices, but for our analysis it is sufficient to take them to be identical.

an $8\mu m$ resolution, corresponding to $r_{\text{min}} = 40\mu m$. To understand the impact of this parameter (and hence the tracking resolution of the future detector) on LLP reach, we also consider a more "optimistic" detector resolution of $5\mu m$, corresponding to $r_{\text{min}} = 25\mu m$, and a "pessimistic" scenario with $16\mu m$ resolution, giving $r_{\text{min}} = 80\mu m$. We emphasize that these values are consistent with the impact parameter resolutions for $\mathcal{O}(10\ \text{GeV})$ tracks with scattering angle above $\sim 5^\circ$ considered in the LHeC CDR [6], and with current resolutions of the LHCb VELO [277].

Moreover, the p_T threshold for reconstruction of a single charged particle is also relevant. In order to study the impact of the p_T threshold, we will consider a benchmark value of $p_T^{\text{min}} = 100\ \text{MeV}$, corresponding to a gyromagnetic radius of $\mathcal{O}(10\text{cm})$ for the B field of 3.5 T. We also consider an optimistic scenario of $p_T^{\text{min}} = 50\ \text{MeV}$ and a pessimistic scenario of $p_T^{\text{min}} = 400\ \text{MeV}$, which corresponds to the threshold for track ID at ATLAS and CMS in a high pile-up environment [278]. [11]

We assume 100% reconstruction efficiency for displaced tracks and vertices. The estimation of the realistic (expected-to-be $\mathcal{O}(1)$) efficiencies requires a full simulation of the detector response to our signal, which is beyond the scope of this work and will be left for future work. We do not expect this to significantly affect our conclusions.

Event simulation and analysis

The production of MSSM Higgsinos is simulated in `MG5_aMC@NLO` [279] at parton-level, which is sufficient given the almost purely geometrical nature of our signal. For

[11] At an $e^- p$ collider the full four momentum can be measured, and employing $|p|$ rather than p_T would lead to a slight increase in sensitivity. However, in order to be comparable with pp collider thresholds, we use p_T in the following.

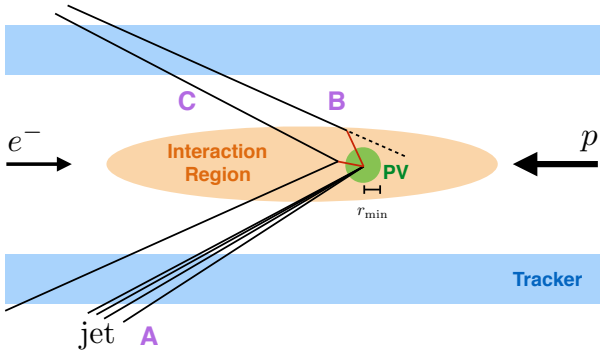

Figure 4.6: Sketch of our LLP search strategy at $e^- p$ colliders. Single or pair-production of weak-scale Higgsino LLPs (red) is practically always associated with the production of a hard jet (A) with $p_T > 20$ GeV and $|\eta| < 4.7$ which reaches the tracker and passes the trigger. The charged jet constituents (black) identify the primary vertex (PV). For Higgsinos decaying into $e/\mu/\pi^\pm + \chi^0_{1,2}$ (B), the LLP is detected if the charged particle trajectory (black solid and dashed) is reconstructed with $p_T > p_T^{\text{min}}$ and has impact parameter greater than r_{min}. For LLPs decaying into two or more charged particles (C), a DV can be reconstructed, and the LLP is identified if the distance to the PV is more than r_{min}. The electron or neutrino in the event as well as neutral final states of LLP decay are not shown.

each chargino k the probability of detecting it as an LLP is

$$P^{(k)}_{\text{detect}} = \sum_i \text{Br}_i(\Delta m(c\tau)) P_i(c\tau) \,, \tag{4.2}$$

where $k = 1, 2$ for chargino pair production events. The index i stands for the decay processes in Fig. 4.2, with branching ratios Br_i. P_i is the probability of detecting this particular chargino if it decays via process i. For 2- and 3-body decays to a single charged particle, it is computed by choosing the charged particle momentum from the appropriate phase space distribution in the chargino rest frame, then computing the minimum distance the chargino must travel for the impact parameter of the resulting charged track to be greater than r_{min}. P_i is the chance of the chargino traveling at least that distance given its boost and the chosen lifetime $c\tau$. $P_i = 0$ if the charged particle p_T lies below threshold

or it does not hit the tracker.

For decays to "jets", defined as three charged pions (all hadronic decays) for Δm below (above) Δm_*, we examine two possibilities. Optimistically, one would expect the jet to contain two or more relatively energetic charged particles, allowing a DV to be reconstructed. P_{jet} is then computed simply by requiring the chargino to travel at least r_{min} from the PV. Pessimistically the jet has to contain at least one charged particle, and we assign $P_{\text{jet}} = P_{\pi^{\pm}\pi^0\pi^0}$. The difference between the optimistic and pessimistic P_{jet} scenarios represents an uncertainty on our sensitivity estimate.

For each event with one chargino, $P^{(1)}_{\text{detect}}$ represents the chance of detecting a single LLP in the event. For each event with two charginos, $1-(1-P^{(1)}_{\text{detect}})(1-P^{(2)}_{\text{detect}})$ is the chance of observing at least one LLP, while $P^{(1)}_{\text{detect}}P^{(2)}_{\text{detect}}$ is the chance of observing two LLPs. This allows us to compute the number of observed events with at least one or two LLPs, $N_{1+\text{LLP}}$ and $N_{2\text{LLP}}$, as a function of chargino mass and chargino lifetime.

We show contours of $N_{1+\text{LLP}}$ and $N_{2\text{LLP}}$ in Fig. 4.7 for $\mu > 0$. The darker (lighter) shading represents the contour with the lowest (highest) estimate of event yield, obtained by minimizing (maximizing) with respect to the two hadronization scenarios of $m_d = 0$ or 0.5 GeV, and adopting the pessimistic (optimistic) P_{jet} reconstruction assumption. The difference between the light and dark shaded regions can be interpreted as a range of uncertainty in projected reach.[12] The $\mu < 0$ case is very similar in all of our studies, so we only show the positive case.

[12]We note that the abrupt "bite" in the green shaded region of the top plot around $(m_\chi, c\tau) \sim (140\ \text{GeV}, 10^{-5}\text{m})$ is an artifact of assuming 100% DV reconstruction once the Higgsino decays to jets of two or more charged particles turn on at larger mass splitting (under the optimistic reconstruction assumption). In reality, this intermediate region would likely be smoothly interpolated by a gradual turn-on, when more efficiently reconstructed DVs start dominating over displaced single tracks.

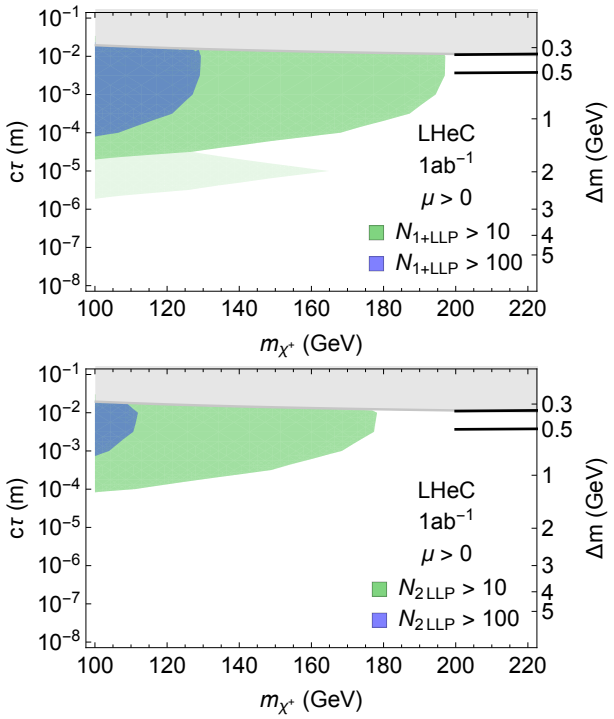

Figure 4.7: Regions in the $(m_{\chi^\pm}, c\tau)$ Higgsino parameter plane where more than 10 or 100 events with at least one (top) or two (bottom) LLPs are observed at the LHeC. Light shading indicates the uncertainty in the predicted number of events due to different hadronization and LLP reconstruction assumptions. Approximately 10 signal events should be discernable against the τ-background at 2σ, in particular for 2 LLPs, so the green shaded region represents an estimate of the exclusion sensitivity. For comparison, the black curves are the optimistic and pessimistic projected bounds from HL-LHC disappearing track searches, see Fig. 4.3.

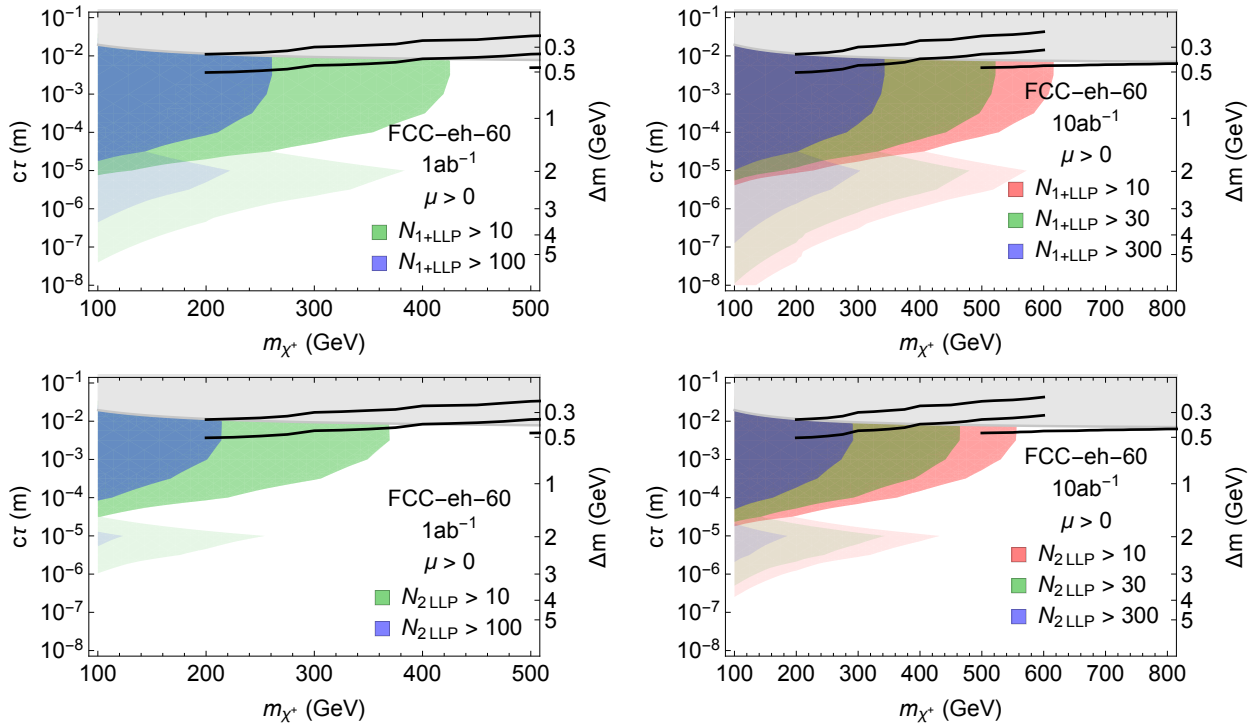

Figure 4.8: Regions in the $(m_{\chi^\pm}, c\tau)$ Higgsino parameter plane where more than the indicated number of one (top) or two (bottom) LLPs are observed at the FCC-eh with a 60 GeV electron beam and 1 ab^{-1} (left) or 10 ab^{-1} (right) of luminosity. Light shading indicates the uncertainty in the predicted number of events due to different hadronization and LLP reconstruction assumptions. As for the LHeC estimate in Fig. 4.7, the green region represents our 2σ sensitivity estimate in the presence of τ backgrounds. For 10 ab^{-1}, red shading is an optimistic sensitivity estimate in case background rejection is better than we anticipate. For comparison, the black curves are projected bounds from disappearing track searches, for the HL-LHC (optimistic and pessimistic) and the FCC-hh, see Fig. 4.3.

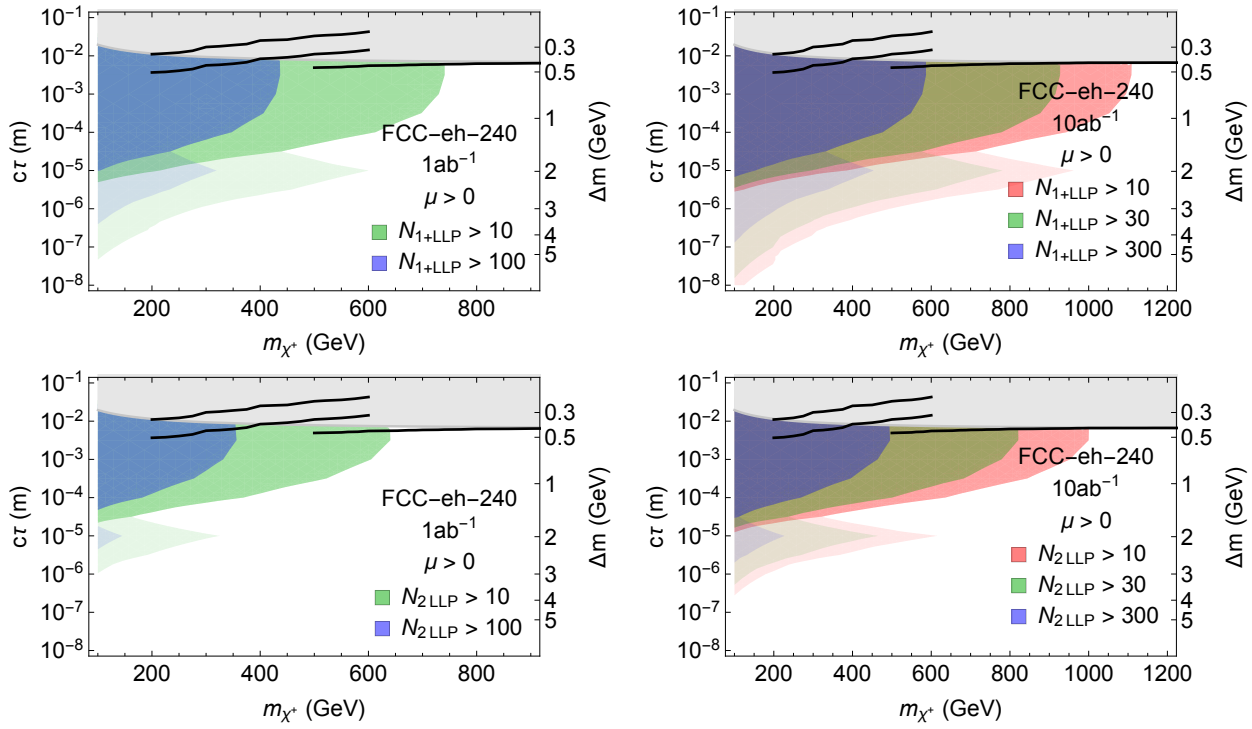

Figure 4.9: Same as Fig. 4.8 for the FCC-eh with a 240 GeV electron beam.

Backgrounds

An important and irreducible background SM background to our LLP signature is the decays of tau leptons, which have a proper lifetime of ~ 0.1mm and beta-decay into the same range of final states as the charginos. Events with one ($\tau^+\nu_\tau$) and two taus ($\tau^+\tau^-$) are produced via VBF together with a jet with $p_T > 20$ GeV, $|\eta| < 4.7$ at LHeC with cross sections of ~ 0.6 and ~ 0.3 pb, respectively.

Since the τ's originate from the decay of on-shell W and Z bosons, their decay products are much more central and energetic than those of charginos. Consequently, despite this background being much larger than the Higgsino signal, it can be suppressed considerably with simple kinematic cuts.

Specifically, by requiring the final states of LLP decay to be forward ($|\eta| > 1$ in the proton beam direction), the missing energy to be high (MET $\gtrsim 30$ GeV) and the LLP final state energy to be very low ($\lesssim 1.5\Delta m$ for a given chargino lifetime), a background rejection of 10^{-3} (10^{-4}) can be achieved for events requiring at least one (two) reconstructed LLPs while keeping a large $\mathcal{O}(1)$ fraction of the Higgsino signal.

Given the above background cross sections, the number of signal events that would be excludable at the 95% confidence level (2σ) above the background are then about 50 (10) for at least one (two) observed LLPs. This purely kinematic background rejection is very effective, but still underestimates the sensitivity. In the space of possible final states and decay lengths, τ's will populate very different regions than the chargino signal. While an in-depth study of such an analysis is beyond our scope, a comparison of the observed LLP data to a background template in that space will clearly increase sensitivity even further.

There are also reducible backgrounds from jets, most importantly the decays of B-mesons, which themselves have macroscopic lifetime. However, the final states of B-decays, which are extremely well studied, are different and distinguishable from the final states of chargino or τ-decay. Furthermore, B-decay can be vetoed by rejecting events with additional soft hadrons that are collinear with the line from the PV to the DV, which are very likely to accompany b-quark production and hadronization. Again, this rejection of QCD backgrounds takes advantage of the clean environment of the ep collider, and we expect its ultimate impact to be smaller than that of the τ-backgrounds we discuss above.

Finally, in any LLP analysis one must generally contend with complicated and difficult-to-estimate backgrounds originating from beam halo, material interactions, mis-

reconstructed tracks, etc. These backgrounds are highly dependent on the final accelerator and detector design, very difficult or impossible to simulate, and far beyond the scope of our simple theoretical study. However, experience at the LHC [223, 225, 280] shows that these backgrounds can be controlled to effectively contribute at the sub-ab cross section level if the LLP decay can be triggered on and is sufficiently distinguishable from the high pile-up levels present at the LHC and HL-LHC. Given the clean environment at the ep colldier, we expect these backgrounds to be under control in our analysis as well.

It is with all this in mind that we have shown contours of $N_{1+\mathrm{LLP},2\mathrm{LLP}} > 10$ and > 100. By the above arguments, the former constitutes a realistic expectation for the approximate number of LLPs which should be excludable at 2σ, while the latter shows how sensitivity is affected if backgrounds are much harder to reject than we anticipated.

FCC-eh

We repeat the above analysis for the FCC-eh scenarios. We assume the same detector dimensions, triggers, and thresholds. The kinematic rejection of τ backgrounds improves, with rejections in the range of $10^{-4} - 10^{-3}$ ($10^{-5} - 10^{-4}$) for one (two) τ events, more than offsetting the modest growth in τ-cross section, which is 2.1 (0.8) pb at the FCC-eh with a 60 GeV electron beam, and 4.4 (1.1) pb with a 240 GeV electron beam.

Figs. 4.8 and 4.9 show the number of observed events with at least 1 or 2 LLPs at the FCC-eh (60) and FCC-eh (240). We recall that we here consider benchmark luminosities of 1 and 10 ab^{-1}. For the latter, we show contours of 300 and 30 events instead of 100

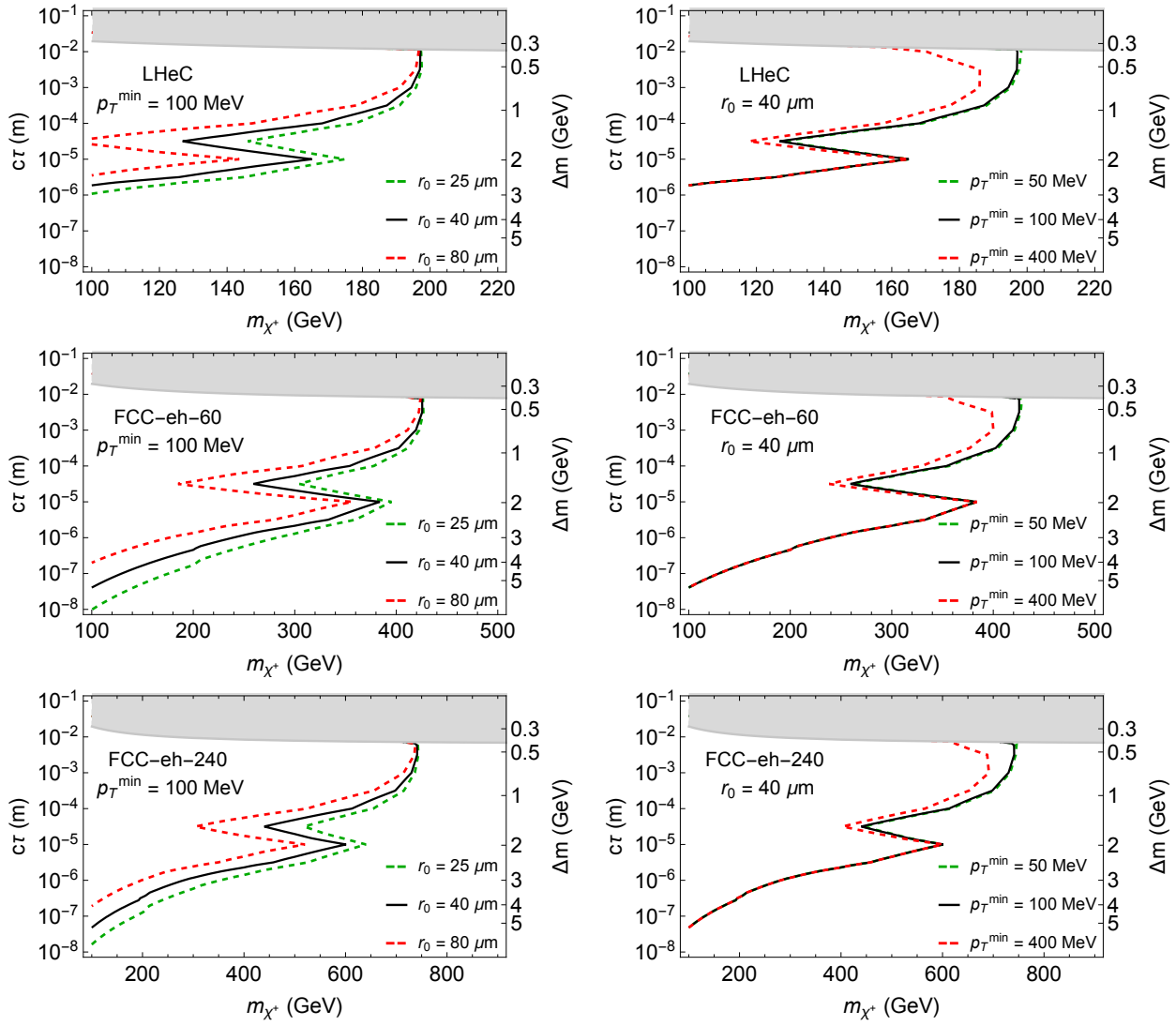

Figure 4.10: Reach dependence on r_0 and $p_T^{\min}$ for the Higgsino search requiring a single tagged LLP decay. All plots assume $1\,\mathrm{ab}^{-1}$ of data, $\mu > 0$, and the most optimistic estimate for event yield given hadronization and displaced jet reconstruction uncertainties.

and 10 to estimate sensitivity. This roughly accounts for the $\sqrt{10}$ larger number of signal events required to stand out against the same background cross section with a factor of 10 higher luminosity. However, we also show contours for 10 events, in the event that background rejection is very good and sensitivity scales more linearly with luminosity. We emphasize that the FCC-eh (240) with $10\ \mathrm{ab}^{-1}$ of luminosity may be able to probe the 1.1 TeV thermal Higgsino DM relic at lifetimes much shorter than FCC-hh disappearing track searches. Furthermore, this reach is theoretically very robust since LLP tagging efficiency at $\mathcal{O}(\mathrm{mm})$ lifetime is excellent at $e^- p$ colliders.

We note that an $\mathcal{O}(1)$ pile-up may become relevant at higher beam energies and luminosities. A detailed discussion is beyond our scope, but we expect that single displaced charged particles should be kinematically clearly distinguishable from a second high-energy primary vertex. Furthermore, given the sizable longitudinal extent of the interaction region, sensitivity at short lifetimes would not be affected by requiring the impact parameter or DV distance from the PV to be much less than the beam spot length. This would further reject pile-up vertices, which are more evenly distributed along the beam axis. While a more thorough investigation is certainly required, we expect our results to be fairly robust against these modest levels of pile-up, especially for the search requiring 2 observed LLPs.

Impact of track resolution and energy thresholds

It is important to determine to what extent the specifications of the detector, like energy thresholds and tracking resolution, affect BSM reach. In Fig. 4.10 we show how

reach of the single-LLP decay search is modified if we deviate from our benchmark assumptions of $p_T^{\rm min} = 100$ MeV as the minimum threshold for single track reconstruction and $r_0^{\rm min} = 40\mu$m as the minimum spatial separation for LLP tagging. (We do not show the corresponding figure for the search requiring two LLP decays, since the conclusions are similar.)

Our results are fairly robust with respect to variation in these two thresholds. Changing the tracking resolution ($r_0^{\rm min}$) unsurprisingly has noticeable effect on reach at the lowest lifetimes, but does not affect mass reach at the larger lifetimes. Conversely, the $p_T^{\rm min}$ threshold has no effect on reach at short lifetimes (where mass splitting is larger, leading the single charged particles to always pass the threshold). At large lifetimes the benchmark threshold of 100 MeV is very close to optimal, with improvements for 50 MeV being very minimal. On the other hand, assuming a much worse threshold of 400 MeV would modestly affect mass reach, which would make it even harder to reach the $m_\chi = 1.1$ TeV goal corresponding to thermal Higgsino dark matter. This provides significant motivation to aim for single track reconstruction thresholds at the ~ 100 MeV level when finalizing detector design.

Discussion and comparison

Our projected LHeC sensitivity for Higgsinos is competitive in mass reach to the monojet projections for the HL-LHC, being sensitive to masses around 200 GeV for the longest theoretically motivated lifetimes. The LHeC search has the crucial advantage of actually observing the charged Higgsino parent of the invisible final state. Proposed disap-

pearing track searches at the HL-LHC may probe higher masses for the longest lifetimes, but lose sensitivity at shorter lifetimes. By comparison, the LHeC search is sensitive to lifetimes as short as microseconds. It is important to note that the mass reach of $e^- p$ colliders is much more robust than the disappearing track projections, since the former are not exponentially sensitive to uncertainties in the Higgsino velocity distribution. While similar lifetime sensitivities may be possible at lepton colliders, only the highest energy proposals would have comparable center-of-mass energy.

The direct collider sensitivities are complementary to the sensitivity of dark matter direct detection experiments, which cover larger mass splittings (shorter lifetimes), and indirect detection constraints. However, these bounds are model-dependent and rely on cosmological assumptions. In the event of a positive dark matter signal, $e^- p$ colliders would play a crucial role in determining the nature of the dark matter candidate.

The mass reach of the FCC-eh is obviously much greater than for the LHeC. Reaching the thermal Higgsino DM mass of $\sim 1.1\ \mathrm{TeV}$ is challenging and would require a high luminosity high energy FCC-eh scenario as shown in Fig. 4.9 (left). However, in all cases the sensitivity to short decay lengths, possibly much less than a single micron, far exceeds what the FCC-hh can accomplish with disappearing track searches, making the FCC-eh coverage crucial in probing the full range of possible Higgsino scenarios.

4.4 LLP Production in Exotic Higgs Decays

The Higgsino analysis of the previous section demonstrates that $e^- p$ colliders have unique capabilities to detect LLPs which decay due to almost-degenerate masses into

extremely soft SM final states with very short lifetimes. However, the excellent tracking resolution, clean environment and longitudinal boost of the collision center-of-mass frame also has significant advantages for detecting LLPs with somewhat higher energy final states.

Exotic Higgs decays are strongly motivated on general theoretical grounds, see e.g. ref. [195]: the small SM Higgs width allows even small BSM couplings to lead to sizable exotic Higgs branching fractions, and the low dimensionality of the gauge- and Lorentz-singlet $|H|^2$ portal operator allows it to couple to any BSM sector via a low-dimensional term in the Lagrangian, making sizable couplings generic.

We consider exotic Higgs decays into a pair of BSM LLPs X. The exotic branching fraction $\mathrm{Br}(h \to XX)$ and the LLP lifetime $c\tau$ are both essentially free parameters. We focus on LLP masses of order 10 GeV to demonstrate that $e^- p$ colliders also offer crucial advantages to LLPs without soft decay products. This simplified model represents many highly motivated theoretical scenarios, including Neutral Naturalness [281] and general Hidden Valleys [59, 60, 61, 62, 63, 64], where the LLPs are hadrons of the hidden sector produced via the Higgs portal.

Analysis strategy

We assume X decays to at least two charged particles with energies above p_T detection threshold to uniquely identify a DV for the LLP decay. The analysis proceeds along very similar lines as the Higgsino case: VBF Higgs production at $e^- p$ colliders, see Fig. 4.4 (right), is simulated to lowest order in MadGraph, with cross sections 0.1, 0.34,

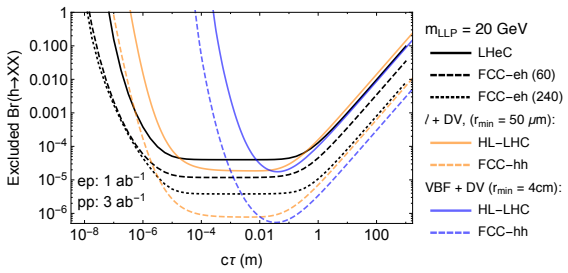

Figure 4.11: Projected exclusion limits on exotic Higgs decay branching fraction to LLPs X as a function of lifetime $c\tau$ for the LHeC, FCC-eh (60) and FCC-eh (240) with $1\ \mathrm{ab}^{-1}$ of data. The excluded branching ratio scales linearly with luminosity under the assumption of no background. The LLP mass in the plot is $20\ \mathrm{GeV}$, but for different masses the curves shift in $c\tau$ roughly by a factor of $m_{\mathrm{LLP}}/(20\ \mathrm{GeV})$. The search at the ep collider requires only the trigger jet to locate the PV and a single DV from LLP decay. For comparison, assuming X decays hadronically, we show a somewhat realistic estimate for the sensitivity of pp colliders with $3\ \mathrm{ab}^{-1}$ and without background (blue), as well as a very optimistic estimate which assumes extremely short-lived LLP reconstruction (orange), from [12].

1.05 pb at the LHeC, FCC-eh (60) and FCC-eh (240) respectively. The search strategy is also the same, shown in Fig. 4.6, but now we are dealing exclusively with displaced vertices (C), which we assume are detected with an efficiency of 100% as long as the final states hit the tracker and the LLP decays at a distance r_{min} away from the primary vertex, which is again identified by the associated jet which passed the trigger.

The decay of a single LLP from exotic Higgs decays, with mass of a few GeV or above, is much more spectacular than in the Higgsino analysis discussed previously. This is because each LLP decays to a DV with either two fairly hard tracks (if the decay is leptonic) or $\mathcal{O}(10)$ charged tracks (if the decay is hadronic), making reconstruction much more robust and strongly distinguishing it from backgrounds including τ and b decay. Additional handles are the DV invariant mass and known Higgs mass. As a result, our exotic Higgs decay search only requires a single LLP with a displacement above $r_{\mathrm{min}} = 40\mu m$, in addition to the triggering jet, and we expect backgrounds to be negligible.

Results and discussion

We show the resulting sensitivity in Fig. 4.11, with the exclusion sensitivity of 4 expected events passing the above signal requirements. From the figure we see that $e^- p$ colliders can probe LLP production in exotic Higgs decays with decay lengths below a micron, due to the lifetime-enhancing longitudinal boost and excellent tracking in a clean environment.

For comparison, we show estimates of the HL-LHC and FCC-hh sensitivity to LLPs produced in exotic Higgs decays [12], where the LLP decays hadronically, which is a challenging scenario for the LHC main detectors. A somewhat realistic estimate assumes triggering on Higgs production from VBF[13] and requiring a single DV displaced more than 3cm from the beamline is enough to eliminate backgrounds (blue curves). A much more optimistic estimate (orange curves) assumes a search triggering on a single high-p_T lepton from associated Higgs Boson production and requiring a single DV with displacement as low as $50\mu m$ can be performed with no backgrounds. It is still unclear whether this optimistic search can be realized at pp colliders.

The sensitivity achievable at the LHeC (FCC-eh) reaches much shorter lifetimes than either projection for the HL-LHC (FCC-hh), especially for the more conservative pp projections. This is especially significant since the optimistic search of [12] was required to cover well-motivated parts of Neutral Naturalness parameter space where the hidden hadrons are very short-lived. Furthermore, the estimated sensitivity of $e^- p$ colliders at short lifetimes is more robust than that of pp colliders, where those searches have to

[13] This reach estimate would be very similar if the search triggered on leptons from associated production instead of VBF.

contend with much higher levels of background and pile-up.

4.5 Discussion

Electron-proton colliders are more commonly associated with DIS studies of the proton than with BSM searches. However, their high center-of-mass energy compared to lepton colliders but clean environment compared to hadron colliders lets them play a unique role in probing a variety of important BSM signals.

Diverse BSM states can be produced in VBF processes, which also ensures triggering and identification of the primary vertex. Any BSM state which looks like hadronic background in the high-energy, high-rate environment of hadron colliders can likely be much better identified and studied in $e^{-}p$ collisions. A prime example of such BSM scenarios are LLPs which decay with short lifetime ($\lesssim$ mm) and/or a small mass splitting ($\lesssim$ GeV) which can arise from compressed spectra. To demonstrate this, we studied searches for pure Higgsinos and exotic Higgs decays to LLPs. In both cases, proposed $e^{-}p$ colliders probe new and important regions of parameter space inaccessible to other experiments. Our most optimistic FCC-eh scenarios could produce and reconstruct the 1.1 TeV thermal Higgsino dark matter relic. It is also important to point out that in both BSM scenarios, the $e^{-}p$ collider reach is more robust than the pp projections.

We used LHeC and FCC-eh proposals as our benchmarks, but took some liberties in exploring higher luminosities and higher energies to show what kind of physics reach may be possible. In that light, our results can serve to guide the detailed design of such a future machine, whether it is built as an add-on to the CERN LHC, CERN FCC-hh, or

a the SppC. Similarly, we found that the reconstruction of soft LLP final states with high tracking resolution ($\lesssim 10\mu m$), single track reconstruction thresholds of ~ 100 MeV and very low pile-up are necessary conditions for this unique BSM sensitivity, and should be a high priority in the design.

We demonstrated that $e^- p$ colliders have unique sensitivity to BSM signals, in particular LLPs with soft final states or very short lifetimes. Further study is needed to identify other BSM scenarios to which these machines could be uniquely sensitive, but our results suggest that difficult final states may be a particularly fruitful avenue of exploration. There may be other diverse classes of signals that can be effectively probed. This adds significant motivation for the construction of future $e^- p$ colliders. Together with the invaluable proton PDF data, as well as precision measurements of EW parameters, top quark couplings and Higgs couplings, our results make clear that adding a DIS program to a pp collider is necessary to fully exploit its discovery potential for new physics.

Chapter 5: Conclusion

This thesis discussed various theoretical ideas to build microscopic models for Cosmic Inflation (see Chap. 2, 3). We explored model-building for inflation at high scales as well as at lower scales, in each case striving for better theoretical control and naturalness. We investigated modeling inflaton as a pseudo-Nambu-Goldstone boson, using multi-axion structure to get an effective super-Planckian field space, the axionic structure originating from extra-dimensional gauge theory, and embedding this in an approximately supersymmetric vacuum in order to address the electroweak hierarchy problem. We also explored the Hybrid Inflation mechanism with a discrete twin symmetry, as a means of naturally realizing relatively low-scale inflation. It is exciting that we will have opportunities to test whether any of these constructions are realized in nature, via the numerous upcoming and near-future experiments. There are various experiments – like BICEP Array [28], Simons Observatory [29], CMB-S4 [30], LiteBIRD [31], and PICO [32] – aiming to improve the constraints on inflationary observables and at measuring the energy scale of inflation, which would be a great discovery. Furthermore, various searches for primordial non-Gaussianities via large scale structure and 21-cm observations [142, 143, 144] will probe the inflaton interactions, and the existence of new fields during inflation. All of these experiments will help us get a detailed view into the physics governing the early

universe, and in particular the phase of cosmic inflation.

The novel signatures of Long-Lived Particles (LLP), explored in Chap. 4, naturally arise from a variety of beyond the Standard Model scenarios, including supersymmetry. It is exciting to see a rich and diverse LLP search program (see e.g. [78, 83, 84, 85]) coming up at the current and future colliders. There are also proposals for dedicated LLP detectors, e.g. MATHUSLA [227, 228], milliQan [229], CODEX-b [230] and FASER [231]. All of these so-called "Lifetime Frontier" searches, will help us better understand the structure of the world of fundamental particles, possibly resolving some of the long-standing puzzles like the electroweak hierarchy problem, nature of dark matter, origin of matter-antimatter asymmetry etc.

It has been the eternal quest of mankind to understand how the world around us works. The theoretical and experimental investigations in particle physics and cosmology explored in this thesis, along with innumerable others not even mentioned here, will hopefully take us further on that path and reveal some of the secrets of the nature!

Appendix A: SUGRA preliminaries

We write here the important SUGRA expressions relevant for Chapter 2. See [33] for review and further details.

For a general Kähler potential and superpotential for chiral superfields Φ_i,

$$K = K(\Phi_i, \bar{\Phi}_i) \ , \ W = W(\Phi_i), \tag{A.1}$$

the SUGRA scalar potential is

$$V_{\text{scalar}}(\Phi_i, \bar{\Phi}_i) = e^K \left[K^{-1}_{\Phi_i \bar{\Phi}_j} \left(D_{\Phi_i} W\right) \left(D_{\bar{\Phi}_j} \overline{W}\right) - 3 W \overline{W} \right], \tag{A.2}$$

with subscripts referring to the respective partial derivatives, and with

$$D_{\Phi_i} W \equiv W_{\Phi_i} + K_{\Phi_i} W. \tag{A.3}$$

$\langle D_{\Phi_i} W \rangle$ is the SUSY order parameter for each of the superfields Φ_i. If there exists spontaneous breaking of SUSY in a model, it gives rise to a massless Goldstino,

$$\psi_{\text{Goldstino}} \propto \langle D_{\Phi_i} W \rangle \ \psi_{\Phi_i}, \tag{A.4}$$

where ψ_{Φ_i} are fermions in the superfields Φ_i. The Goldstino is further "eaten" by the gravitino which then becomes massive. This is called the "super-Higgs mechanism".

Bibliography

[1] Kaustubh Deshpande and Raman Sundrum. Supersymmetric Inflation from the Fifth Dimension. *JHEP*, 08:029, 2019.

[2] Kaustubh Deshpande, Soubhik Kumar, and Raman Sundrum. TwInflation. 1 2021.

[3] David Curtin, Kaustubh Deshpande, Oliver Fischer, and José Zurita. New Physics Opportunities for Long-Lived Particles at Electron-Proton Colliders. *JHEP*, 07:024, 2018.

[4] Daniel Baumann. Inflation. In *Physics of the large and the small, TASI 09, proceedings of the Theoretical Advanced Study Institute in Elementary Particle Physics, Boulder, Colorado, USA, 1-26 June 2009*, pages 523–686, 2011.

[5] Y. Akrami et al. Planck 2018 results. X. Constraints on inflation. *Astron. Astrophys.*, 641:A10, 2020.

[6] J. L. Abelleira Fernandez et al. A Large Hadron Electron Collider at CERN: Report on the Physics and Design Concepts for Machine and Detector. *J. Phys.*, G39:075001, 2012.

[7] Rakhi Mahbubani, Pedro Schwaller, and Jose Zurita. Closing the window for compressed Dark Sectors with disappearing charged tracks. *JHEP*, 06:119, 2017. [Erratum: JHEP 10, 061 (2017)].

[8] E. Aprile et al. Physics reach of the XENON1T dark matter experiment. *JCAP*, 1604(04):027, 2016.

[9] D. S. Akerib et al. LUX-ZEPLIN (LZ) Conceptual Design Report. 2015.

[10] J. Aalbers et al. DARWIN: towards the ultimate dark matter detector. *JCAP*, 1611:017, 2016.

[11] R. Mahbubani and J. Zurita. To appear.

[12] David Curtin and Christopher B. Verhaaren. Discovering Uncolored Naturalness in Exotic Higgs Decays. *JHEP*, 12:072, 2015.

[13] Mary K. Gaillard, Paul D. Grannis, and Frank J. Sciulli. The Standard model of particle physics. *Rev. Mod. Phys.*, 71:S96–S111, 1999.

[14] Particle Data Group, P A Zyla, R M Barnett, J Beringer, O Dahl, D A Dwyer, D E Groom, C J Lin, K S Lugovsky, E Pianori, D J Robinson, C G Wohl, W M Yao, K Agashe, G Aielli, B C Allanach, C Amsler, M Antonelli, E C Aschenauer, D M Asner, H Baer, Sw Banerjee, L Baudis, C W Bauer, J J Beatty, V I Belousov, S Bethke, A Bettini, O Biebel, K M Black, E Blucher, O Buchmuller, V Burkert, M A Bychkov, R N Cahn, M Carena, A Ceccucci, A Cerri, D Chakraborty, R Sekhar Chivukula, G Cowan, G D'Ambrosio, T Damour, D de Florian, A de Gouvêa, T DeGrand, P de Jong, G Dissertori, B A Dobrescu, M D'Onofrio, M Doser, M Drees, H K Dreiner, P Eerola, U Egede, S Eidelman, J Ellis, J Erler, V V Ezhela, W Fetscher, B D Fields, B Foster, A Freitas, H Gallagher, L Garren, H J Gerber, G Gerbier, T Gershon, Y Gershtein, T Gherghetta, A A Godizov, M C Gonzalez-Garcia, M Goodman, C Grab, A V Gritsan, C Grojean, M Grünewald, A Gurtu, T Gutsche, H E Haber, C Hanhart, S Hashimoto, Y Hayato, A Hebecker, S Heinemeyer, B. Review of Particle Physics. *Progress of Theoretical and Experimental Physics*, 2020(8), 08 2020. 083C01.

[15] Gianfranco Bertone and Dan Hooper. History of dark matter. *Rev. Mod. Phys.*, 90:045002, Oct 2018.

[16] Bernard Carr and Florian Kühnel. Primordial black holes as dark matter: Recent developments. *Annual Review of Nuclear and Particle Science*, 70(1):355–394, 2020.

[17] André de Gouvêa. Neutrino mass models. *Annual Review of Nuclear and Particle Science*, 66(1):197–217, 2016.

[18] Michael Dine and Alexander Kusenko. The Origin of the matter - antimatter asymmetry. *Rev. Mod. Phys.*, 76:1, 2003.

[19] Steven Weinberg. The Cosmological Constant Problem. *Rev. Mod. Phys.*, 61:1–23, 1989.

[20] Raphael Bousso. TASI Lectures on the Cosmological Constant. *Gen. Rel. Grav.*, 40:607–637, 2008.

[21] Anson Hook. TASI Lectures on the Strong CP Problem and Axions. *PoS*, TASI2018:004, 2019.

[22] N. Aghanim et al. Planck 2018 results. VI. Cosmological parameters. *Astron. Astrophys.*, 641:A6, 2020.

[23] Adam G. Riess, Stefano Casertano, Wenlong Yuan, J. Bradley Bowers, Lucas Macri, Joel C. Zinn, and Dan Scolnic. Cosmic Distances Calibrated to 1% Precision with Gaia EDR3 Parallaxes and Hubble Space Telescope Photometry of 75 Milky Way Cepheids Confirm Tension with ΛCDM. *Astrophys. J. Lett.*, 908(1):L6, 2021.

[24] Eleonora Di Valentino, Olga Mena, Supriya Pan, Luca Visinelli, Weiqiang Yang, Alessandro Melchiorri, David F. Mota, Adam G. Riess, and Joseph Silk. In the Realm of the Hubble tension − a Review of Solutions. 3 2021.

[25] Judd D. Bowman, Alan E. E. Rogers, Raul A. Monsalve, Thomas J. Mozdzen, and Nivedita Mahesh. An absorption profile centred at 78 megahertz in the sky-averaged spectrum. *Nature*, 555(7694):67–70, 2018.

[26] W. J. G. de Blok. The core-cusp problem. *Advances in Astronomy*, 2010:1–14, 2010.

[27] David H. Lyth. What would we learn by detecting a gravitational wave signal in the cosmic microwave background anisotropy? *Phys. Rev. Lett.*, 78:1861–1863, 1997.

[28] Howard Hui et al. BICEP Array: a multi-frequency degree-scale CMB polarimeter. *Proc. SPIE Int. Soc. Opt. Eng.*, 10708:1070807, 2018.

[29] Peter Ade et al. The Simons Observatory: Science goals and forecasts. *JCAP*, 02:056, 2019.

[30] Kevork Abazajian et al. CMB-S4 Science Case, Reference Design, and Project Plan. 7 2019.

[31] M. Hazumi et al. LiteBIRD: A Satellite for the Studies of B-Mode Polarization and Inflation from Cosmic Background Radiation Detection. *J. Low Temp. Phys.*, 194(5-6):443–452, 2019.

[32] Shaul Hanany et al. PICO: Probe of Inflation and Cosmic Origins. 2 2019.

[33] J. Wess and J. Bagger. *Supersymmetry and supergravity*. Princeton University Press, Princeton, NJ, USA, 1992.

[34] Stephen P. Martin. A Supersymmetry primer. *Adv. Ser. Direct. High Energy Phys.*, 18:1–98, 1998.

[35] Daniele Bertolini, Jesse Thaler, and Zachary Thomas. Super-Tricks for Superspace. In *Theoretical Advanced Study Institute in Elementary Particle Physics: Searching for New Physics at Small and Large Scales*, 2 2013.

[36] Daniel Baumann and Liam McAllister. *Inflation and String Theory*. Cambridge Monographs on Mathematical Physics. Cambridge University Press, 5 2015.

[37] Katherine Freese, Joshua A. Frieman, and Angela V. Olinto. Natural inflation with pseudo nambu-goldstone bosons. *Phys. Rev. Lett.*, 65:3233–3236, Dec 1990.

[38] Renata Kallosh, Andrei D. Linde, Dmitri A. Linde, and Leonard Susskind. Gravity and global symmetries. *Phys. Rev.*, D52:912–935, 1995.

[39] Tom Banks and Nathan Seiberg. Symmetries and Strings in Field Theory and Gravity. *Phys. Rev.*, D83:084019, 2011.

[40] Daniel Harlow and Hirosi Ooguri. Constraints on Symmetries from Holography. *Phys. Rev. Lett.*, 122(19):191601, 2019.

[41] Jihn E. Kim, Hans Peter Nilles, and Marco Peloso. Completing natural inflation. *JCAP*, 0501:005, 2005.

[42] Nima Arkani-Hamed, Hsin-Chia Cheng, Paolo Creminelli, and Lisa Randall. Extra natural inflation. *Phys. Rev. Lett.*, 90:221302, 2003.

[43] Yang Bai and Ben A. Stefanek. Natural millicharged inflation. *Phys. Rev.*, D91(9):096012, 2015.

[44] Anton de la Fuente, Prashant Saraswat, and Raman Sundrum. Natural Inflation and Quantum Gravity. *Phys. Rev. Lett.*, 114(15):151303, 2015.

[45] David J. E. Marsh. Axion Cosmology. *Phys. Rept.*, 643:1–79, 2016.

[46] Alberto Diez-Tejedor and David J. E. Marsh. Cosmological production of ultralight dark matter axions. 2 2017.

[47] John R. Ellis, Andrei D. Linde, and Dimitri V. Nanopoulos. Inflation Can Save the Gravitino. *Phys. Lett. B*, 118:59–64, 1982.

[48] John R. Ellis, Jihn E. Kim, and Dimitri V. Nanopoulos. Cosmological Gravitino Regeneration and Decay. *Phys. Lett. B*, 145:181–186, 1984.

[49] T. Moroi, H. Murayama, and Masahiro Yamaguchi. Cosmological constraints on the light stable gravitino. *Phys. Lett. B*, 303:289–294, 1993.

[50] Lisa Randall and Scott D. Thomas. Solving the cosmological moduli problem with weak scale inflation. *Nucl. Phys. B*, 449:229–247, 1995.

[51] Andrei D. Linde. Hybrid inflation. *Phys. Rev.*, D49:748–754, 1994.

[52] Z. Chacko, Hock-Seng Goh, and Roni Harnik. The Twin Higgs: Natural electroweak breaking from mirror symmetry. *Phys. Rev. Lett.*, 96:231802, 2006.

[53] Asimina Arvanitaki, Nathaniel Craig, Savas Dimopoulos, and Giovanni Villadoro. Mini-Split. *JHEP*, 02:126, 2013.

[54] Nima Arkani-Hamed, Arpit Gupta, David E. Kaplan, Neal Weiner, and Tom Zorawski. Simply Unnatural Supersymmetry. 2012.

[55] G. F. Giudice and R. Rattazzi. Theories with gauge mediated supersymmetry breaking. *Phys. Rept.*, 322:419–499, 1999.

[56] R. Barbier et al. R-parity violating supersymmetry. *Phys. Rept.*, 420:1–202, 2005.

[57] Csaba Csaki, Eric Kuflik, and Tomer Volansky. Dynamical R-Parity Violation. *Phys. Rev. Lett.*, 112:131801, 2014.

[58] JiJi Fan, Matthew Reece, and Joshua T. Ruderman. Stealth Supersymmetry. *JHEP*, 1111:012, 2011.

[59] Matthew J. Strassler and Kathryn M. Zurek. Echoes of a hidden valley at hadron colliders. *Phys.Lett.*, B651:374–379, 2007.

[60] Matthew J. Strassler and Kathryn M. Zurek. Discovering the Higgs through highly-displaced vertices. *Phys.Lett.*, B661:263–267, 2008.

[61] Matthew J. Strassler. Possible effects of a hidden valley on supersymmetric phenomenology. 2006.

[62] Tao Han, Zongguo Si, Kathryn M. Zurek, and Matthew J. Strassler. Phenomenology of hidden valleys at hadron colliders. *JHEP*, 0807:008, 2008.

[63] Matthew J. Strassler. Why Unparticle Models with Mass Gaps are Examples of Hidden Valleys. 2008.

[64] Matthew J. Strassler. On the Phenomenology of Hidden Valleys with Heavy Flavor. 2008.

[65] Matthew Baumgart, Clifford Cheung, Joshua T. Ruderman, Lian-Tao Wang, and Itay Yavin. Non-Abelian Dark Sectors and Their Collider Signatures. *JHEP*, 04:014, 2009.

[66] David E. Kaplan, Markus A. Luty, and Kathryn M. Zurek. Asymmetric Dark Matter. *Phys. Rev.*, D79:115016, 2009.

[67] Yuk Fung Chan, Matthew Low, David E. Morrissey, and Andrew P. Spray. LHC Signatures of a Minimal Supersymmetric Hidden Valley. *JHEP*, 05:155, 2012.

[68] Keith R. Dienes and Brooks Thomas. Dynamical Dark Matter: I. Theoretical Overview. *Phys. Rev.*, D85:083523, 2012.

[69] Keith R. Dienes, Shufang Su, and Brooks Thomas. Distinguishing Dynamical Dark Matter at the LHC. *Phys. Rev.*, D86:054008, 2012.

[70] Ian-Woo Kim and Kathryn M. Zurek. Flavor and Collider Signatures of Asymmetric Dark Matter. *Phys. Rev.*, D89(3):035008, 2014.

[71] Gustavo Burdman, Z. Chacko, Hock-Seng Goh, and Roni Harnik. Folded supersymmetry and the LEP paradox. *JHEP*, 0702:009, 2007.

[72] Haiying Cai, Hsin-Chia Cheng, and John Terning. A Quirky Little Higgs Model. *JHEP*, 0905:045, 2009.

[73] Yanou Cui and Raman Sundrum. Baryogenesis for weakly interacting massive particles. *Phys. Rev.*, D87(11):116013, 2013.

[74] Kurt Barry, Peter W. Graham, and Surjeet Rajendran. Displaced vertices from R -parity violation and baryogenesis. *Phys. Rev.*, D89(5):054003, 2014.

[75] Yanou Cui and Brian Shuve. Probing Baryogenesis with Displaced Vertices at the LHC. *JHEP*, 02:049, 2015.

[76] Seyda Ipek and John March-Russell. Baryogenesis via Particle-Antiparticle Oscillations. *Phys. Rev. D*, 93(12):123528, 2016.

[77] Juan C. Helo, Martin Hirsch, and Sergey Kovalenko. Heavy neutrino searches at the LHC with displaced vertices. *Phys. Rev.*, D89:073005, 2014. [Erratum: Phys. Rev.D93,no.9,099902(2016)].

[78] Stefan Antusch, Eros Cazzato, and Oliver Fischer. Displaced vertex searches for sterile neutrinos at future lepton colliders. *JHEP*, 12:007, 2016.

[79] Michael L. Graesser. Broadening the Higgs boson with right-handed neutrinos and a higher dimension operator at the electroweak scale. *Phys. Rev.*, D76:075006, 2007.

[80] Michael L. Graesser. Experimental Constraints on Higgs Boson Decays to TeV-scale Right-Handed Neutrinos. 2007.

[81] Alessio Maiezza, Miha Nemevšek, and Fabrizio Nesti. Lepton Number Violation in Higgs Decay at LHC. *Phys. Rev. Lett.*, 115:081802, 2015.

[82] Brian Batell, Maxim Pospelov, and Brian Shuve. Shedding Light on Neutrino Masses with Dark Forces. *JHEP*, 08:052, 2016.

[83] Alain Blondel, E. Graverini, N. Serra, and M. Shaposhnikov. Search for Heavy Right Handed Neutrinos at the FCC-ee. *Nucl. Part. Phys. Proc.*, 273-275:1883–1890, 2016.

[84] Stefan Antusch, Eros Cazzato, and Oliver Fischer. Sterile neutrino searches at future e^-e^+, pp, and e^-p colliders. *Int. J. Mod. Phys.*, A32(14):1750078, 2017.

[85] Juliette Alimena et al. Searching for long-lived particles beyond the Standard Model at the Large Hadron Collider. *J. Phys. G*, 47(9):090501, 2020.

[86] Max Klein. The Large Hadron Electron Collider Project. In *Proceedings, 17th International Workshop on Deep-Inelastic Scattering and Related Subjects (DIS 2009): Madrid, Spain, April 26-30, 2009*, 2009.

[87] Oliver Bruening and Max Klein. The Large Hadron Electron Collider. *Mod. Phys. Lett.*, A28(16):1330011, 2013.

[88] Frank Zimmermann, Michael Benedikt, Daniel Schulte, and Jorg Wenninger. Challenges for Highest Energy Circular Colliders. In *Proceedings, 5th International Particle Accelerator Conference (IPAC 2014): Dresden, Germany, June 15-20, 2014*, page MOXAA01, 2014.

[89] P. A. R. Ade et al. Planck 2015 results. XX. Constraints on inflation. *Astron. Astrophys.*, 594:A20, 2016.

[90] Roberto Contino, Yasunori Nomura, and Alex Pomarol. Higgs as a holographic pseudoGoldstone boson. *Nucl. Phys.*, B671:148–174, 2003.

[91] Yutaka Hosotani. Dynamical gauge symmetry breaking as the casimir effect. *Physics Letters B*, 129(3):193 – 197, 1983.

[92] Nima Arkani-Hamed, Lubos Motl, Alberto Nicolis, and Cumrun Vafa. The String landscape, black holes and gravity as the weakest force. *JHEP*, 06:060, 2007.

[93] Michael Czerny, Tetsutaro Higaki, and Fuminobu Takahashi. Multi-Natural Inflation in Supergravity and BICEP2. *Phys. Lett.*, B734:167–172, 2014.

[94] Xin Gao, Tianjun Li, and Pramod Shukla. Combining Universal and Odd RR Axions for Aligned Natural Inflation. *JCAP*, 1410:048, 2014.

[95] Cody Long, Liam McAllister, and Paul McGuirk. Aligned Natural Inflation in String Theory. *Phys. Rev.*, D90:023501, 2014.

[96] Tibra Ali, S. Shajidul Haque, and Vishnu Jejjala. Natural Inflation from Near Alignment in Heterotic String Theory. *Phys. Rev.*, D91(8):083516, 2015.

[97] Ido Ben-Dayan, Francisco G. Pedro, and Alexander Westphal. Towards Natural Inflation in String Theory. *Phys. Rev.*, D92(2):023515, 2015.

[98] Eran Palti. On Natural Inflation and Moduli Stabilisation in String Theory. *JHEP*, 10:188, 2015.

[99] Rolf Kappl, Hans Peter Nilles, and Martin Wolfgang Winkler. Natural Inflation and Low Energy Supersymmetry. *Phys. Lett.*, B746:15–21, 2015.

[100] Renata Kallosh and Andrei D. Linde. Landscape, the scale of SUSY breaking, and inflation. *JHEP*, 12:004, 2004.

[101] Temple He, Shamit Kachru, and Alexander Westphal. Gravity waves and the LHC: Towards high-scale inflation with low-energy SUSY. *JHEP*, 06:065, 2010.

[102] Tatsuo Kobayashi and Manabu Sakai. Inflation, moduli (de)stabilization and supersymmetry breaking. *JHEP*, 04:121, 2011.

[103] Stefan Antusch, Koushik Dutta, and Sebastian Halter. Combining High-scale Inflation with Low-energy SUSY. *JHEP*, 03:105, 2012.

[104] Yusuke Yamada. Instant uplifted inflation: A solution for a tension between inflation and SUSY breaking scale. *JHEP*, 07:039, 2013.

[105] Michael Czerny, Tetsutaro Higaki, and Fuminobu Takahashi. Multi-Natural Inflation in Supergravity. *JHEP*, 05:144, 2014.

[106] Wilfried Buchmuller, Emilian Dudas, Lucien Heurtier, Alexander Westphal, Clemens Wieck, and Martin Wolfgang Winkler. Challenges for Large-Field Inflation and Moduli Stabilization. *JHEP*, 04:058, 2015.

[107] Xingang Chen and Yi Wang. Large non-Gaussianities with Intermediate Shapes from Quasi-Single Field Inflation. *Phys. Rev.*, D81:063511, 2010.

[108] Xingang Chen and Yi Wang. Quasi-Single Field Inflation and Non-Gaussianities. *JCAP*, 1004:027, 2010.

[109] Xingang Chen. Primordial Non-Gaussianities from Inflation Models. *Adv. Astron.*, 2010:638979, 2010.

[110] Daniel Baumann and Daniel Green. Signatures of Supersymmetry from the Early Universe. *Phys. Rev.*, D85:103520, 2012.

[111] Valentin Assassi, Daniel Baumann, and Daniel Green. On Soft Limits of Inflationary Correlation Functions. *JCAP*, 1211:047, 2012.

[112] Xingang Chen and Yi Wang. Quasi-Single Field Inflation with Large Mass. *JCAP*, 1209:021, 2012.

[113] Shi Pi and Misao Sasaki. Curvature Perturbation Spectrum in Two-field Inflation with a Turning Trajectory. *JCAP*, 1210:051, 2012.

[114] Toshifumi Noumi, Masahide Yamaguchi, and Daisuke Yokoyama. Effective field theory approach to quasi-single field inflation and effects of heavy fields. *JHEP*, 06:051, 2013.

[115] Nima Arkani-Hamed and Juan Maldacena. Cosmological Collider Physics. 2015.

[116] Emanuela Dimastrogiovanni, Matteo Fasiello, and Marc Kamionkowski. Imprints of Massive Primordial Fields on Large-Scale Structure. *JCAP*, 1602:017, 2016.

[117] Soubhik Kumar and Raman Sundrum. Heavy-Lifting of Gauge Theories By Cosmic Inflation. *JHEP*, 05:011, 2018.

[118] Xiulian Wang, Bo Feng, Mingzhe Li, Xue-Lei Chen, and Xinmin Zhang. Natural inflation, Planck scale physics and oscillating primordial spectrum. *Int. J. Mod. Phys.*, D14:1347, 2005.

[119] Cedric Pahud, Marc Kamionkowski, and Andrew R Liddle. Oscillations in the inflaton potential? *Phys. Rev.*, D79:083503, 2009.

[120] Raphael Flauger, Liam McAllister, Enrico Pajer, Alexander Westphal, and Gang Xu. Oscillations in the CMB from Axion Monodromy Inflation. *JCAP*, 1006:009, 2010.

[121] Takeshi Kobayashi and Fuminobu Takahashi. Running Spectral Index from Inflation with Modulations. *JCAP*, 1101:026, 2011.

[122] Richard Easther and Raphael Flauger. Planck Constraints on Monodromy Inflation. *JCAP*, 1402:037, 2014.

[123] Raphael Flauger, Liam McAllister, Eva Silverstein, and Alexander Westphal. Drifting Oscillations in Axion Monodromy. *JCAP*, 1710(10):055, 2017.

[124] Tetsutaro Higaki and Fuminobu Takahashi. Axion Landscape and Natural Inflation. *Phys. Lett.*, B744:153–159, 2015.

[125] Kiwoon Choi and Hyungjin Kim. Aligned natural inflation with modulations. *Phys. Lett.*, B759:520–527, 2016.

[126] Layne C. Price. Power spectrum oscillations from Planck-suppressed operators in effective field theory motivated monodromy inflation. *Phys. Rev.*, D92(10):103507, 2015.

[127] Marco Peloso and Caner Unal. Trajectories with suppressed tensor-to-scalar ratio in Aligned Natural Inflation. *JCAP*, 1506(06):040, 2015.

[128] M. Kawasaki, Masahide Yamaguchi, and T. Yanagida. Natural chaotic inflation in supergravity. *Phys. Rev. Lett.*, 85:3572–3575, 2000.

[129] Renata Kallosh, Andrei Linde, and Tomas Rube. General inflaton potentials in supergravity. *Phys. Rev.*, D83:043507, 2011.

[130] Ana Achucarro, Sander Mooij, Pablo Ortiz, and Marieke Postma. Sgoldstino inflation. *JCAP*, 1208:013, 2012.

[131] Sergio Ferrara and Diederik Roest. General sGoldstino Inflation. *JCAP*, 1610(10):038, 2016.

[132] Sergei V. Ketov and Takahiro Terada. Generic Scalar Potentials for Inflation in Supergravity with a Single Chiral Superfield. *JHEP*, 12:062, 2014.

[133] Luis Alvarez-Gaume, Cesar Gomez, and Raul Jimenez. A Minimal Inflation Scenario. *JCAP*, 1103:027, 2011.

[134] J. Polonyi. Generalization of the Massive Scalar Multiplet Coupling to the Supergravity. *Hungary Central Inst Res - KFKI-77-93*, 1977.

[135] Nima Arkani-Hamed, Thomas Gregoire, and Jay G. Wacker. Higher dimensional supersymmetry in 4-D superspace. *JHEP*, 03:055, 2002.

[136] Raman Sundrum. To the fifth dimension and back. In *Theoretical Advanced Study Institute in Elementary Particle Physics: Physics in D >= 4 (TASI 2004), Boulder, Colorado, June 6-July 2, 2004*, pages 585–630, 2004.

[137] Emilian Dudas and Clemens Wieck. Moduli backreaction and supersymmetry breaking in string-inspired inflation models. *JHEP*, 10:062, 2015.

[138] Michael R. Douglas and Shamit Kachru. Flux compactification. *Rev. Mod. Phys.*, 79:733–796, 2007.

[139] Yonatan Kahn, Daniel A. Roberts, and Jesse Thaler. The goldstone and goldstino of supersymmetric inflation. *JHEP*, 10:001, 2015.

[140] Sergio Ferrara, Renata Kallosh, and Jesse Thaler. Cosmology with orthogonal nilpotent superfields. *Phys. Rev.*, D93(4):043516, 2016.

[141] Luca V. Delacretaz, Victor Gorbenko, and Leonardo Senatore. The Supersymmetric Effective Field Theory of Inflation. *JHEP*, 03:063, 2017.

[142] Abraham Loeb and Matias Zaldarriaga. Measuring the small - scale power spectrum of cosmic density fluctuations through 21 cm tomography prior to the epoch of structure formation. *Phys. Rev. Lett.*, 92:211301, 2004.

[143] Julian B. Muñoz, Yacine Ali-Haïmoud, and Marc Kamionkowski. Primordial non-gaussianity from the bispectrum of 21-cm fluctuations in the dark ages. *Phys. Rev.*, D92(8):083508, 2015.

[144] P. Daniel Meerburg, Moritz Münchmeyer, Julian B. Muñoz, and Xingang Chen. Prospects for Cosmological Collider Physics. *JCAP*, 1703(03):050, 2017.

[145] Dalia S. Goldwirth and Tsvi Piran. Initial conditions for inflation. *Phys. Rept.*, 214:223–291, 1992.

[146] Michael Dine and Lawrence Pack. Studies in Small Field Inflation. *JCAP*, 06:033, 2012.

[147] Robert Brandenberger. Initial conditions for inflation — A short review. *Int. J. Mod. Phys. D*, 26(01):1740002, 2016.

[148] Andrei Linde. On the problem of initial conditions for inflation. *Found. Phys.*, 48(10):1246–1260, 2018.

[149] Debika Chowdhury, Jérôme Martin, Christophe Ringeval, and Vincent Vennin. Assessing the scientific status of inflation after Planck. *Phys. Rev. D*, 100(8):083537, 2019.

[150] Edmund J. Copeland, Andrew R. Liddle, David H. Lyth, Ewan D. Stewart, and David Wands. False vacuum inflation with Einstein gravity. *Phys. Rev. D*, 49:6410–6433, 1994.

[151] G. R. Dvali, Q. Shafi, and Robert K. Schaefer. Large scale structure and supersymmetric inflation without fine tuning. *Phys. Rev. Lett.*, 73:1886–1889, 1994.

[152] P. Binetruy and G. R. Dvali. D term inflation. *Phys. Lett. B*, 388:241–246, 1996.

[153] Edi Halyo. Hybrid inflation from supergravity D terms. *Phys. Lett. B*, 387:43–47, 1996.

[154] Renata Kallosh and Andrei D. Linde. P term, D term and F term inflation. *JCAP*, 10:008, 2003.

[155] David E. Kaplan and Neal J. Weiner. Little inflatons and gauge inflation. *JCAP*, 0402:005, 2004.

[156] Nima Arkani-Hamed, Hsin-Chia Cheng, Paolo Creminelli, and Lisa Randall. Pseudonatural inflation. *JCAP*, 0307:003, 2003.

[157] Nima Arkani-Hamed, Andrew G. Cohen, and Howard Georgi. Electroweak symmetry breaking from dimensional deconstruction. *Phys. Lett. B*, 513:232–240, 2001.

[158] Raman Sundrum and Christopher M. Wells. Warped Hybrid Inflation. *JHEP*, 02:097, 2010.

[159] Graham G. Ross, Gabriel German, and J. Alberto Vazquez. Hybrid Natural Inflation. *JHEP*, 05:010, 2016.

[160] Nemanja Kaloper, Morgane König, Albion Lawrence, and James H. C. Scargill. On hybrid monodromy inflation — hic sunt dracones. *JCAP*, 03:024, 2021.

[161] Federico Carta, Nicole Righi, Yvette Welling, and Alexander Westphal. Harmonic Hybrid Inflation. *JHEP*, 12:161, 2020.

[162] Nathaniel Craig, Seth Koren, and Timothy Trott. Cosmological Signals of a Mirror Twin Higgs. *JHEP*, 05:038, 2017.

[163] F. Bezrukov and D. Gorbunov. Light inflaton Hunter's Guide. *JHEP*, 05:010, 2010.

[164] Rouzbeh Allahverdi, Bhaskar Dutta, and Yudi Santoso. MSSM inflation, dark matter, and the LHC. *Phys. Rev. D*, 82:035012, 2010.

[165] Celine Boehm, Jonathan Da Silva, Anupam Mazumdar, and Ernestas Pukartas. Probing the Supersymmetric Inflaton and Dark Matter link via the CMB, LHC and XENON1T experiments. *Phys. Rev. D*, 87(2):023529, 2013.

[166] Joseph Bramante, Jessica Cook, Antonio Delgado, and Adam Martin. Low Scale Inflation at High Energy Colliders and Meson Factories. *Phys. Rev. D*, 94(11):115012, 2016.

[167] David H. Lyth and Ewan D. Stewart. More varieties of hybrid inflation. *Phys. Rev. D*, 54:7186–7190, 1996.

[168] Z. G. Berezhiani, A. D. Dolgov, and R. N. Mohapatra. Asymmetric inflationary reheating and the nature of mirror universe. *Phys. Lett. B*, 375:26–36, 1996.

[169] Ya.B. Zeldovich, I.Yu. Kobzarev, and L.B. Okun. Cosmological Consequences of the Spontaneous Breakdown of Discrete Symmetry. *Zh. Eksp. Teor. Fiz.*, 67:3–11, 1974.

[170] A. Vilenkin and A. E. Everett. Cosmic Strings and Domain Walls in Models with Goldstone and PseudoGoldstone Bosons. *Phys. Rev. Lett.*, 48:1867–1870, 1982.

[171] Mark Hindmarsh. Signals of Inflationary Models with Cosmic Strings. *Prog. Theor. Phys. Suppl.*, 190:197–228, 2011.

[172] Pierre Auclair et al. Probing the gravitational wave background from cosmic strings with LISA. *JCAP*, 04:034, 2020.

[173] A. Vilenkin. Gravitational Field of Vacuum Domain Walls and Strings. *Phys. Rev. D*, 23:852–857, 1981.

[174] Graciela B. Gelmini, Marcelo Gleiser, and Edward W. Kolb. Cosmology of Biased Discrete Symmetry Breaking. *Phys. Rev. D*, 39:1558, 1989.

[175] Ken'ichi Saikawa. A review of gravitational waves from cosmic domain walls. *Universe*, 3(2):40, 2017.

[176] Wilfried Buchmüller, Valerie Domcke, Kohei Kamada, and Kai Schmitz. Hybrid Inflation in the Complex Plane. *JCAP*, 07:054, 2014.

[177] P. Laguna, H. Kurki-Suonio, and R.A. Matzner. Inhomogeneous inflation: The Initial value problem. *Phys. Rev. D*, 44:3077–3086, 1991.

[178] Hannu Kurki-Suonio, Pablo Laguna, and Richard A. Matzner. Inhomogeneous inflation: Numerical evolution. *Phys. Rev. D*, 48:3611–3624, 1993.

[179] Richard Easther, Layne C. Price, and Javier Rasero. Inflating an Inhomogeneous Universe. *JCAP*, 08:041, 2014.

[180] William E. East, Matthew Kleban, Andrei Linde, and Leonardo Senatore. Beginning inflation in an inhomogeneous universe. *JCAP*, 09:010, 2016.

[181] Katy Clough, Eugene A. Lim, Brandon S. DiNunno, Willy Fischler, Raphael Flauger, and Sonia Paban. Robustness of Inflation to Inhomogeneous Initial Conditions. *JCAP*, 09:025, 2017.

[182] Ben Freivogel, Matthew Kleban, Maria Rodriguez Martinez, and Leonard Susskind. Observational consequences of a landscape. *JHEP*, 03:039, 2006.

[183] Koushik Dutta, Pascal M. Vaudrevange, and Alexander Westphal. The Overshoot Problem in Inflation after Tunneling. *JCAP*, 01:026, 2012.

[184] Alan H. Guth, David I. Kaiser, and Yasunori Nomura. Inflationary paradigm after Planck 2013. *Phys. Lett. B*, 733:112–119, 2014.

[185] Ali Masoumi, Alexander Vilenkin, and Masaki Yamada. Initial conditions for slow-roll inflation in a random Gaussian landscape. *JCAP*, 07:003, 2017.

[186] Arushi Bodas, Soubhik Kumar, and Raman Sundrum. The Scalar Chemical Potential in Cosmological Collider Physics. *JHEP*, 02:079, 2021.

[187] Paolo Creminelli, Alberto Nicolis, and Riccardo Rattazzi. Holography and the electroweak phase transition. *JHEP*, 03:051, 2002.

[188] Chris Quigg. Future Colliders Symposium in Hong Kong: Scientific Overview. In *Proceedings, HKUST Jockey Club Institute for Advanced Study: The Future of High Energy Physics (HKUST): Hong Kong, China, January 18-21, 2016*, pages 3–19, 2017.

[189] John Ellis. Prospects for Future Collider Physics. In *Proceedings, HKUST Jockey Club Institute for Advanced Study: The Future of High Energy Physics (HKUST): Hong Kong, China, January 18-21, 2016*, pages 21–38, 2017.

[190] Howard Baer, Tim Barklow, Keisuke Fujii, Yuanning Gao, Andre Hoang, Shinya Kanemura, Jenny List, Heather E. Logan, Andrei Nomerotski, Maxim Perelstein, et al. The International Linear Collider Technical Design Report - Volume 2: Physics. 2013.

[191] James E. Brau, T. Barklow, J. Brau, K. Fujii, J. Gao, J. List, N. Walker, and K. Yokoya. 500 GeV ILC Operating Scenarios. In *Proceedings, Meeting of the APS Division of Particles and Fields (DPF 2015): Ann Arbor, Michigan, USA, 4-8 Aug 2015*, 2015.

[192] CEPC-SPPC Study Group. CEPC-SPPC Preliminary Conceptual Design Report. 1. Physics and Detector. 2015.

[193] M. Bicer et al. First Look at the Physics Case of TLEP. *JHEP*, 01:164, 2014.

[194] M Aicheler, P Burrows, M Draper, T Garvey, P Lebrun, K Peach, N Phinney, H Schmickler, D Schulte, and N Toge. A Multi-TeV Linear Collider Based on CLIC Technology. 2012.

[195] David Curtin, Rouven Essig, Stefania Gori, Prerit Jaiswal, Andrey Katz, et al. Exotic decays of the 125 GeV Higgs boson. *Phys.Rev.*, D90(7):075004, 2014.

[196] T. Golling et al. Physics at a 100 TeV pp collider: beyond the Standard Model phenomena. *CERN Yellow Report*, (3):441–634, 2017.

[197] M. L. Mangano et al. Physics at a 100 TeV pp collider: Standard Model processes. *CERN Yellow Report*, (3):1–254, 2017.

[198] R. Contino et al. Physics at a 100 TeV pp collider: Higgs and EW symmetry breaking studies. *CERN Yellow Report*, (3):255–440, 2017.

[199] Jingyu Tang et al. Concept for a Future Super Proton-Proton Collider. 2015.

[200] David M. South. Search for First Generation Leptoquarks in ep Collisions at HERA. *PoS*, ICHEP2012:141, 2013.

[201] Victor Mukhamedovich Abazov et al. Search for first generation leptoquark pair production in the electron + missing energy + jets final state. *Phys. Rev.*, D84:071104, 2011.

[202] O. Bruning, O. Dominguez, S. Myers, L. Rossi, E. Todesco, and F. Zimmermann. HE-LHC beam-parameters, optics and beam-dynamics issues. In *Proceedings, EuCARD-AccNet-EuroLumi Workshop: The High-Energy Large Hadron Collider (HE-LHC10): Villa Bighi, Malta, Republic of Malta, October 14-16, 2010*, 2011.

[203] Max Klein. Deep inelastic scattering at the energy frontier. *Annalen Phys.*, 528:138–144, 2016.

[204] Uta Klein. Fcc-eh progress on bsm higgs studies, fcc week berlin. *FCC-eh Progress on BSM Higgs Studies, FCC week Berlin*, 2017.

[205] Yi-Lei Tang, Chen Zhang, and Shou-hua Zhu. Invisible Higgs Decay at the LHeC. *Phys. Rev.*, D94(1):011702, 2016.

[206] Mukesh Kumar, Xifeng Ruan, Rashidul Islam, Alan S. Cornell, Max Klein, Uta Klein, and Bruce Mellado. Probing anomalous couplings using di-Higgs production in electron?proton collisions. *Phys. Lett.*, B764:247–253, 2017.

[207] Mukesh Kumar, Xifeng Ruan, Alan S. Cornell, Rashidul Islam, and Bruce Mellado. Double Higgs production at FCC-he and prospects for measurements of self-coupling. *J. Phys. Conf. Ser.*, 623(1):012017, 2015.

[208] Zhiqing Zhang. Top and EW Physics at the LHeC. *PoS*, EPS-HEP2015:342, 2015.

[209] O. Cakir, A. Senol, and A. T. Tasci. Single Production of Fourth Family t-prime Quarks at LHeC. *EPL*, 88(1):11002, 2009.

[210] Han Liang, Xiao-Gang He, Wen-Gan Ma, Shao-Ming Wang, and Ren-You Zhang. Seesaw Type I and III at the LHeC. *JHEP*, 09:023, 2010.

[211] Carl Blaksley, Mattias Blennow, Florian Bonnet, Pilar Coloma, and Enrique Fernandez-Martinez. Heavy Neutrinos and Lepton Number Violation in lp Colliders. *Nucl. Phys.*, B852:353–365, 2011.

[212] Subhadeep Mondal and Santosh Kumar Rai. Probing the Heavy Neutrinos of Inverse Seesaw Model at the LHeC. *Phys. Rev.*, D94(3):033008, 2016.

[213] Lucia Duarte, Gabriel A. Gonzalez-Sprinberg, and Oscar Alfredo Sampayo. Majorana neutrinos production at LHeC in an effective approach. *Phys. Rev.*, D91(5):053007, 2015.

[214] Subhadeep Mondal and Santosh Kumar Rai. Polarized window for left-right symmetry and a right-handed neutrino at the Large Hadron-Electron Collider. *Phys. Rev.*, D93(1):011702, 2016.

[215] Manfred Lindner, Farinaldo S. Queiroz, Werner Rodejohann, and Carlos E. Yaguna. Left-Right Symmetry and Lepton Number Violation at the Large Hadron Electron Collider. *JHEP*, 06:140, 2016.

[216] Bastian Diaz, Martin Schmaltz, and Yi-Ming Zhong. The leptoquark Hunter?s guide: Pair production. *JHEP*, 10:097, 2017.

[217] I. Dorner, S. Fajfer, A. Greljo, J. F. Kamenik, and N. Konik. Physics of leptoquarks in precision experiments and at particle colliders. *Phys. Rept.*, 641:1–68, 2016.

[218] Nirmal Raj. Anticipating nonresonant new physics in dilepton angular spectra at the LHC. *Phys. Rev.*, D95(1):015011, 2017.

[219] Vardan Khachatryan et al. Search for excited leptons in proton-proton collisions at sqrt(s) = 8 TeV. *JHEP*, 03:125, 2016.

[220] Georges Aad et al. Search for single production of a vector-like quark via a heavy gluon in the $4b$ final state with the ATLAS detector in pp collisions at $\sqrt{s} = 8$ TeV. *Phys. Lett.*, B758:249–268, 2016.

[221] Georges Aad et al. Search for the production of single vector-like and excited quarks in the Wt final state in pp collisions at $\sqrt{s}$ = 8 TeV with the ATLAS detector. *JHEP*, 02:110, 2016.

[222] A. Ferrari, Johann Collot, M-L. Andrieux, B. Belhorma, P. de Saintignon, J-Y. Hostachy, Ph. Martin, and M. Wielers. Sensitivity study for new gauge bosons and right-handed Majorana neutrinos in pp collisions at s = 14-TeV. *Phys. Rev.*, D62:013001, 2000.

[223] Vardan Khachatryan et al. Search for long-lived particles that decay into final states containing two electrons or two muons in proton-proton collisions at $\sqrt{s} = 8$ TeV. *Phys. Rev.*, D91(5):052012, 2015.

[224] The ATLAS collaboration. Search for long-lived neutral particles decaying into displaced lepton jets in proton–proton collisions at $\sqrt{s}$ = 13 TeV with the ATLAS detector. 2016.

[225] Vardan Khachatryan et al. Search for Long-Lived Neutral Particles Decaying to Quark-Antiquark Pairs in Proton-Proton Collisions at $\sqrt{s} = 8$ TeV. *Phys. Rev.*, D91(1):012007, 2015.

[226] Georges Aad et al. Search for long-lived, weakly interacting particles that decay to displaced hadronic jets in proton-proton collisions at $\sqrt{s} = 8$ TeV with the ATLAS detector. *Phys. Rev.*, D92(1):012010, 2015.

[227] John Paul Chou, David Curtin, and H. J. Lubatti. New Detectors to Explore the Lifetime Frontier. *Phys. Lett.*, B767:29–36, 2017.

[228] David Curtin and Michael E. Peskin. Analysis of Long Lived Particle Decays with the MATHUSLA Detector. *Phys. Rev. D*, 97(1):015006, 2018.

[229] Austin Ball et al. A Letter of Intent to Install a milli-charged Particle Detector at LHC P5. 2016.

[230] Vladimir V. Gligorov, Simon Knapen, Michele Papucci, and Dean J. Robinson. Searching for Long-lived Particles: A Compact Detector for Exotics at LHCb. *Phys. Rev. D*, 97(1):015023, 2018.

[231] Jonathan L. Feng, Iftah Galon, Felix Kling, and Sebastian Trojanowski. ForwArd Search ExpeRiment at the LHC. *Phys. Rev. D*, 97(3):035001, 2018.

[232] James E. Brau, Martin Breidenbach, Charles Baltay, Raymond E. Frey, and David M. Strom. Silicon detectors at the ILC. *Nucl. Instrum. Meth.*, A579:567–571, 2007.

[233] Halina Abramowicz et al. The International Linear Collider Technical Design Report - Volume 4: Detectors. 2013.

[234] Naomi van der Kolk. CLIC Detector and Physics Status. In *Proceedings, International Workshop on Future Linear Colliders 2016 (LCWS2016): Morioka, Iwate, Japan, December 05-09, 2016*, 2017.

[235] Georges Aad et al. Search for direct production of charginos, neutralinos and sleptons in final states with two leptons and missing transverse momentum in pp collisions at $\sqrt{s} = 8$ TeV with the ATLAS detector. *JHEP*, 05:071, 2014.

[236] A. M. Sirunyan et al. Search for electroweak production of charginos and neutralinos in multilepton final states in proton-proton collisions at $\sqrt{s} = 13$ TeV. *JHEP*, 03:166, 2018.

[237] C. Patrignani et al. Review of Particle Physics. *Chin. Phys.*, C40(10):100001, 2016.

[238] Matthew Low and Lian-Tao Wang. Neutralino dark matter at 14 TeV and 100 TeV. *JHEP*, 08:161, 2014.

[239] Marco Cirelli, Filippo Sala, and Marco Taoso. Wino-like Minimal Dark Matter and future colliders. *JHEP*, 10:033, 2014. [Erratum: JHEP01,041(2015)].

[240] Hajime Fukuda, Natsumi Nagata, Hidetoshi Otono, and Satoshi Shirai. Higgsino Dark Matter or Not: Role of Disappearing Track Searches at the LHC and Future Colliders. *Phys. Lett. B*, 781:306–311, 2018.

[241] Tao Han, Sanjay Padhi, and Shufang Su. Electroweakinos in the Light of the Higgs Boson. *Phys. Rev.*, D88(11):115010, 2013.

[242] Stefania Gori, Sunghoon Jung, and Lian-Tao Wang. Cornering electroweakinos at the LHC. *JHEP*, 10:191, 2013.

[243] Pedro Schwaller and Jose Zurita. Compressed electroweakino spectra at the LHC. *JHEP*, 03:060, 2014.

[244] Zhenyu Han, Graham D. Kribs, Adam Martin, and Arjun Menon. Hunting quasidegenerate Higgsinos. *Phys. Rev.*, D89(7):075007, 2014.

[245] Howard Baer, Azar Mustafayev, and Xerxes Tata. Monojets and mono-photons from light higgsino pair production at LHC14. *Phys. Rev.*, D89(5):055007, 2014.

[246] Howard Baer, Azar Mustafayev, and Xerxes Tata. Monojet plus soft dilepton signal from light higgsino pair production at LHC14. *Phys. Rev.*, D90(11):115007, 2014.

[247] Marcin Badziak, Antonio Delgado, Marek Olechowski, Stefan Pokorski, and Kazuki Sakurai. Detecting underabundant neutralinos. *JHEP*, 11:053, 2015.

[248] Chengcheng Han, Doyoun Kim, Shoaib Munir, and Myeonghun Park. Accessing the core of naturalness, nearly degenerate higgsinos, at the LHC. *JHEP*, 04:132, 2015.

[249] Daniele Barducci, Alexander Belyaev, Aoife K. M. Bharucha, Werner Porod, and Veronica Sanz. Uncovering Natural Supersymmetry via the interplay between the LHC and Direct Dark Matter Detection. *JHEP*, 07:066, 2015.

[250] N. Arkani-Hamed, A. Delgado, and G. F. Giudice. The Well-tempered neutralino. *Nucl. Phys.*, B741:108–130, 2006.

[251] Laura Lopez Honorez, Emmanuel Nezri, Josep F. Oliver, and Michel H. G. Tytgat. The Inert Doublet Model: An Archetype for Dark Matter. *JCAP*, 0702:028, 2007.

[252] Marco Cirelli, Nicolao Fornengo, and Alessandro Strumia. Minimal dark matter. *Nucl. Phys.*, B753:178–194, 2006.

[253] Oliver Fischer and Jochum J. van der Bij. The scalar Singlet-Triplet Dark Matter Model. *JCAP*, 1401:032, 2014.

[254] Kazuo Fujikawa. A Vector - like extension of the standard model. *Prog. Theor. Phys.*, 92:1149–1160, 1994.

[255] Aniket Joglekar, Pedro Schwaller, and Carlos E. M. Wagner. Dark Matter and Enhanced Higgs to Di-photon Rate from Vector-like Leptons. *JHEP*, 12:064, 2012.

[256] Nima Arkani-Hamed, Kfir Blum, Raffaele Tito D'Agnolo, and JiJi Fan. 2:1 for Naturalness at the LHC? *JHEP*, 01:149, 2013.

[257] Aniket Joglekar, Pedro Schwaller, and Carlos E. M. Wagner. A Supersymmetric Theory of Vector-like Leptons. *JHEP*, 07:046, 2013.

[258] Adam Falkowski, David M. Straub, and Avelino Vicente. Vector-like leptons: Higgs decays and collider phenomenology. *JHEP*, 05:092, 2014.

[259] Nilanjana Kumar and Stephen P. Martin. Vectorlike leptons at the Large Hadron Collider. *Phys. Rev.*, D92(11):115018, 2015.

[260] D. Emmanuel-Costa and R. Gonzalez Felipe. Minimal string-scale unification of gauge couplings. *Phys. Lett.*, B623:111–118, 2005.

[261] Biplob Bhattacherjee, Pritibhajan Byakti, Ashwani Kushwaha, and Sudhir K Vempati. Unification with Vector-like fermions and signals at LHC. *JHEP*, 05:090, 2018.

[262] Howard E. Haber and Gordon L. Kane. The Search for Supersymmetry: Probing Physics Beyond the Standard Model. *Phys. Rept.*, 117:75–263, 1985.

[263] David Tucker-Smith and Neal Weiner. Inelastic dark matter. *Phys. Rev.*, D64:043502, 2001.

[264] David Tucker-Smith and Neal Weiner. The Status of inelastic dark matter. *Phys. Rev.*, D72:063509, 2005.

[265] C. H. Chen, Manuel Drees, and J. F. Gunion. A Nonstandard string / SUSY scenario and its phenomenological implications. *Phys. Rev.*, D55:330–347, 1997. [Erratum: Phys. Rev.D60,039901(1999)].

[266] C. H. Chen, Manuel Drees, and J. F. Gunion. Addendum/erratum for 'searching for invisible and almost invisible particles at e+ e- colliders' [hep-ph/9512230] and 'a nonstandard string/SUSY scenario and its phenomenological implications' [hep-ph/9607421]. 1999.

[267] Vardan Khachatryan et al. Search for supersymmetry in events with soft leptons, low jet multiplicity, and missing transverse energy in proton-proton collisions at $\sqrt{s}$=8 TeV. *Phys. Lett.*, B759:9–35, 2016.

[268] Morad Aaboud et al. Search for long-lived charginos based on a disappearing-track signature in pp collisions at $\sqrt{s} = 13$ TeV with the ATLAS detector. *JHEP*, 06:022, 2018.

[269] Gian F. Giudice, Tao Han, Kai Wang, and Lian-Tao Wang. Nearly Degenerate Gauginos and Dark Matter at the LHC. *Phys. Rev.*, D81:115011, 2010.

[270] Stefania Gori, Sunghoon Jung, Lian-Tao Wang, and James D. Wells. Prospects for Electroweakino Discovery at a 100 TeV Hadron Collider. *JHEP*, 12:108, 2014.

[271] Joseph Bramante, Patrick J. Fox, Adam Martin, Bryan Ostdiek, Tilman Plehn, Torben Schell, and Michihisa Takeuchi. Relic neutralino surface at a 100 TeV collider. *Phys. Rev.*, D91:054015, 2015.

[272] Giovanni Grilli di Cortona. Hunting electroweakinos at future hadron colliders and direct detection experiments. *JHEP*, 05:035, 2015.

[273] Joseph Bramante, Nishita Desai, Patrick Fox, Adam Martin, Bryan Ostdiek, and Tilman Plehn. Towards the Final Word on Neutralino Dark Matter. *Phys. Rev.*, D93(6):063525, 2016.

[274] Clifford Cheung, Lawrence J. Hall, David Pinner, and Joshua T. Ruderman. Prospects and Blind Spots for Neutralino Dark Matter. *JHEP*, 05:100, 2013.

[275] Lorenzo Calibbi, Alberto Mariotti, and Pantelis Tziveloglou. Singlet-Doublet Model: Dark matter searches and LHC constraints. *JHEP*, 10:116, 2015.

[276] Rebecca Krall and Matthew Reece. Last Electroweak WIMP Standing: Pseudo-Dirac Higgsino Status and Compact Stars as Future Probes. *Chin. Phys. C*, 42(4):043105, 2018.

[277] R. Aaij et al. Performance of the LHCb Vertex Locator. *JINST*, 9:P09007, 2014.

[278] *ATLAS inner detector: Technical Design Report, 1*. Technical Design Report ATLAS. CERN, Geneva, 1997.

[279] J. Alwall, R. Frederix, S. Frixione, V. Hirschi, F. Maltoni, O. Mattelaer, H. S. Shao, T. Stelzer, P. Torrielli, and M. Zaro. The automated computation of tree-level and next-to-leading order differential cross sections, and their matching to parton shower simulations. *JHEP*, 07:079, 2014.

[280] Georges Aad et al. Search for massive, long-lived particles using multitrack displaced vertices or displaced lepton pairs in pp collisions at $\sqrt{s}$ = 8 TeV with the ATLAS detector. *Phys. Rev.*, D92(7):072004, 2015.

[281] Nathaniel Craig, Andrey Katz, Matt Strassler, and Raman Sundrum. Naturalness in the Dark at the LHC. *JHEP*, 07:105, 2015.